



Technische Universität München

Fakultät für Medizin

Mapping the fate decision of single NK cells *in vivo*

Sophie Flommersfeld

Vollständiger Abdruck der von der Fakultät für Medizin der Technischen Universität München zur Erlangung des akademischen Grades einer

Doktorin der Naturwissenschaften (Dr. rer. nat.)

genehmigten Dissertation.

Vorsitz: Prof. Dr. Marc Schmidt-Supprian

Prüfer*innen der Dissertation:

1. TUM Junior Fellow Dr. Veit Buchholz
2. Prof. Dr. Benjamin Schusser
3. Prof. Dr. Adelheid Cerwenka

Die Dissertation wurde am 08.12.2021 bei der Fakultät für Medizin der Technischen Universität München eingereicht und durch die Fakultät für Medizin am 12.07.2022 angenommen.

Parts of this thesis have previously been published:

Flommersfeld S*, Böttcher JP*, Ersching J, Flossdorf M, Meiser P, Pachmayr LO, Leube J, Hensel I, Jarosch S, Zhang Q, Chaudhry MZ, Andrae I, Schiemann M, Busch DH, Cicin-Sain L, Sun JC, Gasteiger G, Victora GD, Höfer T, Buchholz VR[†], Grassmann S[†]. Fate mapping of single NK cells identifies a type 1 innate lymphoid-like lineage that bridges innate and adaptive recognition of viral infection. *Immunity* (2021)

Grassmann S*, Mihatsch L*, Mir J, Kazeroonian A, Rahimi R, **Flommersfeld S**, Schober K, Hensel I, Leube J, Pachmayr LO, Kretschmer L, Zhang Q, Jolly A, Chaudhry MZ, Schiemann M, Cicin-Sain L, Höfer T, Busch DH, Flossdorf M, Buchholz VR. Early emergence of T central memory precursors programs clonal dominance during chronic viral infection. *Nature Immunology* (2020)

Grassmann S*, Pachmayr LO*, Leube J, Mihatsch L, Andrae I, **Flommersfeld S**, Oduro J, Cicin-Sain L, Schiemann M, Flossdorf M, Buchholz VR. Distinct surface expression of activating receptor Ly49H drives differential expansion of NK cell clones upon murine cytomegalovirus infection. *Immunity* (2019)

* These authors contributed equally

[†] Senior authors

Table of Contents

1	INTRODUCTION	9
1.1	NK cells are key players of cellular innate immunity.....	9
1.2	Target recognition by NK cells.....	9
1.3	NK cell maturation and phenotype.....	12
1.4	Tissue-resident NK cells	14
1.5	Innate lymphoid cells (ILCs).....	15
1.6	Adaptive-like responses of NK cells.....	17
1.6.1	Hapten-induced memory-like NK cells.....	17
1.6.2	Cytokine-induced memory-like NK cells.....	19
1.6.3	Adaptive-like NK cell responses in cytomegalovirus infection	19
1.7	Crosstalk between NK cells, dendritic cells and T cells upon MCMV infection.....	22
1.8	Single-cell fate mapping of immune cells.....	24
1.8.1	Cellular barcoding.....	25
1.8.2	Congenetic matrix.....	26
1.8.3	Retroviral fluorescent barcoding.....	28
2	AIM OF THIS THESIS.....	30
3	MATERIAL AND METHODS	31
3.1	Material	31
3.1.1	Devices	31
3.1.2	Chemicals and reagents	32
3.1.3	Antibodies.....	33
3.1.4	Buffers and media	36
3.1.5	Cell lines	37
3.1.6	Plasmids and recombinant DNA.....	37
3.1.7	Oligonucleotides	37
3.1.8	Mice.....	38
3.1.9	Viruses	39
3.1.10	Software.....	39
3.2	Methods.....	39
3.2.1	Tissue culture.....	39
3.2.2	Generation of retroviral fluorescent barcodes	40
3.2.2.1	Transfection of virus-producing cell lines.....	40
3.2.2.2	Generation of stably transduced Plat-E cell lines	40

3.2.2.3	Generation of retrogenic mice.....	40
3.2.3	MCMV generation and infection.....	41
3.2.3.1	Generation of virus stocks from salivary glands.....	41
3.2.3.2	Plaque Assay.....	42
3.2.3.3	Infections.....	42
3.2.3.4	Measurement of MCMV titers.....	43
3.2.4	Generation of single-cell suspensions.....	43
3.2.4.1	Spleen and lymph nodes.....	43
3.2.4.2	Blood.....	43
3.2.4.3	Liver.....	43
3.2.5	Adoptive transfer of Ly49H ⁺ NK cells.....	44
3.2.5.1	Pre-enrichment of NK1.1 ⁺ cells.....	44
3.2.5.2	Cell sorting and adoptive transfer.....	44
3.2.5.3	Retransfer of Ly49H ⁺ NK cells.....	44
3.2.6	Adoptive transfer of OT-1 T cells.....	45
3.2.6.1	Priming of OT-1 T cells.....	45
3.2.6.2	Retransfer of OT-1 T cells.....	45
3.2.7	Flow cytometry.....	46
3.2.8	RNA sequencing.....	46
3.2.8.1	Bulk RNA sequencing.....	46
3.2.8.2	Single cell RNA sequencing.....	46
3.2.9	Confocal immunofluorescence imaging and image analysis.....	47
3.2.10	Parabiosis.....	47
3.2.11	Mixed bone marrow chimeras.....	47
3.2.12	Functional assays.....	48
3.2.12.1	Stimulation of Ly49H ⁺ NK cells with PMA/ionomycin.....	48
3.2.12.2	<i>Ex vivo</i> cytokine staining.....	48
3.2.12.3	Ba/F3 co-culture.....	48
3.2.12.4	<i>In vitro</i> killing assay.....	49
3.2.13	Statistics.....	49
4	RESULTS.....	50
4.1	Ly49H ⁺ NK cells show high phenotypic diversity upon MCMV infection.....	50
4.2	Single-cell fate mapping of Ly49H ⁺ NK cells identifies two distinct response patterns upon MCMV infection.....	51
4.3	Distinct response patterns emerge from pre-existing NK cell subsets and are stable throughout infection.....	54

4.4	The identified NK cell subsets are transcriptionally distinct	57
4.5	CD27 ⁺ CD62L ⁻ NK cells share features with ILC1s	60
4.6	ILC1-like NK cells unite important characteristics of NK cells and ILC1s	62
4.7	ILC1-like NK cells are not immature precursors of conventional NK cells	65
4.8	ILC1-like NK cells are restricted to lymphoid organs and tissue-resident in the spleen.....	68
4.9	ILC1-like NK cells and cDC1s form clusters early during MCMV infection	71
4.10	Clustering of ILC1-like NK cells and cDC1s is critical for optimal priming of CD8 T cells early during MCMV infection.....	75
5	DISCUSSION.....	79
5.1	Individual Ly49H ⁺ NK cells can adopt separate fates upon MCMV infection.....	79
5.2	Classification of ILC1-like NK cells within the growing family of innate lymphocytes.....	81
5.3	ILC1-like NK cells play a unique role in bridging innate and adaptive immunity	83
5.4	From murine to human NK cell subsets.....	86
6	SUMMARY.....	88
7	BIBLIOGRAPHY.....	89
8	ACKNOWLEDGEMENTS.....	108

Index of Figures

Figure 1: Target recognition by NK cells.....	10
Figure 2: NK cell licensing.....	11
Figure 3: Different subsets of group 1 innate lymphoid cells.	16
Figure 4: Adaptive-like responses of Ly49H ⁺ NK cells upon MCMV infection.	21
Figure 5: Efficient NK cell activation is critical to ensure early control of viral replication and rapid CD8 ⁺ T cell responses during MCMV infection.	23
Figure 6: Two concepts of immune cell differentiation on single-cell level.....	25
Figure 7: The congenic matrix as a tool for single-cell fate mapping of immune cells.....	27
Figure 8: Retroviral fluorescent barcoding.....	28
Figure 9: Ly49H ⁺ NK cells show phenotypic heterogeneity upon MCMV infection.	50
Figure 10: Retrogenic color-barcoding enables single-cell fate mapping of Ly49H ⁺ NK cells.	52
Figure 11: Single-cell fate mapping of Ly49H ⁺ NK cells identifies two distinct response patterns upon MCMV infection.....	53
Figure 12: CD62L ⁻ clones originate from CD27 ⁺ CD62L ⁻ Ly49H ⁺ NK cells in the spleen. ..	55
Figure 13: Distinct response patterns are maintained during memory phase and upon secondary infection.	56
Figure 14: CD27 ⁺ CD62L ⁻ NK cells have a unique transcriptional profile.	58
Figure 15: Distinct transcriptional signatures are conserved among Ly49H ⁺ and Ly49H ⁻ NK cells and mirror differences in protein levels of marker proteins.	60
Figure 16: CD27 ⁺ CD62L ⁻ NK cells share features with ILC1s.	61
Figure 17: CD27 ⁺ CD62L ⁻ NK cells are <i>bona fide</i> NK cells.	62
Figure 18: ILC1-like NK cells show enhanced cytokine production.....	63
Figure 19: ILC1-like NK cells receive signaling via Ly49H and show target-specific cytotoxicity.	64
Figure 20: ILC1-like NK cells do not serve as precursors of cNK cells.....	65

Figure 21: RNA velocities suggest no differentiation activity of ILC1-like NK cells towards cNK cells.	67
Figure 22: Transcriptional profiles of cNK and ILC1-like NK cells remain distinct upon MCMV infection.....	68
Figure 23: ILC1-like NK cells are overrepresented in lymphoid tissues.....	69
Figure 24: ILC1-like NK cells are tissue-resident in the spleen at steady state, but show a similar homing profile compared to cNK cells upon adoptive transfer.	70
Figure 25: ILC1-like NK cells cluster with cDC1s early during MCMV infection in an XCR1-dependant manner.	72
Figure 26: Clustering of ILC1-like NK cells and cDC1s requires Ly49H.....	73
Figure 27: Clustering of ILC1-like NK cells and cDC1s requires NK-cell intrinsic expression of Batf3.....	74
Figure 28: Co-localization of cDC1s and MCMV-infected cells is impaired in <i>Klra8^{-/-}</i> mice at 24 hours p.i.....	75
Figure 29: Optimal CD8 T cell priming upon MCMV requires expression of Ly49H.	77
Figure 30: NK-cell intrinsic expression of Batf3 is critical to achieve optimal CD8 T cell priming upon infection.	78

Abbreviations

ACT	Ammonium chloride-Tris
ADCC	Antibody-dependent cellular cytotoxicity
BSA	Bovine serum albumin
CHS	Contact hypersensitivity
DC	Dendritic cell
cDC1	Conventional type 1 dendritic cell
DMEM	Dulbecco's Modified Eagle Medium
DMSO	Dimethyl sulfoxide
DNFB	2,4-dinitrofluorobenzene
DTA	Diphtheria toxin
EDTA	Ethylenediaminetetraacetic acid
EMA	Ethidium monoazide bromide
FACS	Fluorescence activated cell sorting
FCS	Fetal calf serum
GeoMFI	Geometric mean fluorescence intensity
GM-CSF	Granulocyte-macrophage colony-stimulating factor
Gy	Gray
HCl	Hydrochloride
HCMV	Human cytomegalovirus
HSC	Hematopoietic stem cell
IFN-γ	Interferon- γ
IL	Interleukin
IL2rg	IL-2 receptor subunit gamma
mIL-3	Murine IL-3
mIL-6	Murine IL-6
ILC	Innate lymphoid cell
i.p.	Intraperitoneal
ITIM	Immunoreceptor tyrosine-based inhibitory motif
i.v.	Intravenous
KDE	Kernel density estimate
KIR	Killer cell immunoglobulin-like receptors
Ltb	Lymphotoxin beta
MCMV	Murine cytomegalovirus
MHC	Major histocompatibility complex

NK	Natural killer
cNK	Conventional NK
trNK	Tissue-resident NK
PBS	Phosphate buffered saline
PCA	Principal component analysis
PFA	Paraformaldehyde
PI	Propidium iodide
Plat-E	Platinum-E
RNA-seq	RNA sequencing
scRNA-seq	Single cell RNA sequencing
RT	Room temperature
mSCF	Murine SCF
SPF	Specific pathogen-free
TCR	T cell receptor
TNF-α	Tumor necrosis factor alpha

1 Introduction

1.1 NK cells are key players of cellular innate immunity

Natural killer (NK) cells are a critical constituent of cellular innate immunity. They belong to the lymphoid lineage, originate from the bone marrow and undergo terminal maturation in secondary lymphoid tissues (Caligiuri, 2008). NK cells represent a first line of defense against viral infections and cancers. Several studies have shown that patients with NK cell deficiency display increased susceptibility to herpesviruses and other viral pathogens (Biron et al., 1989, Orange, 2013). Different functions of NK cells have been described so far. First of all, NK cells mediate direct cytotoxicity to infected and malignant cells. Target cells are recognized specifically by the integration of various signals from both activating and inhibitory receptors and are killed via the release of pre-formed cytolytic effector molecules such as perforin and granzymes or via death receptor-related pathways, e.g. FasL or TRAIL (Prager and Watzl, 2019). In addition to that, NK cells also secrete cytokines and chemokines that shape the host's immune responses. A main effector molecule secreted by NK cells is Interferon- γ (IFN- γ) which stimulates the expression of MHC molecules on tumor and antigen-presenting cells, activates macrophages, induces protective T cell responses and mediates antiviral effects (Wallach et al., 1982, Heise and Virgin, 1995, Mocikat et al., 2003, Lucin et al., 1994). Furthermore, NK cells can also secrete pro-inflammatory Tumor necrosis factor alpha (TNF- α) and Granulocyte-macrophage colony-stimulating factor (GM-CSF) that promotes proliferation and maturation of monocytes and dendritic cells (Caligiuri, 2008).

1.2 Target recognition by NK cells

NK cells express an array of activating and inhibitory receptors that enable them to identify infected and malignant cells with high specificity and control NK cell reactivity. So far, three different mechanisms of NK cell activation have been described.

First, NK cells recognize antibody-coated target cells via CD16, also known as Fc γ RIII. The receptor binds to the Fc portion of surface-bound immunoglobulin G molecules and induces target cell lysis in a process called antibody-dependent cellular cytotoxicity (ADCC) (Lanier et al., 1988).

Second, target cells might express stress-induced ligands that are detected by activating NK cell receptors (**Figure 1A, left panel**). NKG2D is a well-described example of such a receptor that

Introduction

recognizes stress-induced self-ligands such as ULBP and MIC molecules in humans or RAE1, H60 and MULT1 proteins in mice – molecules that are absent or expressed at low levels by healthy cells, but are upregulated upon infection or malignant transformation of these cells (Raulet et al., 2013). NKG2D interactions are of significant importance for the antitumor activity of NK cells (Jamieson et al., 2002). Other activating receptors bind to foreign ligands, e.g. Ly49H on murine NK cells recognizes the cytomegalovirus-encoded glycoprotein m157 (Arase et al., 2002, Smith et al., 2002) and NKp46 binds to influenza virus hemagglutinin (Mandelboim et al., 2001).

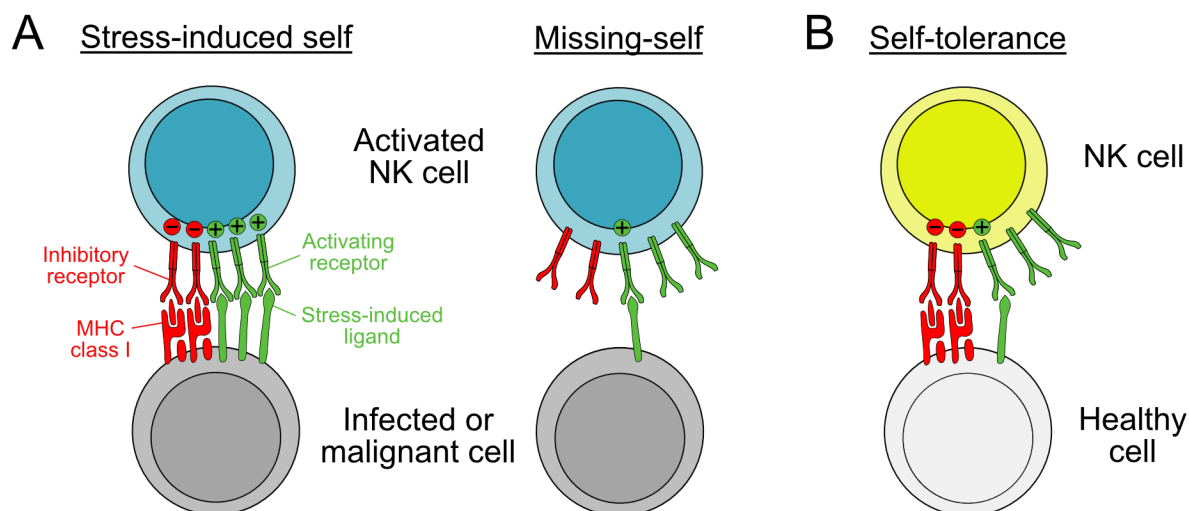


Figure 1: Target recognition by NK cells.

(A) Recognition of target cells that express stress-induced ligands (left) or display aberrant MHC class I expression (right). (B) Self-tolerance of NK cells towards healthy cells.

As a third option, NK cells can detect target cells with aberrant major histocompatibility complex (MHC) class I surface expression via “missing-self” recognition (Karre et al., 1986) (Figure 1A, right panel). The majority of inhibitory NK cell receptors bind to MHC class I molecules, such as killer cell immunoglobulin-like receptors (KIR) in humans, inhibitory Ly49 receptors in mice and NKG2A/CD94 heterodimers in both species (Moretta et al., 1996, Raulet et al., 1997, Lanier, 2005). All of these receptors contain at least one intracytoplasmic signaling domain called immunoreceptor tyrosine-based inhibitory motif (ITIM) mediating their inhibitory function (Vivier et al., 2004). MHC class I molecules are constitutively expressed by healthy cells, but surface expression of MHC class I is often downregulated by tumor cells and virus-infected cells to avoid recognition by CD8⁺ T cells (Stern et al., 1980, Restifo et al., 1993, Campbell and Slater, 1994, Ziegler et al., 1997). NK cells prevent this mechanism of immune escape and specifically target these cells that are “missing-self”. To avoid autoimmunity, NK cells undergo an education process called “licensing” during maturation. More precisely, NK

Introduction

cells have to interact with self-MHC class I molecules to achieve functional maturation (Kim et al., 2005) (**Figure 2**). A high number of self-MHC-specific inhibitory receptors increases NK cell responsiveness, but also ensures self-tolerance and optimizes sensitivity to changes in MHC expression by infected or malignant cells (Joncker et al., 2009) (**Figure 1B**). In line with that, NK cells from mice that lack MHC class I or Ly49 expression, kill missing-self targets less efficiently (Liao et al., 1991, Hoglund et al., 1991, Belanger et al., 2012). NK cells that do not express self-MHC-specific inhibitory receptors remain “unlicensed” and are hyporesponsive to activation (Fernandez et al., 2005) (**Figure 2**).

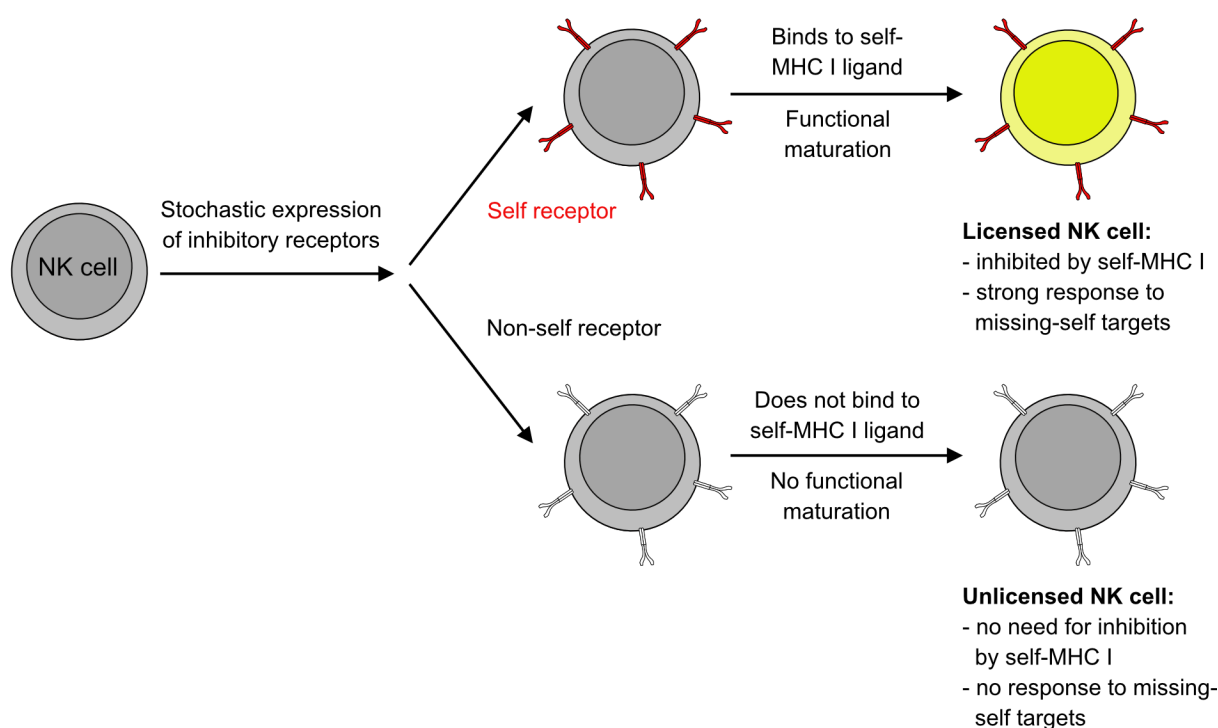


Figure 2: NK cell licensing

Schematic depiction of NK cell licensing. Developing NK cells express either self-reactive or non-self-reactive inhibitory receptors. NK cells expressing self-specific receptors undergo functional maturation and become licensed NK cells that are inhibited by self-MHC I, but are able to recognize missing-self targets. NK cells expressing non-self receptors do not undergo functional maturation and remain unlicensed. Unlicensed NK cells do not respond to missing-self targets, but are also self-tolerant due to the lack of self-reactive receptors. Adapted from (Kim et al., 2005).

However, it has been demonstrated that unlicensed NK cells kill tumor cells that express high levels of MHC class I molecules, more efficiently than licensed NK cells (Orr et al., 2010), and that blockade of inhibitory receptors can enhance the NK cell-mediated anti-tumor response (Koh et al., 2001). Furthermore, all NK cells show similar activation upon recognition of stress-induced ligands (Nishimura et al., 1988, Leiden et al., 1989) suggesting that signals received from activating receptors might compensate for the hyporesponsiveness of unlicensed NK cells (Tu et al., 2016). In some cases, unlicensed NK cells are also required for effective immune

Introduction

responses against viral infections. For example, the immune response against murine cytomegalovirus (MCMV) is supposed to be dominated by unlicensed NK cells (Orr et al., 2010). Similar observations were made upon influenza virus infection in mice or human immunodeficiency virus infection (Mahmoud et al., 2016, Alter et al., 2009). In general, unlicensed NK cells are of particular importance whenever inhibitory receptors are engaged by MHC class I or virus-induced mimics that dampen NK cell activation of licensed NK cells (Tu et al., 2016).

1.3 NK cell maturation and phenotype

Like B and T lymphocytes, NK cells originate from common lymphoid progenitors and – similar to B cells – develop in the bone marrow. The development of mature NK cells critically depends on several transcription factors, especially Nfil3 and Eomes (Gascoyne et al., 2009, Gordon et al., 2012), as well as the cytokine IL-15 (Vosshenrich et al., 2005). After egress from the bone marrow, NK cells undergo terminal maturation in secondary lymphoid tissues (Caligiuri, 2008). Human NK cells are commonly defined by the absence of CD3 and expression of CD56. So far, two major subsets of human NK cells have been described: CD56^{dim} CD16⁺ and CD56^{bright} CD16^{dim/-} NK cells (Lanier et al., 1983, Lanier et al., 1986). While CD56^{dim} NK cells constitute approximately 90 % of circulating NK cells in peripheral blood, CD56^{bright} NK cells compose the majority of NK cells in secondary lymphoid organs (Fehniger et al., 2003). Furthermore, CD56^{bright} NK cells were described to be less cytotoxic but more potent cytokine producers compared to their CD56^{dim} counterparts, suggesting that CD56^{dim} and CD56^{bright} NK cells represent functionally distinct subsets (Nagler et al., 1989, Fehniger et al., 1999, Cooper et al., 2001). Different studies indicate that CD56^{bright} NK cells might be precursors of CD56^{dim} NK cells as they acquire characteristics of CD56^{dim} NK cells after stimulation *in vitro* and *in vivo* upon adoptive transfer into immunodeficient mice (Chan et al., 2007, Romagnani et al., 2007). In addition, CD56^{bright} NK cells were shown to have longer telomere repeats than CD56^{dim} NK cells indicating a more immature phenotype (Chan et al., 2007, Romagnani et al., 2007). However, whether human NK cells indeed differentiate from CD56^{bright} to CD56^{dim} phenotype is still controversially discussed. Evidence against the linear differentiation model comes from recent studies by Wu et al., where genetically barcoded hematopoietic stem cells were transplanted into rhesus macaques and the clonal composition of different immune cell subsets was analyzed in peripheral blood several months post-transplant, revealing stably distinct clonal patterns in CD56⁻ vs. CD56⁺ NK cells and arguing against

Introduction

constant replenishment of CD56⁻ NK cells from the CD56⁺ NK cell compartment (Wu et al., 2014, Wu et al., 2018).

In contrast to human NK cells, murine NK cells do not express CD56. In C57BL/6 mice, NK cells are historically defined by their reactivity with the monoclonal antibody PK136 that binds to NK1.1 (Koo and Peppard, 1984). Expression of NK1.1 is acquired already early during NK cell development and stably maintained during maturation (Rosmaraki et al., 2001). However, NK1.1 is an alloantigen, the expression of which is restricted to few inbred strains (Carlyle et al., 2006). Therefore, further lineage markers have been proposed, namely CD49b (Arase et al., 2001) and NKp46 (Walzer et al., 2007). NKp46 has the additional advantage that it is nearly absent from NKT cells, which express NK1.1 but also T cell markers like CD3. Maturation of mouse NK cells has been described to happen in a 4-stage developmental process: Immature CD11b^{low} CD27^{low} NK cells first acquire expression of CD27, followed by upregulation of CD11b, and then terminally differentiate into CD11b^{high} CD27^{low} NK cells (Chiossone et al., 2009). CD27 expression dissects mature murine NK cells into two distinct subsets, of which CD27^{high} NK cells display enhanced responsiveness to activation signals and cytokine stimulation (Hayakawa and Smyth, 2006). Similarly, also human NK cells consist of a CD27^{high} and a CD27^{low} fraction that correspond with CD56^{bright} and CD56^{dim} NK cells, respectively (Silva et al., 2008, Vossen et al., 2008). In both humans and mice, CD62L was shown to be a relevant maturation marker upon viral infection that marks a polyfunctional NK cell subset important for protective immunity (Juelke et al., 2010, Peng et al., 2013b). Moreover, a study by Peng et al. indicates that CD62L⁻ NK cells give rise to CD62L⁺ cells upon stimulation (Peng et al., 2013b). Another marker that has been described to be expressed by a fraction of NK cells, is the receptor CD160 which binds to classical and non-classical MHC class I molecules (Maeda et al., 2005). CD160 expression is associated with enhanced IFN- γ production and tumor control in mice (Tu et al., 2015) and high cytotoxicity in humans (Maiza et al., 1993). In addition to the aforementioned markers, several other markers are also differentially expressed by NK cells and contribute to the enormous phenotypic diversity of the NK cell compartment (Crinier et al., 2018). Recently, the discovery of tissue-resident NK cells and further innate lymphoid cell (ILC) subsets has even more increased the heterogeneity within the pool of innate lymphocytes (Robinette et al., 2015, McFarland et al., 2021). Phenotype and characteristics of these subsets as well as their commonalities and differences in comparison to conventional NK cells will be summarized in the following sections. However, the developmental relationship, functionality and plasticity of this large number of different subsets of innate lymphocytes is still under intensive investigation.

1.4 Tissue-resident NK cells

Besides conventional circulating NK cells, several subsets of tissue-restricted NK cells with organ-specific phenotypes and functionalities have been described. Localization of these tissue-resident NK (trNK) cells mainly comprise liver, skin, small intestine, uterus, thymus and salivary glands. Liver NK cells consist of a circulating CD49b⁺ CD49a⁻ and a resident CD49b⁻ CD49a⁺ subset (Peng et al., 2013a). Liver-resident NK cells have an immature phenotype as they express low levels of CD11b and CD49b (Peng et al., 2013a). Furthermore, they display reduced expression of Ly49 receptors and CD62L, but higher levels of the activation markers CD160 and CD69 in comparison to conventional NK (cNK) cells (Sojka et al., 2014). Similar to cNK cells, trNK cells in the liver were capable of producing IFN- γ , but in contrast to them also produced high levels of TNF- α and GM-CSF upon stimulation (Sojka et al., 2014). Moreover, liver trNK cells were shown to mount hapten-induced memory responses (Paust et al., 2010, Peng et al., 2013a) (see also 1.6.1). Liver-resident NK cells develop independent of conventional NK cells, they do not require the transcription factors Eomes and Nfil3, but instead depend on the expression of T-bet and Hobit (Sojka et al., 2014, Daussy et al., 2014, Mackay et al., 2016).

Subsets of CD49b⁻ CD49a⁺ NK cells with similar phenotypic properties are also present in skin, small intestine and uterus (Sojka et al., 2014). Uterine NK cells are characterized by a unique receptor repertoire that distinguishes them from cNK cells (Yadi et al., 2008) and execute highly specialized functions especially during early pregnancy where uterine NK cells release molecules that are involved in vascular modifications and decidual remodeling (Ashkar et al., 2000, Lash et al., 2006, Hanna et al., 2006).

Thymic NK cells develop in the thymus from double negative thymocytes (Vargas et al., 2011) and, in contrast to cNK cells, depend on the expression of CD127 and the transcription factor GATA-3 (Vosshenrich et al., 2006). Furthermore, they display reduced cytotoxicity, increased cytokine production and high expression of CD69 (Vosshenrich et al., 2006). Salivary glands also contain a phenotypically and functionally unique NK cell population. These develop independently of Nfil3, but express Eomes and T-bet (Cortez et al., 2014, Erick et al., 2016). In line with other trNK cell subsets, they display increased expression of CD69 (Cortez et al., 2014). NK cells from salivary glands of MCMV-infected mice show minimal IFN- γ production and degranulation upon re-stimulation, a defect that might contribute to the persistence of the virus in this organ (Tessmer et al., 2011, Erick et al., 2016). In addition, also when isolated from uninfected hosts, these cells display general hyporesponsiveness *ex vivo* (Tessmer et al., 2011).

Introduction

All of these examples show, that tissue-specific NK cell subsets can develop independently from cNK cells and harbor a distinct phenotype and functionality. However, how all these individual NK cell populations contribute to the immune response against viral pathogens for example, remains largely unclear.

1.5 Innate lymphoid cells (ILCs)

Besides NK cells, several other subsets of innate lymphoid cells have been described recently, namely ILC1, ILC2 and ILC3. In general, ILCs are tissue-resident (Gasteiger et al., 2015) and strong cytokine producers, representing the innate counterparts of T helper cell subsets (Spits et al., 2013). This tissue residency contrasts with NK cells which have been described as cytotoxic ILCs that circulate in the bloodstream (Vivier et al., 2018). Like NK cells, ILCs require the common cytokine receptor γ -chain and the transcription factor Id2 for their development, but unlike them, ILCs rely on GATA-3 and signaling via the interleukin-7 receptor subunit- α (also known as CD127) for maintenance and survival (Spits et al., 2013, Vosshenrich et al., 2006).

ILC2s are characterized by the ability to produce the type 2 cytokines IL-4, IL-5 and IL-13 (Vivier et al., 2018). They require the transcription factors GATA-3 (Hoyler et al., 2012) and ROR α (Wong et al., 2012) for development and are involved in the immune response against extracellular parasites (Fallon et al., 2006) as well as tissue homeostasis (Monticelli et al., 2011).

ILC3s are defined by their capacity to produce type 17 cytokines such as IL-22 and IL-17A (Cella et al., 2009, Takatori et al., 2009) and the requirement of the transcription factor ROR γ t (Sanos et al., 2009). They are abundant in mucosal tissues and involved in innate immune responses against extracellular bacteria (Satoh-Takayama et al., 2008, Zheng et al., 2008) as well as the containment of commensal bacteria in the intestine (Sonnenberg et al., 2012).

NK cells themselves belong to group 1 innate lymphoid cells, as do ILC1s. These cells are involved in the immune responses against intracellular pathogens and tumors (Klose et al., 2014, Abt et al., 2015, Weizman et al., 2017). ILC1s and NK cells share the capacity to produce IFN- γ in a T-bet-dependent manner as well as the expression of some phenotypic markers, such as NK1.1 and NKp46 (Vivier et al., 2018). However, they follow different developmental pathways (Klose et al., 2014). While ILC1 development strictly relies on the expression of T-bet, NK cells are present in T-bet deficient host. Instead, NK cells depend on the transcription factor Eomes which is dispensable for ILC1 development (Daussy et al., 2014). Furthermore,

Introduction

NK cells and ILC1s are functionally distinct. ILC1s produce higher amounts of TNF- α and GM-CSF than NK cells, but in contrast to them are not or only weakly cytotoxic (Vivier et al., 2018). Moreover, NK cells express MHC class I-specific inhibitory receptors, such as Ly49 receptors or NKG2A, as well as activating receptors, such as Ly49H and NKG2D, that allow direct recognition of infected or malignant cells (Diefenbach et al., 2014, Vivier et al., 2018). Phenotypic markers that have been suggested to distinguish ILC1s from NK cells are TRAIL, CD49a, CD127 and CD200R, while NK cells express CD49b (Vivier et al., 2018, Weizman et al., 2017). However, the expression of these markers can be lost upon activation and is often tissue-dependent which makes the phenotypic identification of ILC1s rather difficult. Therefore, the expression of the transcription factor Eomes is commonly used to distinguish NK cells from ILC1s (Vivier et al., 2018).



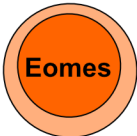


conventional NK cells	tissue-specific group 1 ILCs			
	liver, skin, intestine (ILC1)	uterus	thymus	salivary gland
 NKp46 ⁺ NK1.1 ⁺ CD49b ⁺ CD49a ⁻ CD11b ^{low/+} CD27 ^{+/-} CD16 ⁺ NKG2D ⁺ Ly49 ⁺	 NKp46 ⁺ NK1.1 ⁺ CD49b ⁻ CD49a ⁺ CD127 ⁺ TRAIL ⁺ CD69 ⁺ CD160 ⁺ CD200R ⁺	 NKp46 ⁺ NK1.1 ⁺ CD49b ⁻ CD49a ⁺ CD127 ⁻ TRAIL ⁺ CD16 ⁺ CD69 ⁺ Ly49 ⁺	 NKp46 ⁺ NK1.1 ⁺ CD49b ⁺ CD49a ⁻ CD127 ⁺ CD69 ⁺ Ly49 ^{low}	 NKp46 ⁺ NK1.1 ⁺ CD49b ⁺ CD49a ⁺ TRAIL ⁺ CD69 ⁺ CD103 ⁺ Ly49 ⁺
IFN- γ +++ TNFa + GM-CSF + Cytotoxicity +++	IFN- γ +++ TNFa +++ GM-CSF +++ Cytotoxicity +/-	IFN- γ +++ TNFa +++ Cytotoxicity +	IFN- γ +++ TNFa +++ GM-CSF +++ Cytotoxicity +	IFN- γ + Cytotoxicity +

Figure 3: Different subsets of group 1 innate lymphoid cells.

Phenotypic identity and functionality of conventional NK cells, ILC1s and tissue-resident NK cells from different organs.

Adapted from (Diefenbach et al., 2014, Hashemi and Malarkannan, 2020).

Introduction

The identification of the ILC1 lineage also complicated the definition of the aforementioned tissue-resident NK cell subsets, some of which express markers such as CD49a and CD127, show increased cytokine production and less cytotoxicity and develop independently from Eomes expression (Vosshenrich et al., 2006, Sojka et al., 2014). Therefore, some of them, especially liver trNK cells, are nowadays often referred to as ILC1s. In summary, together with distinct receptor expression and maturation states, the different subsets of trNK cells as well as ILC1s, all of which are distinct from cNK cells, contribute to the enormous diversity and complexity of group 1 innate lymphoid cells (**Figure 3**).

1.6 Adaptive-like responses of NK cells

Historically, NK cells, as a part of innate immunity, were thought to be short-lived cytolytic cells that recognize infected cells and tumor cells in an antigen-independent manner. In contrast, adaptive immune cells such as B and T lymphocytes, undergo antigen-specific expansion and persist as long-lived memory cells. However, recent evidence has shown that different subsets of NK cells are able to mount adaptive-like responses comprising clonal expansion, long-term maintenance and the formation of immunological memory which are hallmarks of adaptive immunity (Adams et al., 2020). These memory cells show increased functionality and host protection against previously encountered pathogens. Currently, three different models of NK cell memory have been described (O'Sullivan et al., 2015). The context in which these memory-like NK cells are generated as well as their functional and phenotypic characteristics will be summarized in the following.

1.6.1 Hapten-induced memory-like NK cells

NK cell memory has initially been described in a model of hapten-induced contact hypersensitivity (CHS) (O'Leary et al., 2006). Haptens are low-molecular non-immunogenic molecules that are able to bind and chemically modify proteins. These modified proteins are then recognized as foreign antigens and induce immune reactions including long-lived B and T cell memory. After prior sensitization, administration of the hapten to previously unexposed sites causes CHS resulting from a local recall response associated with tissue swelling. In the mentioned study, mice are immunized with 2,4-dinitrofluorobenzene (DNFB) and then re-challenged with the same hapten. Strikingly, this re-challenge induces robust and hapten-specific CHS, even in Rag2-deficient (*Rag2*^{-/-}) mice that lack B and T lymphocytes (O'Leary et al., 2006). It was shown that NK cells accumulate in hapten-challenged tissues and that

Introduction

depletion of NK cells in *Rag2^{-/-}* mice completely abrogates CHS induction (O'Leary et al., 2006, Paust et al., 2010). Furthermore, hapten-induced memory can be transferred to naïve recipients by adoptive transfer of hepatic but not splenic NK cells from sensitized donor mice (O'Leary et al., 2006, Paust et al., 2010). These hepatic memory cells require CXCR6 expression for long-term survival and full effector potential. Neutralizing antibodies against CXCR6 or its ligand CXCL16 abrogate NK-cell mediated recall responses to haptens (Paust et al., 2010). Further studies showed that these memory responses are mediated by a subset of hepatic NK cells that are liver-resident and do not express the marker DX5 ($\alpha 2\beta 1$ integrin, also known as CD49b) which is expressed by the majority of mature NK cells, but instead show surface expression of $\alpha 1\beta 1$ integrin (CD49a) (Peng et al., 2013a). Furthermore, liver-resident NK cells differ from conventional NK cells as they are Eomes⁻, but their development depends on T-bet and Hobit expression (Daussy et al., 2014, Sojka et al., 2014, Mackay et al., 2016). Memory formation of these hapten-induced NK cells is driven by type I interferons and Il-12 (Majewska-Szczepanik et al., 2013). In addition, CD49a⁺ liver-resident NK cells can also mount memory-like responses to viral antigens (Paust et al., 2010, Li et al., 2017). As mentioned before, these liver-resident NK cells are nowadays often considered as ILC1s (O'Sullivan et al., 2015).

More recently, it has been reported that conventional CD49b⁺ NK cells in the liver can also confer hapten-induced memory responses (van den Boorn et al., 2016). This study showed that monobenzene sensitization induces activation of the NLRP3 inflammasome in macrophages and that IL-18 derived from these macrophages is critical in the formation of NK cell memory (van den Boorn et al., 2016). There is also evidence for a CXCR6⁺ liver-resident NK cell subset in humans. These NK cells also display an immature phenotype (CD56^{bright} CD16⁻), expression of CD69 and a distinct transcription factor profile (Stegmann et al., 2016). In contrast to murine NK cells, the human CXCR6⁺ subset in the liver is T-bet^{low} Eomes^{high} while circulating human NK cells are T-bet^{high} Eomes^{low} (Stegmann et al., 2016).

However, many aspects of hapten-induced memory still have to be elucidated. To date the receptors responsible for hapten recognition remain unknown as well as the mode of recognition, i.e. whether NK cells recognize haptens directly or proteins that have been modified by these (O'Sullivan et al., 2015). Some early studies already provided evidence that only licensed Ly49C/I⁺ NK cells can confer hapten-induced memory (O'Leary et al., 2006, Majewska-Szczepanik et al., 2013). In line with that, a recent study has shown that hapten-induced CHS is impaired in Rag-deficient mice with severely reduced Ly49 receptor expression, but can be rescued by Ly49I knock-in (Wight et al., 2018). Moreover, antigens that bind to MHC class I, which is recognized by Ly49 receptors, can elicit memory-like NK cell

Introduction

responses similar to haptens (Wight et al., 2018). These findings suggest that inhibitory Ly49 receptors might be involved in hapten recognition by liver NK cells.

1.6.2 Cytokine-induced memory-like NK cells

In 2009, a study by Cooper et al. demonstrated that splenic NK cells which are adoptively transferred into *Rag1*^{-/-} recipients after *in vitro* stimulation with the cytokines IL-12, IL-15 and IL-18, generate cells with memory-like properties. In detail, when re-stimulated *ex vivo* with cytokines or plate-bound antibodies, these pre-activated NK cells show enhanced IFN- γ production compared to control NK cells (Cooper et al., 2009). This enhanced cytokine production can be detected for up to 3 weeks after adoptive transfer and is also passed on to daughter cells (Cooper et al., 2009). A more recent study showed that differences in IFN- γ production can be observed for up to 12 weeks after adoptive transfer and that they are NK-cell-intrinsic (Keppel et al., 2013). Of note, the cytotoxic capacity of cytokine-activated NK cells is similar to that of control NK cells (Cooper et al., 2009, Keppel et al., 2013). In addition, administration of cytokine-activated NK cells was shown to substantially reduce the growth of established tumors in irradiated mice (Ni et al., 2012). In that model, transferred cells are detectable for up to 3 months even after tumor rejection (Ni et al., 2012).

Similar to murine NK cells, human NK cells generate memory-like cells following stimulation with IL-12, IL-15 and IL-18 (Romee et al., 2012). These pre-activated NK cells display enhanced IFN- γ production for up to 6 weeks after *in vitro* culture and re-stimulation with cytokines or tumor targets (Romee et al., 2012). Moreover, cytokine-induced memory-like NK cells show enhanced functionality against leukemia cell lines as well as primary leukemic blasts *in vitro* and improved control of leukemia burden in a humanized mouse model (Romee et al., 2016). Thereby, cytokine-induced memory-like NK cells provide a promising tool for cancer immunotherapy which was already proven in preclinical studies against several types of cancer (Boieri et al., 2017, Zhuang et al., 2019, Uppendahl et al., 2019). In contrast to hapten-induced or virus-induced memory NK cells, cytokine-induced memory cells are not antigen-specific and are therefore broadly applicable.

1.6.3 Adaptive-like NK cell responses in cytomegalovirus infection

In the early 2000s, several studies demonstrated that the activating NK cell receptor Ly49H, which is expressed by approximately 50 % of all NK cells in C57BL/6 mice, binds exclusively to the MCMV-encoded glycoprotein m157 (Arase et al., 2002, Smith et al., 2002) (**Figure 4A**).

Introduction

m157 is a decoy receptor with homologies to MHC class I molecules (Adams et al., 2007) that was also reported to bind to inhibitory NK cell receptors in MCMV-susceptible mouse strains, e.g. Ly49I in 129/J (Arase et al., 2002). These findings suggest that m157 initially evolved as an inhibitor of NK cell immunity that prevents missing-self recognition of MCMV-infected cells despite downregulation of MHC class I expression (Lanier, 2008). The activating receptor Ly49H probably evolved more recently in C57BL/6 mice as a result of host-pathogen co-evolution conferring a selective advantage to that mouse strain (Lanier, 2008). This virus-specificity results in selective activation and expansion of Ly49H⁺ NK cells during the acute phase of MCMV infection (Dokun et al., 2001, Brown et al., 2001). Mice that lack Ly49H expression show increased susceptibility to MCMV infection (Lee et al., 2001, Fodil-Cornu et al., 2008, Cheng et al., 2008). Furthermore, MCMV titers are up to 1000-fold increased after antibody depletion of Ly49H expressing cells (Daniels et al., 2001). Similarly, infection with an m157-deficient MCMV variant leads to enhanced virulence of the virus and abrogates activation of Ly49H⁺ NK cells (Bubic et al., 2004). In summary, these studies demonstrate that Ly49H⁺ NK cells protect against MCMV infection due to their specificity to a viral antigen.

In 2009, a study by Sun et al. showed that adoptive transfer of Ly49H⁺ NK cells into mice that lack this receptor, leads to robust antigen-driven expansion of these cells after infection with MCMV (**Figure 4B+C**). After control of the infection, transferred cells contract and form a stable pool of long-lived antigen-experienced cells that can be recovered from several tissues for up to 70 days post infection (p.i.) (Sun et al., 2009). These long-lived cells display enhanced IFN- γ production as well as degranulation after re-stimulation *ex vivo* with plate-bound antibodies (Sun et al., 2009) (**Figure 4C**). Moreover, memory cells undergo secondary expansion after re-transfer into naïve recipients followed by recall infection with MCMV and were shown to be more protective than their unexperienced counterparts (Sun et al., 2009). Besides Ly49H receptor engagement, pro-inflammatory cytokine signaling via IL-12, IL-18 and type I interferons (Beaulieu et al., 2014) as well as co-stimulation via DNAM-1 (Nabekura et al., 2014) are necessary to induce optimal expansion and memory differentiation of Ly49H⁺ NK cells upon MCMV infection. Taken together, these studies demonstrate that Ly49H-expressing NK cells – similar to T cells – undergo selective expansion and contraction upon MCMV infection and generate a pool of long-lived self-renewing memory cells that are able to re-expand and provide enhanced protection upon re-infection. These features make MCMV a suitable model to probe NK cell responses *in vivo* and study infection-driven NK cell differentiation starting out from small cell populations or even single cells.

Introduction

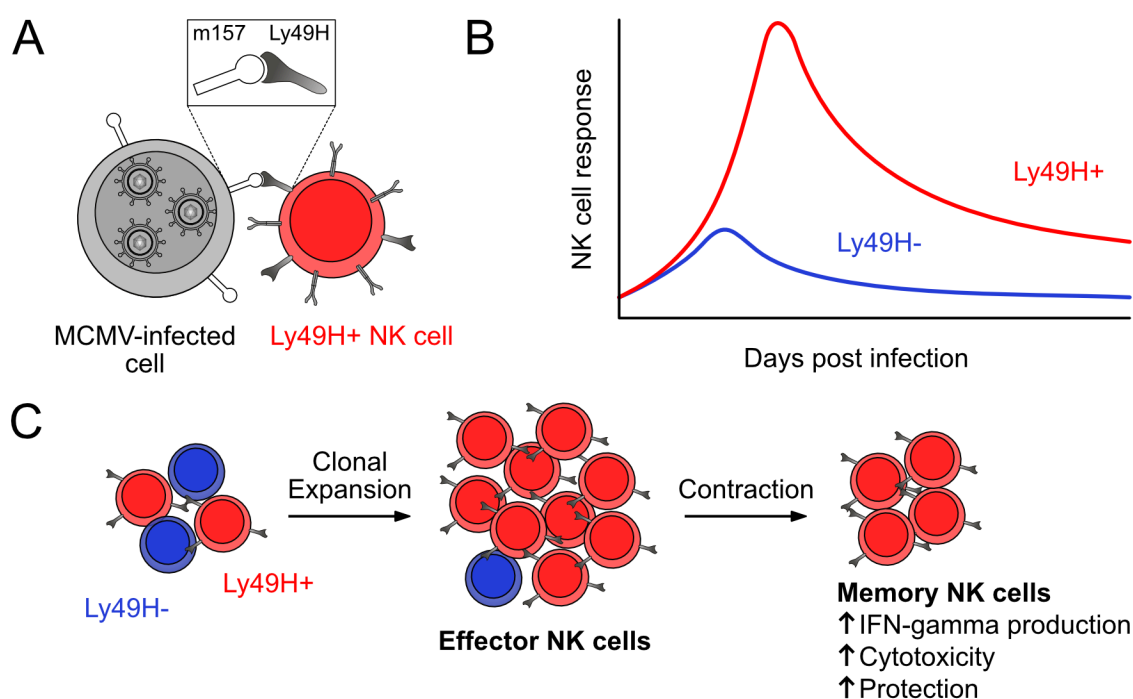


Figure 4: Adaptive-like responses of Ly49H⁺ NK cells upon MCMV infection.

(A) Engagement of the activating NK cell receptor Ly49H with MCMV-encoded glycoprotein m157 at the cell surface of infected cells. (B) Schematic depiction of the response kinetics of Ly49H⁺ (red) and Ly49H⁻ (blue) NK cells upon MCMV infection. (C) Clonal expansion and contraction of Ly49H⁺ NK cells result in the generation of functionally enhanced memory NK cells.

Memory NK cells display a distinct transcriptional and epigenetic signature in comparison to naïve NK cells, i.e. NK cells at steady state, before infection-driven activation and expansion. This signature at least in part overlaps with that of memory CD8⁺ T cells (Bezman et al., 2012, Lau et al., 2018). Furthermore, memory NK cells express KLRG1 and Ly6C (Sun et al., 2009) which is equivalent to a mature phenotype, and they show elevated surface levels of Ly49H in comparison to naïve NK cells (Adams et al., 2019). In line with this, initial Ly49H surface levels correlate positively with the expansion capacity of individual Ly49H⁺ NK cells (Grassmann et al., 2019). Consequently, NK cells can adapt to MCMV infection by selective expansion of Ly49H^{high} NK cell clones (Grassmann et al., 2019) with enhanced functional avidity towards m157-expressing targets (Adams et al., 2019). This avidity selection of NK cell clones represents another parallel to immune responses mediated by antigen-specific T cells. During infection, selective expansion of T cell clones expressing TCRs with optimal affinity to their cognate antigen skews the TCR repertoire towards high-affinity TCRs (Busch and Pamer, 1999). However, whereas the affinity selection of antigen-specific T cells is based on the expression of different TCRs, avidity selection of Ly49H⁺ NK cells relies on distinct expression levels of the same receptor. Moreover, in contrast to naïve T cells, distinct maturation states of NK cells already exist at steady state (Chiossone et al., 2009). Among these, immature KLRG1⁻

Introduction

NK cells were reported to expand better and preferentially generate memory cells upon MCMV infection (Kamimura and Lanier, 2015).

Similar to MCMV, human cytomegalovirus (HCMV) infection also induces adaptive-like responses of NK cells. Seropositive individuals display an increased frequency of NK cells expressing the receptor NKG2C (Guma et al., 2004, Lopez-Verges et al., 2011). NKG2C is an activating NK cell receptor that forms heterodimers with CD94 and binds to HLA-E (Braud et al., 1998). Indeed, it was shown that NKG2C⁺ NK cells undergo expansion *ex vivo* in response to HCMV-infected or HLA-E expressing targets (Guma et al., 2006, Rolle et al., 2014). HLA-E also binds to NKG2A (Braud et al., 1998), the inhibitory counterpart of NKG2C. HLA-E expression at the surface of HCMV-infected cells is stabilized by the HCMV-encoded peptide *UL40*, which reduces missing-self recognition by NK cells (Tomasec et al., 2000, Ulbrecht et al., 2000). A recent study has shown that the activation of NKG2C⁺ NK cells by different *UL40* peptides, derived from various HCMV strains, is highly variable and depends on the affinity between NKG2C and *UL40* peptides presented in the context of HLA-E, with highest-affinity interactions inducing strongest NK cell activation and proliferation (Hammer et al., 2018).

Importantly, memory-like NK cell responses have also been observed in the context of infection with other herpesviruses (Azzi et al., 2014, Abdul-Careem et al., 2012), human and simian immunodeficiency virus (Alter et al., 2009, Reeves et al., 2015), vaccinia (Gillard et al., 2011) or influenza virus (Dou et al., 2015).

1.7 Crosstalk between NK cells, dendritic cells and T cells upon MCMV infection

Several studies have shown that both NK cells and T cells critically contribute to the immune response against MCMV. Mice with selective NK cell deficiency display increased susceptibility to lethal MCMV infection and develop higher virus titers in several organs after infection with a sublethal dose of MCMV in comparison to NK cell-competent mice (Shellam et al., 1981). A protective NK cell response is especially important for the control of early viral replication. Furthermore, CD8⁺ T cells also significantly contribute to host protection against MCMV infection. They are essential to fight acute infection in mice that lack effective NK cell responses (Lathbury et al., 1996), but in addition are necessary to control long-term virus replication (French et al., 2004) and prevent reactivation of the virus from latency even in NK cell-competent mice (Simon et al., 2006).

Introduction

The activation of both NK and T cells is dependent on the crosstalk of these lymphocyte subsets with dendritic cells (DCs). MCMV is recognized early upon infection by innate immune cells via pattern recognition receptors. It has been shown that Toll-like receptor 9, that is mainly expressed by DCs, is critical for this early MCMV sensing (Krug et al., 2004). After pathogen recognition, DCs produce cytokines, such as type I interferons or IL-12, that mediate NK cell activation (Dalod et al., 2002). In particular, type I interferons are necessary to stimulate NK cell-mediated cytotoxicity while IL-12 increases IFN- γ production by NK cells (Orange and Biron, 1996). While type I interferons are mainly produced by plasmacytoid dendritic cells (pDCs) (Dalod et al., 2002), conventional type 1 dendritic cells (cDC1s), that are characterized by the expression of the chemokine receptor XCR1, are the major source of IL-12 (Weizman et al., 2019) and indispensable for effective NK cell activation as well as expansion of Ly49H⁺ NK cells upon MCMV infection (Andrews et al., 2003). On the other hand, effective antiviral NK cell activity is necessary to ensure maintenance of cDC1s in the spleen during MCMV infection (Andrews et al., 2003, Robbins et al., 2007) and to promote DC maturation (Gerosa et al., 2002, Alexandre et al., 2014). In line with this enhanced maintenance of cDC1s, the activation of NK cells via Ly49H-m157 interaction results in an increased frequency and activation status of epitope-specific CD8⁺ T cells early during MCMV infection (Robbins et al., 2007) (**Figure 5, left panel**). In contrast, infection with an m157-deficient MCMV variant that is unable to activate NK cells via Ly49H, induces enhanced CD8⁺ T cell responses at later timepoints resulting from an increased viral load and higher levels of innate cytokines in these mice (Mitrovic et al., 2012) (**Figure 5, right panel**).

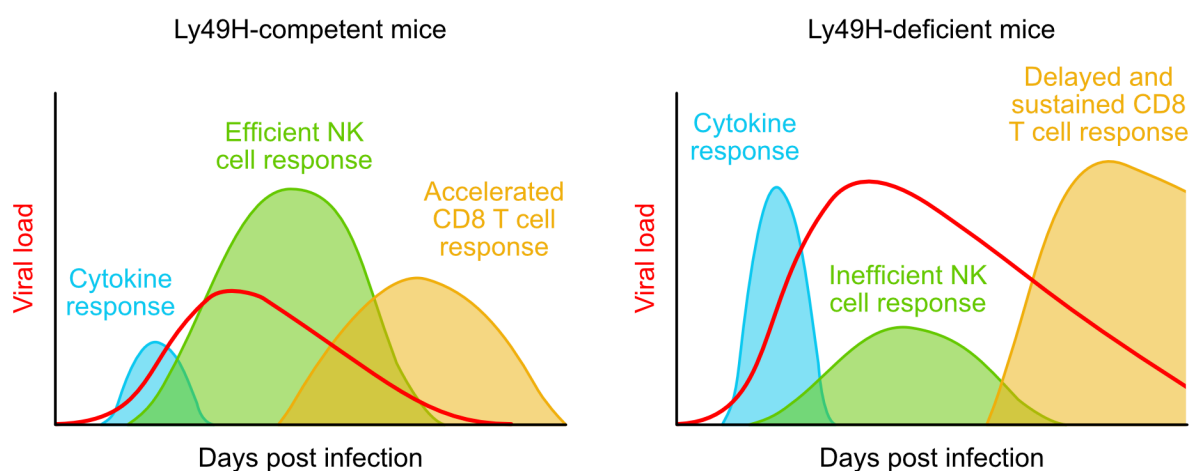


Figure 5: Efficient NK cell activation is critical to ensure early control of viral replication and rapid CD8⁺ T cell responses during MCMV infection.

Schematic depiction of viral load as well as the kinetics of innate and adaptive immune responses against MCMV in Ly49H-competent (left) and Ly49H-deficient (right) mice. Adapted from (Alexandre et al., 2014).

Introduction

cDC1s are specialized to take up extracellular antigens by internalization of apoptotic cells, process these antigens and present them in the context of MHC class I in a process called cross-presentation (den Haan et al., 2000, Schulz and Reis e Sousa, 2002, Iyoda et al., 2002). In contrast to that, classical antigen presentation to CD8⁺ T cells relies on directly infected dendritic cells. Several MCMV encoded proteins induce downregulation of cell-surface MHC class I molecules in infected cells (Campbell and Slater, 1994, Ziegler et al., 1997, Reusch et al., 1999) and thereby reduce the capacity of directly infected cells to present antigens to CD8⁺ T cells (Andrews et al., 2001). In line with that, several studies demonstrated that cross-presentation mediated by cDC1s is both necessary and sufficient to efficiently prime CD8⁺ T cells *in vivo* upon MCMV infection (Snyder et al., 2010, Busche et al., 2013, Torti et al., 2011). In summary, the crosstalk between NK cells, dendritic cells and T cells is essential to efficiently control viral replication and rapidly induce effective early T cell responses during MCMV infection (**Figure 5**). In this context, it has been proposed that Ly49H⁺ NK cells mainly affect cDC1s indirectly, through enhanced viral control and the resulting reduction of type I interferon production by pDCs, which otherwise has deleterious effects on cDC1 survival (Robbins et al., 2007). Enhanced cDC1 survival is then thought to promote improved cross-presentation to and early expansion of antigen-specific CD8⁺ T cells. However, whether a direct interaction of Ly49H⁺ NK cells and cDC1s also plays a role in this innate/adaptive crosstalk has not been explored. Moreover, it remains unclear, whether all Ly49H⁺ NK cell or only a specialized subset are engaged in this crosstalk.

1.8 Single-cell fate mapping of immune cells

Lymphocyte populations that respond to a given pathogen, show substantial phenotypic and functional diversity. Upon infection, antigen-specific lymphocytes are selectively expanded and differentiate into various effector and memory subsets. Especially for T cells, a great number of phenotypically and functionally distinct subsets have been described (Buchholz et al., 2012, Kallies et al., 2020). As argued before, NK cells also represent a phenotypically and functionally diverse population of immune cells – already at steady state (see 1.3). However, the developmental relationship of these different NK cell subsets and their functionality, especially during the immune response to different pathogens, is still under investigation. Furthermore, it is unclear how individual NK cells responding to a certain pathogen contribute to the overall heterogeneity of the response. Previous studies from our laboratory utilized adoptive single-cell transfer to demonstrate that the output generated from individual T cell clones is highly diverse concerning size of the progeny as well as subset composition and

Introduction

memory capacity (Buchholz et al., 2013, Cho et al., 2017, Grassmann et al., 2020). In general, there exist two concepts of immune cell differentiation: In the first scenario, individual clones undergo phenotypic diversification upon differentiation and give rise to a phenotypically and functionally diverse offspring (“one cell, multiple fates”); the second hypothesis assumes that individual clones adopt distinct fates (“one cell, one fate”) and that the observed overall heterogeneity of the immune response results from a combination of multiple individual clones (Buchholz et al., 2016) (**Figure 6**). Whereas the first concept holds true for T cell differentiation, this has so far not been studied in detail for NK cells.

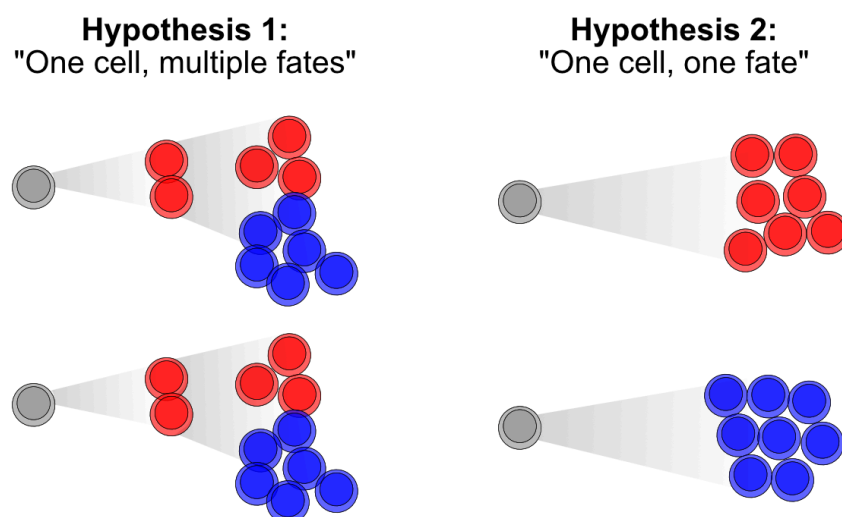


Figure 6: Two concepts of immune cell differentiation on single-cell level.

Phenotypic heterogeneity of immune responses might result from phenotypic diversification during differentiation (left) or combining multiple individual clones with distinct fates (right). Adapted from (Flommersfeld et al., 2021).

Recently, we demonstrated that single Ly49H⁺ NK cells indeed upon adoptive transfer into MCMV-infected mice, also generate offspring that massively varies in size ranging from 10 to 10.000 cells per clone (Grassmann et al., 2019). However, it is still unclear whether these individual NK cell clones also differ in the expression of phenotypic markers and in their functionality, aspects that will be subject of this study. Different approaches that allow adoptive transfer and fate mapping of single cells, their virtues and limitations are described in the following.

1.8.1 Cellular barcoding

In 2008, Schepers et al. adapted an approach called cellular barcoding to enable the analysis of lineage relationships originating from single T cells *in vivo*. Therefore, cells are transduced with a retroviral plasmid library containing GFP and a random 98-bp DNA barcode (Schepers et al.,

Introduction

2008). These unique identifiers are passed on to all daughter cells and can be recovered via microarray (Schepers et al., 2008, Gerlach et al., 2010) or next generation sequencing (Gerlach et al., 2013) after activation and expansion of the individual clones. By comparing the barcode composition within different organs or immune cell subsets, conclusions can be drawn concerning the lineage relationships of distinct “T cell families” (Schepers et al., 2008, Gerlach et al., 2010, Gerlach et al., 2013). The term “T cell family” was introduced to define a population of T cells that derives from the same single cell, while “clone” is used for all T cells harboring the same TCR and can therefore be misleading in this context (Buchholz and Flossdorf, 2018).

Polylox barcoding represents another approach that uses unique genetic labels to track the fate of hematopoietic stem cells *in vivo* (Pei et al., 2017). The *Polylox* cassette is a DNA element that is composed of several *loxP*-flanked segments. These *loxP* sites are targeted by the Cre recombinase resulting in more than one million unique recombination products (Pei et al., 2017). For *in vivo* fate mapping, the *Polylox* cassette is targeted into the *Rosa26* locus and then crossed into mice that express Cre recombinase under the control of a tamoxifen-inducible promoter (Pei et al., 2017). Consequently, recombination of the *Polylox* cassette can be induced by the administration of tamoxifen and allows endogenous labeling of hematopoietic stem cells. The barcode composition of different cell populations can then be determined by PCR amplification and sequencing (Pei et al., 2017).

The advantage of these cellular barcoding approaches is the enormous number of clones that can be analyzed simultaneously. However, since detection of the barcode labels requires techniques such as microarray or sequencing, phenotyping of the expanded clones via antibody staining or isolation of immune cells from distinct precursors for re-transfer or functional analyses are difficult. Furthermore, the *Polylox* system is limited by the fact that some of the generated codes are highly redundant (Pei et al., 2017). Consequently, the approach is not suitable to study lineage relationships based on immune responses of only 100-1000 epitope-specific T cells as the number of uniquely labelled T cells is too low in this setup.

1.8.2 Congenic matrix

Another option to track the offspring of individual immune cells *in vivo* is the use of congenic markers. Congenic mice are basically identical to wildtype C57BL/6 mice except that they have differing alleles at one specific gene locus. The most common congenic mouse strain carries a functionally identical variant of the pan-leukocyte marker CD45, called CD45.1, while

Introduction

wildtype C57BL/6 mice express CD45.2 (Shen et al., 1985). The advantage of these congenic markers is that they are expressed at the cell surface and can be labelled with monoclonal antibodies. This enables the simultaneous identification of single-cell-derived lymphocyte families as well as their direct phenotypic or functional analysis via flow cytometry (Stemberger et al., 2007). Additionally, offspring belonging to distinct single-cell-derived families can be isolated by fluorescence activated cell sorting (FACS) and re-transferred to secondary hosts (Graef et al., 2014) or subjected to further analyses such as RNA sequencing (Grassmann et al., 2020). However, one single congenic marker only allows adoptive transfer of a maximum of two single cells per recipient (CD45.1/1 and CD45.1/2). Therefore, the so-called congenic matrix was developed that combines differential expression of two congenic markers (CD45.1 and CD90.1) and consequently allows adoptive transfer of up to 8 single cells that are distinguishable from each other and the recipient via flow cytometry (Buchholz et al., 2013) (Figure 7).

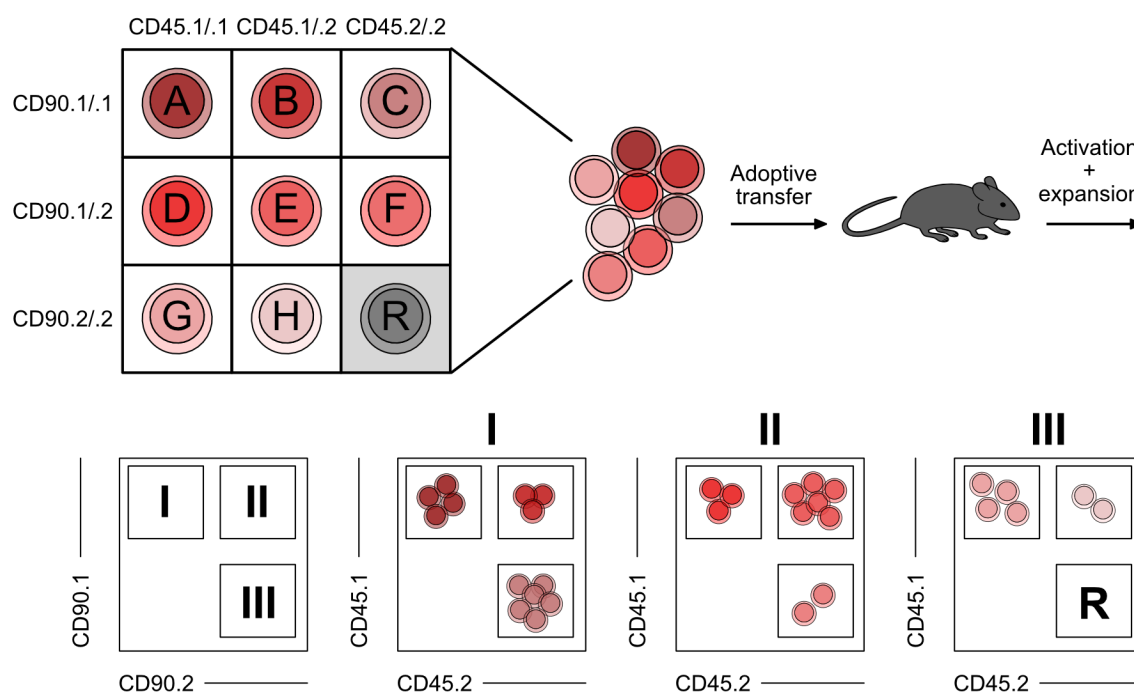


Figure 7: The congenic matrix as a tool for single-cell fate mapping of immune cells.

Schematic depiction of the composition of the congenic matrix and the identification of the different components via flow cytometry.

However, the number of single cells that can be tracked within one and the same recipient is still limited which makes the approach inefficient for experimental systems with a very low recovery rate. This recovery rate describes the amount of successfully recovered clones at the timepoint of analysis relative to the number of initially transferred single cells. For example, detectable offspring was recovered from only 3,1 % of all transferred single Ly49H⁺ NK cells

Introduction

upon MCMV infection (Grassmann et al., 2019). Furthermore, the majority of NK cells does not stably express CD90 which makes the congenic matrix inefficient for multiplexed tracking of this immune cell type (Grassmann et al., 2019).

1.8.3 Retroviral fluorescent barcoding

To circumvent the limitations of the aforementioned models, an approach called retrogenic fluorescent barcoding was developed in our laboratory that enables simultaneous tracking of a larger number of single cells as well as visualization of their unique labels via flow cytometry (Grassmann et al., 2019). Therefore, hematopoietic stem cells are isolated and retrovirally transduced with the five fluorescent proteins GFP, YFP, Ametrine (or T-Sapphire), CFP and BFP in a combinatorial manner. These transduced stem cells are then transplanted into irradiated recipients and give rise to color-barcode immune cells expressing diverse combinations of the used fluorochromes (**Figure 8**).

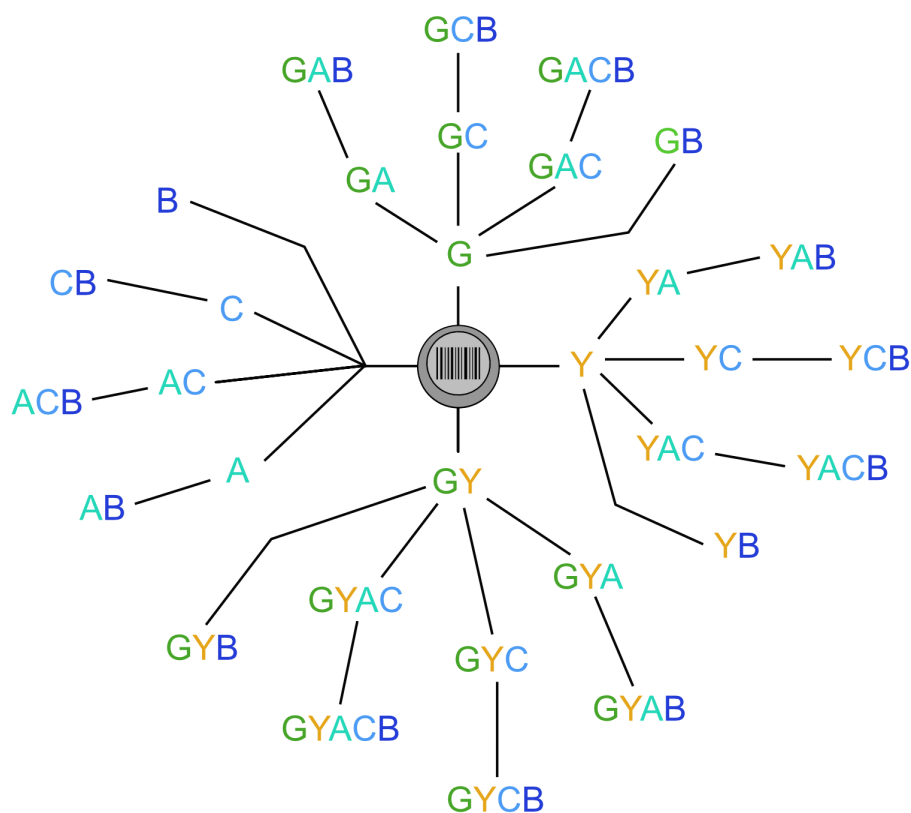


Figure 8: Retroviral fluorescent barcoding.

Fluorescent labels generated by retroviral transduction of hematopoietic stem cells with the five fluorescent proteins GFP (G), YFP (Y), Ametrine (A), CFP (C) and BFP (B). The combination of these five distinct fluorochromes allows to generate >30 unique color barcodes which can be used to track the offspring of individual immune cells *in vivo*.

Adapted from (Kretschmer et al., 2021).

Introduction

Single cells harboring unique color barcodes are then sorted from these retrogenic donors and adoptively transferred. As color barcodes are passed on to all daughter cells, they allow tracking of up to 30 individual cells and their progeny *in vivo* within one and the same recipient. Furthermore, color barcodes are distinguishable by flow cytometry and thereby enable phenotypic and functional analyses of the expanded clones.

2 Aim of this thesis

NK cells represent a first line of defense against viral infections and cancer. They recognize infected and malignant cells with high specificity by integrating various signals from activating and inhibitory receptors. As a special case, the only known ligand of the activating receptor Ly49H is the MCMV-encoded glycoprotein m157 (Arase et al., 2002, Smith et al., 2002). Thereby, Ly49H⁺ NK cells possess a defined antigen-specificity and are preferentially activated upon MCMV infection (Dokun et al., 2001). They undergo clonal expansion (Grassmann et al., 2019) and persist for extended periods of time after resolution of acute infection, both of which are hallmarks of adaptive immunity (Sun et al., 2009). This adaptive-like behavior of Ly49H⁺ NK cells allows for the study of their response to a viral pathogen *in vivo*. In this study, we aimed to use retroviral fluorescent barcoding and single-cell fate mapping to study the infection-driven differentiation of NK cells starting out from single Ly49H⁺ NK cells. Thereby, we wanted to investigate whether all NK cells differentiate along a common pathway or whether different subsets of NK cells exist that show distinct response patterns. It is already known that CD8⁺ T cells, for example, develop within a common differentiation framework but individual T cells generate highly variable output (Buchholz et al., 2013). For NK cells, it is much less understood, how the overall immune response is composed of individual responses. On the other hand, naïve NK cells already consist of many different subpopulations with distinct homing patterns, phenotype and functionality. Therefore, it is important to understand how individual subsets contribute to the immune response. Moreover, it was reported that NK cells can contribute to the immune response against MCMV in different ways: they control early viral replication, recognize and kill infected cells, produce cytokines and are involved in the crosstalk with other immune cell types such as DCs and T cells. Whether these distinct functions are mediated by all NK cells or specialized subsets, is so far not understood. To decipher the heterogeneity of NK cells responding to MCMV infection, we aimed to transfer populations and single cells into MCMV-susceptible recipients, infect the mice and then analyze the offspring of these cells at the peak of the immune response by flow cytometry. Our goal was to examine which subsets of Ly49H⁺ NK cells respond to MCMV or are generated during the immune response and to identify their molecular signatures as well as their specific functional contribution.

3 Material and Methods

3.1 Material

3.1.1 Devices

Device	Model	Supplier
10x Instrument	Chromium Controller	10x Genomics, Pleasanton, USA
Balance	EG 2200-2NM	Kern & Sohn GmbH, Balingen, Germany
	ACJ 320-4M	Kern & Sohn GmbH, Balingen, Germany
Centrifuge	Biofuge fresco	Heraeus, Hanau, Germany
	Pico 17	Heraeus, Hanau, Germany
	Multifuge 3 S-R	Heraeus, Hanau, Germany
	Multifuge X3R	Heraeus, Hanau, Germany
	Mega Star 3.OR	VWR, Darmstadt, Germany
Counting chamber	Neubauer improved	Paul Marienfeld & Co. KG, Lauda-Königshofen, Germany
Dounce tissue grinder		Sigma-Aldrich, Taufkirchen, Germany
Flow cytometer/ cell sorter	CytoFLEX LX	Beckman Coulter, Fullerton, USA
	CytoFLEX S	Beckman Coulter, Fullerton, USA
	FACS Aria II	Becton Dickinson, Heidelberg, Germany
	MoFlo Astrios	Beckman Coulter, Fullerton, USA
Incubator	HERAcell 240	Heraeus, Hanau, Germany
Laminar flow hood	HERAsafe	Heraeus, Hanau, Germany
Microscope	Primovert	Carl Zeiss, Jena, Germany
	TCS SP8	Leica, Wetzlar, Germany
pH-meter	766	Knick, Berlin, Germany
Sequencer	HiSeq2500	Illumina, San Diego, USA
	HiSeq4000	Illumina, San Diego, USA
	NovaSeq6000	Illumina, San Diego, USA
Water bath		GFL, Burgwedel, Germany

Material and Methods

3.1.2 Chemicals and reagents

Reagent	Supplier
Ammonium chloride (NH ₄ Cl)	Carl Roth, Karlsruhe, Germany
Bovine serum albumin (BSA)	Sigma-Aldrich, Taufkirchen, Germany
Calcium chloride (CaCl ₂)	Merck, Darmstadt, Germany
Cytofix/Cytoperm™ Kit	Becton Dickinson, Heidelberg, Germany
Dimethyl sulfoxide (DMSO)	Sigma-Aldrich, Taufkirchen, Germany
Disodium phosphate (Na ₂ HPO ₄)	Carl Roth, Karlsruhe, Germany
Dulbecco's Modified Eagle Medium (DMEM)	Life Technologies, Carlsbad, USA
2X DMEM	Sigma-Aldrich, Taufkirchen, Germany
Ethanol	Klinikum rechts der Isar, München, Germany
Ethidium monoazide bromide (EMA)	Thermo Fischer, Darmstadt, Germany
Ethylenediaminetetraacetic acid (EDTA)	Carl Roth, Karlsruhe, Germany
Fetal calf serum (FCS)	Sigma-Aldrich, Taufkirchen, Germany
Gentamycin	Life Technologies, Carlsbad, USA
L-Glutamine	Sigma-Aldrich, Taufkirchen, Germany
Golgi Plug™	Becton Dickinson, Heidelberg, Germany
Heparin-sodium (5000 IU/mL)	Ratiopharm, Ulm, Germany
HEPES	Carl Roth, Karlsruhe, Germany
Ionomycin	Sigma-Aldrich, Taufkirchen, Germany
Recombinant murine IL-3	PeptoTech, Hamburg, Germany
Recombinant murine IL-6	PeptoTech, Hamburg, Germany
β-Mercaptoethanol	Life Technologies, Carlsbad, USA
Methylcellulose	Sigma-Aldrich, Taufkirchen, Germany
Paraformaldehyde (PFA)	Sigma-Aldrich, Taufkirchen, Germany
Phorbol-12-myristat-13-acetat	Sigma-Aldrich, Taufkirchen, Germany

Material and Methods

Reagent	Supplier
Phosphate buffered saline (PBS)	Carl Roth, Karlsruhe, Germany
PBS solution	Life Technologies, Carlsbad, USA
Penicillin	Life Technologies, Carlsbad, USA
Percoll	Sigma-Aldrich, Taufkirchen, Germany
Potassium chloride (KCl)	Carl Roth, Karlsruhe, Germany
Propidium iodide (PI)	Thermo Fischer, Darmstadt, Germany
RPMI 1640	Life Technologies, Carlsbad, USA
Recombinant murine SCF	PeproTech, Hamburg, Germany
Skim milk powder	Sigma-Aldrich, Taufkirchen, Germany
Sodium chloride (NaCl)	Carl Roth, Karlsruhe, Germany
Streptomycin	Life Technologies, Carlsbad, USA
eBioscience™ Foxp3 Transcription Factor Staining Buffer Set	Thermo Fischer, Darmstadt, Germany
True-Nuclear™ Transcription Factor Buffer Set	BioLegend, San Diego, USA
Tris-Hydrochloride (Tris-HCl)	Carl Roth, Karlsruhe, Germany
Trypan Blue solution	Carl Roth, Karlsruhe, Germany
Trypsin-EDTA	Life Technologies, Carlsbad, USA

3.1.3 Antibodies

All antibodies have been titrated to the optimal dilutions.

Antibody	Supplier	Identifier
Anti-mouse NK1.1	BioLegend, San Diego, USA	PK136
Anti-mouse NK1.1	Thermo Fisher, Darmstadt, Germany	PK136
Anti-mouse Ly49H	Thermo Fisher, Darmstadt, Germany	3D10
Anti-mouse CD45.1	BioLegend, San Diego, USA	A20

Material and Methods

Antibody	Supplier	Identifier
Anti-mouse CD45.2	BioLegend, San Diego, USA	104
Anti-mouse CD27	BioLegend, San Diego, USA	LG.3A10
Anti-mouse CD27	Thermo Fisher, Darmstadt, Germany	LG7.F9
Anti-mouse CD62L	BioLegend, San Diego, USA	MEL-14
Anti-mouse CD62L	Becton Dickinson, Heidelberg, Germany	MEL-14
Anti-mouse CD160	BioLegend, San Diego, USA	7H1
Anti-mouse CD160	R&D Systems, Minneapolis, USA	Cat# AF3899
Anti-mouse CD11b	Becton Dickinson, Heidelberg, Germany	M1/70
Anti-mouse CD11b	BioLegend, San Diego, USA	M1/70
Anti-mouse KLRG1	Thermo Fisher, Darmstadt, Germany	2F1
Anti-human Granzyme B (crossreactive)	Thermo Fisher, Darmstadt, Germany	GB11
Anti-mouse CD3e	Becton Dickinson, Heidelberg, Germany	145-2C11
Anti-mouse CD3e	BioLegend, San Diego, USA	145-2C11
Anti-mouse TCR beta	Becton Dickinson, Heidelberg, Germany	H57-597
Anti-mouse CD4	Thermo Fisher, Darmstadt, Germany	RM4-5
Anti-mouse CD8a	BioLegend, San Diego, USA	53-6.7
Anti-mouse CD19	Becton Dickinson, Heidelberg, Germany	1D3
Anti-mouse Sca-1	BioLegend, San Diego, USA	D7
Anti-mouse CD16/32	BioLegend, San Diego, USA	93
Anti-mouse CD49a	BioLegend, San Diego, USA	HMa1
Anti-mouse CD49b	BioLegend, San Diego, USA	DX5
Anti-mouse Ly-6C	Becton Dickinson, Heidelberg, Germany	AL-21
Anti-mouse CD69	BioLegend, San Diego, USA	H1.2F3
Anti-mouse CD127	BioLegend, San Diego, USA	A7R34
Anti-mouse Ly49A	Thermo Fisher, Darmstadt, Germany	A1(Ly49A)
Anti-mouse Ly49I	Thermo Fisher, Darmstadt, Germany	YLI-90

Material and Methods

Antibody	Supplier	Identifier
Anti-mouse Ly49F	Miltenyi Biotec, Bergisch Gladbach, Germany	HBF-719
Anti-mouse Ly49G2	Miltenyi Biotec, Bergisch Gladbach, Germany	4D11
Anti-mouse Ly49D	Thermo Fisher, Darmstadt, Germany	eBio4E5
Anti-mouse IFN-gamma	Thermo Fisher, Darmstadt, Germany	XMG1.2
Anti-mouse TNF-alpha	BioLegend, San Diego, USA	MP6-XT22
Anti-mouse GM-CSF	BioLegend, San Diego, USA	MP1-22E9
Anti-mouse XCR1	BioLegend, San Diego, USA	ZET
Anti-mouse CD200r	Thermo Fisher, Darmstadt, Germany	0X110
Anti-sheep IgG	Jackson Immuno Research, Cambridge, UK	RRID: AB_2340747
Donkey anti-rabbit IgG	BioLegend, San Diego, USA	RRID: AB_1575130
Donkey anti-rabbit IgG	BioLegend, San Diego, USA	RRID: AB_2563306
Anti-GFP	Thermo Fisher, Darmstadt, Germany	RRID: AB_221477
Anti-Collagen IV	Abcam, Cambridge, UK	Cat# ab6586
TotalSeq™-B0301 anti-mouse Hashtag 1	BioLegend, San Diego, USA	M1/42; 30-F11
TotalSeq™-B0302 anti-mouse Hashtag 2	BioLegend, San Diego, USA	M1/42; 30-F11
TotalSeq™-B0304 anti-mouse Hashtag 4	BioLegend, San Diego, USA	M1/42; 30-F11
TotalSeq™-B0305 anti-mouse Hashtag 5	BioLegend, San Diego, USA	M1/42; 30-F11
TotalSeq™-B0306 anti-mouse Hashtag 6	BioLegend, San Diego, USA	M1/42; 30-F11
TotalSeq™-B0307 anti-mouse Hashtag 7	BioLegend, San Diego, USA	M1/42; 30-F11

Material and Methods

3.1.4 Buffers and media

Buffer	Composition
Ammonium chloride-Tris (ACT)	90 % (v/v) 0.17 M NH ₄ Cl 10 % (v/v) 0.17 M Tris HCl, pH 7.2
FACS Buffer, pH 7.5	1x PBS 0.5 % (w/v) BSA 2 mM EDTA
Complete DMEM (cDMEM)	1x DMEM 10 % (v/v) FCS 0.12 % (w/v) HEPES 0.02 % (w/v) L-Glutamine 1 % (v/v) Penicillin/Streptomycin 0.1 % (v/v) Gentamycin 0.1 % (v/v) β-Mercaptoethanol
Complete RPMI (cRPMI)	1x RPMI 1640 10 % (v/v) FCS 0.12 % (w/v) HEPES 0.02 % (w/v) L-Glutamine 1 % (v/v) Penicillin/Streptomycin 0.1 % (v/v) Gentamycin 0.1 % (v/v) β-Mercaptoethanol
Freezing Medium	FCS 10 % (v/v) DMSO
Transfection Buffer, pH 6.76	ddH ₂ O 1.6 % (w/v) NaCl 0.074 % (w/v) KCl 0.05 % (w/v) Na ₂ HPO ₄ 1 % (w/v) HEPES

Material and Methods

3.1.5 Cell lines

Cell line	Organism	Origin
Ba/F3	Mouse	UCSF, San Francisco, USA
Ba/F3-m157	Mouse	UCSF, San Francisco, USA
M2-10B4	Mouse	ATCC, Manassas, USA
Platinum-E (Plat-E)	Human	Cell Biolabs, San Diego USA
RD114	Human	ATCC, Manassas, USA
RMA	Mouse	MSKCC, New York, USA
RMA-S	Mouse	MSKCC, New York, USA

3.1.6 Plasmids and recombinant DNA

Plasmid/recombinant DNA	Origin
pMP71	Wolfgang Uckert, MDC Berlin, Germany
EGFP	MIH, TU Munich, Germany
EYFP	MIH, TU Munich, Germany
CFP	MIH, TU Munich, Germany
Ametrine	MIH, TU Munich, Germany
EBFP2	MIH, TU Munich, Germany

3.1.7 Oligonucleotides

Oligonucleotide	Sequence	Supplier
GFP family Not1 fwd	5'ATTAGCGGCCGCGCCACCAT GGTGAGCAAGGGCG 3'	Sigma-Aldrich, Taufkirchen, Germany
GFP family EcoR1 rev	5' TAATGAATTCTTACTTGTAC AGCTCG 3'	Sigma-Aldrich, Taufkirchen, Germany

Material and Methods

3.1.8 Mice

Mouse strain	Official name	Origin
C57BL/6	C57BL/6J OlaHsd	Envigo, Indianapolis, USA
BALB/c	BALB/c OlaHsd	Envigo, Indianapolis, USA
OT-1	C57BL/6- Tg(TcraTcrb)1100Mjb/J	The Jackson Laboratory, Bar Harbor, USA
CD45.1	B6.SJL-Ptprca Pepcb/BoyJ	The Jackson Laboratory, Bar Harbor, USA
<i>Rag2^{-/-} Il2rg^{-/-}</i>	C;129S4-Rag2tm1.1Flv Il2rgtm1.1Flv/J	The Jackson Laboratory, Bar Harbor, USA
<i>Klra8^{-/-}</i>	B6.BXD8-Klra8Cmv1- del/WumJ	The Jackson Laboratory, Bar Harbor, USA
<i>Nkp46^{iCre}</i>	B6.Cg-Ncr1 tm1.1(icre)Viv	Eric Vivier, Centre d'Immunologie de Marseille-Luminy, Marseille, France
<i>R26-LSL-iDTA</i>	Gt(ROSA)26Sortm1(DTA)J pmb/J	The Jackson Laboratory, Bar Harbor, USA
<i>Xcr1^{Venus DTR}</i>	B6.Cg-Xcr1tm2 (HBEGF/Venus)Ksho	The Jackson Laboratory, Bar Harbor, USA
<i>Batf3^{-/-}</i>	B6.129S(C)-Batf3 ^{tm1Kmm} /J	Jan Böttcher, IMI, TU Munich, Germany
<i>Eomes^{GFP}</i>	Eomes<tm2.1Rob>	Yakup Tanriver, UK Freiburg, Freiburg, Germany
<i>Eomes^{flox/flox}</i>	Eomes<tm1Srn>	Joseph Sun, MSKCC, New York, USA

C57BL/6 (females, 6-12 weeks) and BALB/c (males, 3 weeks) were purchased from Envigo. TCR transgenic OT-1, CD45.1, *Rag2^{-/-} Il2rg^{-/-}*, *Klra8^{-/-}*, *Nkp46^{iCre}*, *R26-LSL-iDTA*, *Batf3^{-/-}* and *Xcr1^{Venus DTR}* mice were bred and maintained under specific pathogen-free (SPF) conditions at the mouse facility at the Technical University of Munich. *Eomes^{GFP}* mice were bred under SPF conditions at the mouse facility at the University of Freiburg, *Nkp46^{iCre} x Eomes^{flox/flox}* mice were maintained under SPF conditions at the Memorial Sloan Kettering Cancer Center (New York, USA). All animal experiments were approved by local authorities and performed in accordance with national guidelines.

Material and Methods

3.1.9 Viruses

MCMV-wildtype (wt) was prepared from the BAC-derived mouse cytomegalovirus clone pSM3fr 3.3 (Smith strain). The MCMV-*ie2*-SIINFEKL was generated by fusing the SIINFEKL epitope at the C-terminus of the *ie2* sequence using *en passant* mutagenesis as described before (Dekhtiarenko et al., 2016). For the MCMV-*ie2*-SIINFEKL-GFP, P2A-linked GFP was inserted before the second exon of *ie1/ie3* (Chaudhry et al., 2020). Viruses were kindly provided by Luka Cicin-Sain (Helmholtz Centre for Infection Research, Braunschweig).

3.1.10 Software

Software	Supplier
FlowJo V10	FlowJo LLC, Ashland, USA
Prism 9	Graphpad, La Jolla, USA
Imaris 9.5	Bitplane, Zürich, Switzerland
SCANPY (v 1.4.4)	Theis lab (GitHub) (Wolf et al., 2018)
Velocity (v 0.17.17)	Velocity-team (Github) (La Manno et al., 2018)
Cellranger (v 5.0.1)	10x Genomics, Pleasanton, USA
Affinity Designer (v1.10.1)	Serif Europe Ltd., Nottingham, Great Britain
Microsoft Office (v16.16.27)	Microsoft, Redmond, USA

3.2 Methods

3.2.1 Tissue culture

M2-10B4, Plat-E, RD114, Ba/F3 and Ba/F3-m157 cells were grown in cDMEM in tissue-culture treated cell culture flasks. RMA and RMA-S cells were grown in cRPMI in tissue-culture treated cell culture flasks. Cell lines were incubated at 37 °C and 5 % CO₂ in humidified atmosphere and were splitted every 2-4 days depending on their confluence. M2-10B4, Plat-E and RD114 were treated with Trypsin-EDTA (5 min, 37 °C) to detach from the bottom of the flask prior to splitting.

Material and Methods

3.2.2 Generation of retroviral fluorescent barcodes

3.2.2.1 Transfection of virus-producing cell lines

Retroviral packaging cell lines were transfected via calcium phosphate precipitation with the retroviral vectors encoding for the five fluorescent proteins GFP, YFP, CFP, BFP and Ametrine. Therefore, Plat-E (ecotropic) and RD114 cells (amphotropic), respectively, were seeded in 6-well plates and grown until they reached 70 % confluence. 15 μ l of a 3,3 M CaCl₂ solution were mixed with 18 μ g of the retroviral plasmid dissolved in 135 μ l ddH₂O. For calcium-phosphate precipitation, the mixture was added dropwise to an equal volume of transfection buffer under vortexing. The precipitate was incubated for 15-20 minutes at room temperature (vortex after 10 minutes) and then carefully distributed onto the cells. After 6 hours, the medium was removed from the cells and fresh DMEM was added. After 48 h, viral supernatants were collected, purified from remaining cells by centrifugation (1500 rpm, 4 °C, 7 min) and stored at 4 °C for up to 4 weeks.

3.2.2.2 Generation of stably transduced Plat-E cell lines

Plat-E cell lines with a stable genomic integration of the retroviral plasmid DNA were generated by spinoculation. Therefore, 400 μ l of the respective RD114 supernatant was added per well of a tissue-culture treated 48-well plate and centrifuged at 3.000 g and 32 °C for 2 hours. Platinum-E cells were counted and cell density was adjusted to 5x10⁵ cells/mL in cDMEM. Then, 50 μ l of the cell suspension (25.000 cells) were added carefully to the viral supernatant and the plate was centrifuged again at 800 g and 32 °C for 1,5 hours. Transduction efficacy was determined after 2 days by flow cytometry. To enhance the virus production of the Plat-E cell lines and get rid of remaining untransduced cells, transduced cells were purified by fluorescence activated cell sorting (FACS). Viral supernatants were collected when cells reached ~ 70 % confluence, purified from remaining cells by centrifugation (1500 rpm, 4 °C, 7 min) and stored at 4 °C for up to 4 weeks.

3.2.2.3 Generation of retrogenic mice

Femora and tibiae of 8-15 weeks old CD45.1 or C57BL/6 mice were cut out and muscles were removed. Epiphyses were cut off and bone marrow cells were flushed out with 2-3 mL cDMEM per bone using a 10 mL syringe with a 26G needle. Cells were centrifuged at 1500 rpm for 6 minutes and resuspended in 3 mL ACT buffer for red blood cell lysis. Samples were incubated for 3 minutes at room temperature (RT) before the reaction was stopped by adding 7 mL cDMEM. Afterwards, bone marrow cells were centrifuged again, resuspended in 500 μ l FACS

Material and Methods

buffer containing anti-mouse CD3, anti-mouse CD19 and anti-mouse Ly6A/E (Sca-1) antibodies and incubated for 30 minutes at 4 °C protected from light. Cells were washed with 10 mL FACS buffer and finally resuspended in 500 µl cDMEM for FACS. PI was added 1/100 for live/dead discrimination. CD3⁻ CD19⁻ Sca-1⁺ hematopoietic stem cells (HSCs) were sorted into 15 mL tubes containing 1 mL FCS. Sorted cells were washed with 5 mL PBS and resuspended in cDMEM, supplemented with 2 ng/mL murine IL-3 (mIL-3), 50 ng/mL murine IL-6 (mIL-6) and 50 ng/mL murine SCF (mSCF). HSCs were cultivated in a tissue-culture treated 48-well plate (250.000-350.000 cells/400 µl). After 3 days, cells were splitted 1:1 or 1:2 depending on their confluence.

For retroviral transduction, a tissue-culture untreated 48-well plate was coated with 10 µg/mL RetroNectin in PBS (150 µl per well) overnight at 4 °C. Expanded HSCs were retrovirally transduced after 4 days of culture. Viral supernatants were collected either from Plat-E cells transfected with retroviral vectors encoding for the different fluorescent proteins or stably transduced Plat-E cell lines as described (see 3.2.2.1 and 3.2.2.2). These supernatants were pooled to achieve combinatorial transduction of the HSCs. RetroNectin was removed and the wells were washed once with PBS. 400 µl of the pooled supernatants were added per well and centrifuged at 3.000 g and 32 °C for 2 hours. Stem cells were collected in a 15 mL tube, centrifuged at 1500 rpm for 6 minutes and resuspended in fresh cDMEM, supplemented with 2 ng/mL mIL-3, 50 ng/mL mIL-6 and 50 ng/mL mSCF (final cell density: 300.000 cells/400 µl). Viral supernatants were removed and 400 µl of the prepared HSCs were added per well. The plate was centrifuged at 800 g and 32 °C for 1,5 h and then incubated at 37 °C and 5 % CO₂ until injection.

After two days, C57BL/6 recipient mice were irradiated using a cesium irradiator. The mice received a total dose of 9 grays (Gy) that were delivered in two equal doses 4 hours apart. After the second irradiation, stem cells were collected in a 15 mL tube, washed with PBS and resuspended in FCS at a final density of 1-3x10⁶ cells/100 µl. 100 µl of the cell suspension were injected intravenously (i.v.) into the irradiated hosts. After 4 weeks, chimerism of the retrogenic mice was determined in peripheral blood samples via flow cytometry (see 3.2.4.2 and 3.2.7).

3.2.3 MCMV generation and infection

3.2.3.1 Generation of virus stocks from salivary glands

For *in vivo* propagation of MCMV strains, 3 weeks old male BALB/c mice were infected intraperitoneally (i.p.) with 2x10⁵ plaque-forming units (pfu) of the respective MCMV variant.

Material and Methods

After 21 days, salivary glands were harvested and homogenized in 5 % skim milk/DMEM (1 mL for three salivary glands) using the loose pestle of a dounce tissue grinder. Cell suspensions were centrifuged (800 g, 4 °C, 5 min) and supernatants were transferred into a fresh dounce tissue grinder. After a second round of homogenization with the tight pestle and centrifugation, supernatants were collected and stored in small aliquots at -80 °C for further usage. All preparation steps were conducted on ice under a laminar flow hood with sterile reagents. For passaging MCMV, the same protocol was performed but lower virus doses (500-2.500 pfu) were used for infection of BALB/c mice. For infection experiments, 3-times-passaged virus stocks were used.

3.2.3.2 Plaque Assay

The concentrations of all generated virus stocks were determined by plaque assays. Therefore, M2-10B4 cells were grown in a tissue-culture treated 48-well plate until they reached 100 % confluence. Serial dilutions were made of all virus stocks including a control virus with known concentration. Virus stocks were diluted in cDMEM and dilutions from 10^{-3} to 10^{-6} were used for viruses isolated from salivary glands. Medium was removed from the cell layers and triplicates of each dilution were added to the cells (400 μ l per well). Cells were incubated for 1,5 hours at 37 °C. Afterwards, the virus was removed and the cells were layered with 1X Methylcellulose/DMEM. After four to six days, appropriate dilutions were chosen and plaques were counted manually under an inverted microscope. To correct for interexperimental deviations, a correction factor was determined by dividing the measured concentration of the control virus by its known concentration. All measured virus titers were multiplied by this correction factor.

3.2.3.3 Infections

Upon adoptive transfer experiments, *Rag2^{-/-} Il2rg^{-/-}*, *Klra8^{-/-}* and *Nkp46^{iCre} x R26-LSL-iDTA* mice were infected with 100 pfu MCMV-wt (3rd passage) by intraperitoneal (i.p.) injection. C57BL/6 and *Xcr1^{Venus DTR}* mice were infected i.p. with 2.000 pfu MCMV-wt (3rd passage). *Klra8^{+/+}* and *Klra8^{-/-}* mice were infected i.p. with 2.000 pfu MCMV-wt or MCMV-*ie2-SIINFEKL-GFP* (3rd passage) for confocal immunofluorescence imaging. *Klra8^{-/-} : Batf3^{+/+}* or *Klra8^{-/-} : Batf3^{-/-}* mixed bone marrow chimeras, *Klra8^{+/+}* and *Klra8^{-/-}* mice were infected with MCMV-*ie2-SIINFEKL* (500 pfu, 3rd passage) by i.p. injection.

Material and Methods

3.2.3.4 Measurement of MCMV titers

To determine viral titers, spleens were harvested from MCMV-infected *Klra8^{-/-}* and *Klra8^{+/+}* mice and virus titration was done in close collaboration with M. Zeeshan Chaudry and Luca Cicin-Sain (Helmholtz Centre for Infection Research, Braunschweig) via plaque assay. All experimental steps are described in detail in Flommersfeld et al., 2021.

3.2.4 Generation of single-cell suspensions

3.2.4.1 Spleen and lymph nodes

Spleens and lymph nodes were harvested and mashed through a 40 µm cell strainer in a 60 mm petri dish containing 5 mL cRPMI. The resulting single cell suspension was transferred to a 15 mL tube and both cell strainer and petri dish were rinsed with another 5 mL cRPMI. Splenocytes were centrifuged at 1500 rpm for 6 minutes and resuspended in 3 mL ACT buffer for 3 minutes at RT. Red blood cell lysis was stopped by adding 7 mL cRPMI. Cell numbers were determined using a Neubauer counting chamber.

3.2.4.2 Blood

50-100 µl blood were collected in heparinized tubes by puncture of the *vena facialis* using a 2,9 mm lancet. 10 mL ACT buffer were added and samples were incubated for 10 minutes at RT to lyse erythrocytes. Blood cells were centrifuged at 1500 rpm for 6 minutes and pellets were resuspended in 5 mL ACT buffer for another 5 minutes at RT. The reaction was stopped by adding 5 ml cRPMI.

3.2.4.3 Liver

Livers were homogenized in 3 mL PBS by using a dounce tissue grinder with the loose pestle. The single-cell suspension was transferred to a 15 mL tube and centrifuged at 1500 rpm for 6 minutes. Pellets were resuspended in 40 % Percoll/PBS and gradient centrifugation was performed at 2600 rpm and RT for 20 minutes (accel = 5, decel = 0) to isolate lymphocytes. The lymphocyte fraction was resuspended in 3 mL ACT buffer for 3 minutes at RT. Red blood cell lysis was stopped by adding 7 mL cRPMI.

Material and Methods

3.2.5 Adoptive transfer of Ly49H⁺ NK cells

3.2.5.1 Pre-enrichment of NK1.1⁺ cells

Spleens of CD45.1 or retrogenic donor mice were harvested and brought into single-cell suspension as described (see 3.2.4.1). Splenocytes were stained in FACS buffer (1 mL per 1×10^8 cells) with an anti-mouse NK1.1 APC antibody for 30 minutes at 4 °C protected from light. Cells were washed with 10 mL FACS Buffer and resuspended in 1 mL cRPMI. NK1.1⁺ cells were enriched by flow cytometric sorting on a MoFlo Astrios cell sorter. Therefore, a threshold was set for the APC channel so that only APC-positive events were detected. This allowed to run samples at high speed while collecting all droplets containing APC-positive cells. APC-negative droplets were discarded by the cell sorter. Collected samples were enriched 5- to 10-fold for NK1.1⁺ cells and were then subjected to purity sorting.

3.2.5.2 Cell sorting and adoptive transfer

Enriched samples were suspended in FACS buffer (200 μ l per 1×10^7 cells) and stained with respective antibodies for 30 minutes at 4 °C in the dark. Cells were washed with 10 mL PBS and resuspended in cRPMI (final cell density: 5×10^7 cells/mL). PI was added 1/100 for live/dead discrimination.

For single-cell adoptive transfers, CD3⁻ CD19⁻ NK1.1⁺ Ly49H⁺ CD27⁺ cells harboring distinct color-barcodes were sorted from retrogenic donors. Expression of CD62L and CD11b was indexed or considered for sort decisions in some experiments. 20-30 single cells with distinct barcodes were sorted into the same well and subsequently co-transferred into the same host. This multiplexing allowed to track several NK cell clones within the same recipient, as barcodes are heritable and can be distinguished by flow cytometry.

For bulk transfers, CD3⁻ CD19⁻ NK1.1⁺ Ly49H⁺ NK cell populations were sorted. In most experiments, surface expression of the markers CD27, CD62L, CD160 and/or CD11b was used to identify and sort different NK cell subsets. NK cells were sorted into a 96-well v-bottom plate containing 400.000 feeder splenocytes in 200 μ l FCS. NK cells were injected intravenously into *Rag2*^{-/-} *Il2rg*^{-/-}, *Klra8*^{-/-} or *Nkp46*^{iCre} x *R26-LSL-iDTA* recipient mice.

3.2.5.3 Retransfer of Ly49H⁺ NK cells

Ly49H⁺ NK cell subsets were sorted and adoptively transferred into *Nkp46*^{iCre} x *R26-LSL-iDTA* recipients as described (see 3.2.5.2). Mice were subsequently infected with MCMV-wt by intraperitoneal injection. Spleens of primary recipients were harvested at day 8 p.i. and splenocytes were stained with an anti-mouse CD45.1 antibody. CD45.1⁺ cells were enriched by

Material and Methods

flow cytometric sorting (MoFlo Astrios) as described (see 3.2.5.1). Afterwards, enriched cells were stained with respective antibodies and CD19⁻ CD3⁻ CD45.1⁺ NK1.1⁺ Ly49H⁺ cells were sorted into a 96-well v-bottom plate containing 400.000 *Rag2*^{-/-} *Il2rg*^{-/-} splenocytes in 200 µl FCS. NK cells were injected i.v. into *Rag2*^{-/-} *Il2rg*^{-/-} as secondary recipients. After 20 days, secondary recipients were either infected with MCMV-wt or spleens were harvested and analyzed by flow cytometry. Spleens from the infected cohort were analyzed at day 8 p.i.

3.2.6 Adoptive transfer of OT-1 T cells

3.2.6.1 Priming of OT-1 T cells

Klra8^{-/-} : *Batf3*^{+/+} and *Klra8*^{-/-} : *Batf3*^{-/-} mixed bone marrow chimeras, *Klra8*^{+/+} and *Klra8*^{-/-} mice were infected i.p. with 500 pfu MCMV-*ie2*-SIINFEKL. CD45.1⁺ *Rag1*^{-/-} OT-1 splenocytes were harvested and stained with antibodies directed against CD8 and CD44 and PI for live/dead discrimination for 30 minutes at 4 °C protected from light. Cells were washed with 10 mL FACS buffer and resuspended in FCS. Absolute number of naïve SIINFEKL-specific OT-1 T cells (CD8⁺ CD44^{low}) in the sample was determined by analyzing a small aliquot of the stained sample via flow cytometry and final cell density was adjusted to 1x10⁶ naïve OT-1 T cells per 200 µl FCS. 1x10⁶ naïve OT-1 T cells were injected i.p. at 24, 48, 72 or 96 hours post infection. After 21 hours, spleens were harvested and analyzed by flow cytometry as described (see 3.2.4.1 and 3.2.7).

3.2.6.2 Retransfer of OT-1 T cells

1x10⁶ CD45.1^{+/+} and CD45.1^{+/-} *Rag1*^{-/-} OT-1 splenocytes were adoptively transferred into *Klra8*^{-/-} and *Klra8*^{+/+} mice, respectively, as described (see 3.2.6.1). On the next day, mice were infected i.p. with 500 pfu MCMV-*ie2*-SIINFEKL. At day 2 p.i., spleens of primary recipients were harvested and brought into single-cell suspension. Splenocytes were stained with an anti-mouse CD45.1 antibody and CD45.1⁺ cells were enriched by flow cytometric sorting on a MoFlo Astrios as described (see 3.2.5.1). Afterwards, enriched cells were stained with respective antibodies and CD19⁻ CD4⁻ CD45.1⁺ CD8⁺ OT-1 T cells were sorted into a 96-well v-bottom plate containing 400.000 C57BL/6 splenocytes in 200 µl FCS. To directly compare the expansion capacity of OT-1 T cells primed in either mouse strain, identical numbers of CD45.1^{+/+} OT-1 T cells from *Klra8*^{-/-} and CD45.1^{+/-} OT-1 T cells from *Klra8*^{+/+} mice were sorted into the same well and co-transferred into infection-matched C57BL/6 recipient mice. Expansion of OT-1 cells was monitored by flow cytometric analysis of peripheral blood samples.

Material and Methods

3.2.7 Flow cytometry

Lymphocytes were isolated from respective organs as described (see 3.2.4) and stained in a v-bottom 96-well plate. A maximum of 2×10^7 cells were added per well and centrifuged at 1500 rpm and 4 °C for 3 minutes. Pellets were resuspended in 100 µl FACS buffer containing EMA 1/1000 for live/dead discrimination and anti-mouse CD16/CD32 1/500 for blocking of Fc receptors to avoid unspecific binding of antibodies and incubated for 20 minutes at 4 °C exposed to light. Afterwards, cells were washed 1,5 times with FACS buffer and stained with the respective antibodies – diluted in 100 µl FACS buffer per well – for 30 minutes at 4 °C in the dark. Cells were washed 2,5 times with FACS buffer and either analyzed by flow cytometry or intracellular staining was performed. Transcription factor staining was done using eBioscience™ Foxp3 Transcription Factor Staining Buffer Set or True-Nuclear™ Transcription Factor Buffer Set according to the manufacturer's instructions. Therefore, after final washing, cells were fixed in 200 µl Fixation/Permeabilization working solution for 30 minutes at 4 °C in the dark. Cells were centrifuged at 1800 rpm and 4 °C for 4 minutes and then washed with 200 µl 1X Perm Wash buffer. Intracellular staining was performed in 100 µl 1X Perm Wash buffer containing the respective antibodies directed against transcription factors or granzyme B at appropriate dilutions (30 min, 4 °C, in the dark). Finally, cells were washed 2,5 times with 1X Perm Wash buffer and resuspended in 200 µl FACS buffer for flow cytometric analysis.

3.2.8 RNA sequencing

3.2.8.1 Bulk RNA sequencing

For bulk RNA sequencing (RNA-seq), distinct NK cell populations were sorted as described (see 3.2.5.2) into RNase-free tubes containing 20 µl PBS and 1 µl RNase inhibitor. Samples were frozen in liquid nitrogen and stored at -80 °C. RNA extraction, library preparation and sequencing were performed in the laboratory of Thomas Höfer at the German Cancer Research Center in Heidelberg, Germany. Data analysis was performed by Michael Floßdorf at the Institute for Medical Microbiology, Immunology and Hygiene (TUM). A detailed protocol of both experimental procedures and data analysis is given in Flommersfeld et al., 2021.

3.2.8.2 Single cell RNA sequencing

For single cell RNA-seq (scRNA-seq) Experiments, NK cells were sorted as described (see 3.2.5.2) in an FCS-coated v-bottom 96-well plate containing 200 µl FACS buffer (without EDTA) per well. Single cell partitioning, barcoding, RNA extraction and library preparation

Material and Methods

were performed by Simon Graßmann and Sebastian Jarosch at the Institute for Medical Microbiology, Immunology and Hygiene (TUM) using the 10x Genomics platform (Flommersfeld et al., 2021). Data analysis was performed by Simon Grassmann and Michael Floßdorf as described in Flommersfeld et al., 2021.

3.2.9 Confocal immunofluorescence imaging and image analysis

Confocal immunofluorescence imaging was performed by Jan Böttcher and Philippa Meiser at the Institute for Molecular Immunology (TUM), including organ fixation, preparation of spleen sections, staining and imaging as well as image analysis and quantification. A detailed description of the procedure can be taken from Flommersfeld et al., 2021.

3.2.10 Parabiosis

Parabiosis experiments were performed by Jonatan Ersching and Gabriel Victora at the Rockefeller University in New York, USA, in accordance to previously published protocols (Coleman and Hummel, 1969, Harris, 1997). C57BL/6 mice were parabiotically joined to congenic CD45.1 mice. A detailed protocol of the procedure is given in Flommersfeld et al., 2021. Four weeks after the surgery, spleens were harvested and subjected to flow cytometric analysis. Due to the distinct congenic background of the parabiotic partners, the origin of different immune cell populations could be determined by antibody staining for CD45.1 and CD45.2.

3.2.11 Mixed bone marrow chimeras

Bone marrow cells were isolated from femora and tibiae of 8-15 weeks old *Klra8^{-/-}*, *Batf3^{-/-}* and C57BL/6 mice as described (see 3.2.2.3). Cell numbers were determined using an a Neubauer improved counting chamber. Equal numbers of respective bone marrows were mixed at a final density of 5×10^6 cells per 200 μ l FCS. Recipient mice received total body irradiation with 2 times 4,5 Gy 4 hours apart using a cesium irradiator. After the second irradiation, 200 μ l of the prepared bone marrow cells were injected i.v. Reconstitution of the Ly49H⁺ NK cell compartment was analyzed after 6 weeks by blood sampling.

Material and Methods

3.2.12 Functional assays

3.2.12.1 Stimulation of Ly49H⁺ NK cells with PMA/ionomycin

Spleens were harvested from CD45.1 mice and brought into single-cell suspension as described (see 3.2.4.1). Splenocytes were stained with respective antibodies and CD27⁻ CD62L⁺, CD27⁺ CD62L⁺ and CD27⁺ CD62L⁻ Ly49H⁺ NK cells, respectively, were sorted into a u-bottom 96-well plate containing 400.000 C57BL/6 splenocytes per well in cRPMI. After sorting, PMA and ionomycin were added at a final concentration of 20 ng/ml and 1.25 µg/ml, respectively. An equal volume of DMSO, diluted 1/10 in cRPMI, was added to the negative control. Cells were incubated at 37 °C and 5 % CO₂ for 1 hour before Golgi plug was added 1/1000. After another 4 hours, cells were washed with FACS buffer and staining of surface molecules was performed as described (see 3.2.7). Intracellular cytokine staining was done using Cytofix/Cytoperm™ Fixation/Permeabilization Solution Kit. Therefore, cells were fixed by adding 100 µl Fixation/Permeabilization solution per well for 30 minutes at 4 °C protected from light. Afterwards, cells were washed 1,5 times with 1X Perm/Wash Buffer and resuspended in 100 µl 1X Perm/Wash Buffer containing antibodies directed against the respective cytokines. After another 30 minutes at 4°C in the dark, cells were washed 2,5 times with 1X Perm/Wash Buffer and finally resuspended in 200 µl FACS buffer for flow cytometry.

3.2.12.2 Ex vivo cytokine staining

For restimulation with plate-bound antibodies, a 96-well ELISA plate was coated with 1 µg/ml purified anti-mouse NK1.1 in PBS overnight at 4 °C. At the following day, splenocytes were isolated and cell numbers were determined using a Neubauer improved counting chamber. Final cell density was adjusted to 2,5x10⁷ cells per mL cRPMI. Coated wells were washed with PBS and 5x10⁶ cells were added per well. Identical numbers of splenocytes were added to uncoated wells without restimulation. After 1 hour, Golgi Plug™ was added 1/500 and intracellular cytokine staining was performed as described (see 3.2.12.1).

3.2.12.3 Ba/F3 co-culture

Ba/F3-neo (WT) and Ba/F3-m157 were a kind gift from Hisashi Arase and Lewis Lanier. Both cell lines were transferred to 15 mL tubes and cell numbers were determined using a Neubauer improved counting chamber. Ba/F3 cells were centrifuged at 1500 rpm for 6 minutes and resuspended in cRPMI with a final cell density of 2,5x10⁵ cells/mL. 50.000 cells were added per well to a u-bottom 96-well plate. Splenocytes of CD45.1 mice were harvested and stained with respective antibodies. 2.000 CD27⁺ CD62L⁺ or CD27⁺ CD62L⁻ Ly49H⁺ NK cells were

Material and Methods

sorted into the prepared 96-well plate and co-incubated with Ba/F3-neo or Ba/F3-m157 cells for 24 hours in cRPMI. After co-culture, cells were analyzed by flow cytometry.

3.2.12.4 *In vitro* killing assay

RMA and RMA-S cells were a kind gift from Joseph Sun. To generate cell lines expressing fluorescent labels detectable by flow cytometry, Plat-E cell lines were transfected with retroviral vectors encoding for GFP and BFP as described (see 3.2.2.1). RMA and RMA-S cells were retrovirally transduced with the collected supernatants as described for Plat-E cells (see 3.2.2.2). Successfully transduced cells were purified from untransduced cells by FACS and expanded.

To pre-activate the NK cells, C57BL/6 mice were infected with MCMV-wt 24 hours prior to NK cell sorting. At the day of the experiment, RMA and RMA-S cells were counted using a Neubauer improved counting chamber and 1.500 GFP⁺ RMA as well as 1.500 BFP⁺ RMA-S cells were added to each well of a u-bottom 96-well plate. Splens of infected C57BL/6 mice were harvested and stained with respective antibodies. 3.000 CD27⁺ CD62L⁺ or CD27⁺ CD62L⁻ Ly49H⁺ NK cells were sorted to the respective wells. RMA, RMA-S and NK cells were co-incubated for 42 hours in cRPMI. After co-culture, PI was added 1/100 for live/dead discrimination and the numbers of living GFP⁺ and BFP⁺ cells were analyzed by flow cytometry.

3.2.13 Statistics

Prism software was used for quantification and statistical analysis. A detailed description of each statistical test is given in the respective figure legend. Significance is defined as * $p < 0.05$, ** $p < 0.01$, *** $p < 0.001$, **** $p < 0.0001$. Normality tests were performed to decide whether to use parametric or nonparametric tests, where applicable.

4 Results

4.1 Ly49H⁺ NK cells show high phenotypic diversity upon MCMV infection

Upon MCMV infection, Ly49H⁺ NK cells adoptively transferred to immunodeficient hosts undergo vigorous proliferation. To assess the phenotypic diversity of such an expanded NK cell population, we adoptively transferred Ly49H⁺ NK cells into either *Klra8*^{-/-} or *Rag2*^{-/-} *Il2rg*^{-/-} recipients and analyzed their offspring via flow cytometry at day 7–8 p.i. (**Figure 9A**). *Klra8*^{-/-} mice lack expression of the activating receptor Ly49H and are thereby highly susceptible to MCMV infection (Lee et al., 2001).

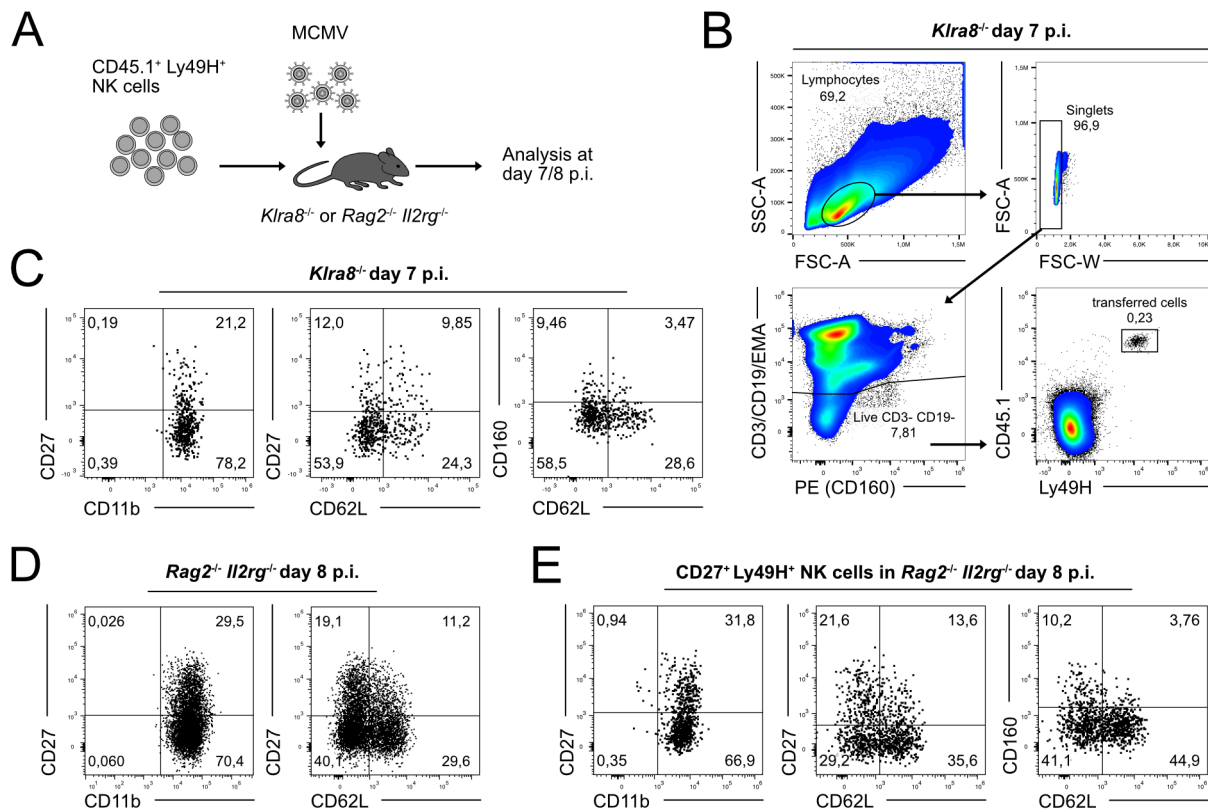


Figure 9: Ly49H⁺ NK cells show phenotypic heterogeneity upon MCMV infection.

(A) 3×10^4 or 1×10^3 CD45.1⁺ Ly49H⁺ NK cells were adoptively transferred into *Klra8*^{-/-} or *Rag2*^{-/-} *Il2rg*^{-/-} mice followed by infection of recipients with MCMV and analysis of expanded NK cell populations in spleen at day 7 or 8 post infection, respectively. (B) Representative pseudocolor plots show gating strategy of transferred Ly49H⁺ NK cells in *Klra8*^{-/-} recipients at day 7 p.i. (C) Representative dot plots show marker expression by transferred Ly49H⁺ NK cells in *Klra8*^{-/-} recipients at day 7 p.i. (D) As in (C) but in *Rag2*^{-/-} *Il2rg*^{-/-} recipients at day 8 p.i. (E) Representative dot plots show marker expression by transferred CD27⁺ Ly49H⁺ NK cells in *Rag2*^{-/-} *Il2rg*^{-/-} recipients at day 8 p.i.

Data are representative of at least 2 independent, similar experiments. (modified from (Flommersfeld et al., 2021))

Results

Rag2^{-/-} *Il2rg*^{-/-} recipients have neither B nor T cells due to the deficiency of the Rag2 recombinase. Furthermore, they do not develop functional NK cells as the IL-2 receptor subunit gamma (*Il2rg*) – also known as common cytokine receptor gamma chain – is necessary to form functional receptors for many cytokines including IL-15 that is critical for NK cell development and maintenance. Both immunodeficient strains provide a model in which strong clonal expansion of Ly49H⁺ NK cells can be achieved. The transferred populations expressed the congenic marker CD45.1 to enable tracking of these cells *in vivo* (**Figure 9B**). Recipient mice were infected with MCMV and expanded NK cell populations were analyzed at the peak of the response, which is at day 7 in *Klra8*^{-/-} and day 8 in *Rag2*^{-/-} *Il2rg*^{-/-} recipients, respectively. Analysis of the expression of different phenotypic markers, that have been described to play a role in NK cell differentiation – such as CD27, CD11b, CD62L and CD160 (Hayakawa and Smyth, 2006, Chiossone et al., 2009, Peng et al., 2013b, Anumanthan et al., 1998) – indicated that Ly49H⁺ NK cells show high phenotypic diversity at the peak of expansion. Whereas all cells expressed CD11b, the other markers were detectable in only a fraction of the expanded population (**Figure 9C+D**). This differentiation pattern was similar for both mouse models and conserved even when transferring only immature NK cells, identified by the expression of CD27 at steady state (**Figure 9E**).

4.2 Single-cell fate mapping of Ly49H⁺ NK cells identifies two distinct response patterns upon MCMV infection

However, adoptive transfer experiments of NK cell populations do not give any insight into the clonal origin of these phenotypically distinct NK cells. Therefore, one aim of this work was to study how the phenotypic diversity of the NK cell response, observed at day 7–8 p.i., is composed starting out from single Ly49H⁺ NK cells. Phenotypic heterogeneity might result from different scenarios. One hypothesis could be that Ly49H⁺ NK cells undergo phenotypic diversification during expansion. This means that all NK cells follow a common differentiation path ending up in the generation of a diverse progeny. Alternatively, individual Ly49H⁺ NK cells could adopt separate NK cell fates, which are then restricted to a certain phenotype. In this second scenario, phenotypic diversity is generated by the combination of multiple NK cell clones. All these aspects can be addressed by performing single-cell adoptive transfers.

Retrogenic color-barcoding, which was previously established in the laboratory (Grassmann et al., 2019, Grassmann et al., 2020), was used to generate color-barcoded NK cells that are trackable *in vivo*. Therefore, hematopoietic stem cells were isolated from the bone marrow of

Results

C57BL/6 mice expressing distinct congenic markers and expanded *in vitro*. Expanded HSCs were retrovirally transduced with the five fluorescent proteins GFP, YFP, Ametrine, CFP and BFP in a combinatorial manner and transplanted into irradiated hosts (**Figure 10A**). Within 4-6 weeks these HSCs develop into various color-barcoded hematopoietic lineages, including NK cells (**Figure 10B**). Single color-barcoded CD27⁺ Ly49H⁺ NK cells were then sorted from the spleen of retrogenic donors and transferred into *Rag2*^{-/-} *Il2rg*^{-/-} recipients in a multiplexed manner (**Figure 10C**). This means that 20-30 single NK cells harboring distinct color barcodes were co-transferred into the same recipient, but the offspring of every one of these single NK cells could be analyzed separately, based on its heritable color-barcode (**Figure 10D**). Recipients were infected with MCMV and expanded NK cell clones were analyzed at day 8 p.i. (**Figure 10C**).

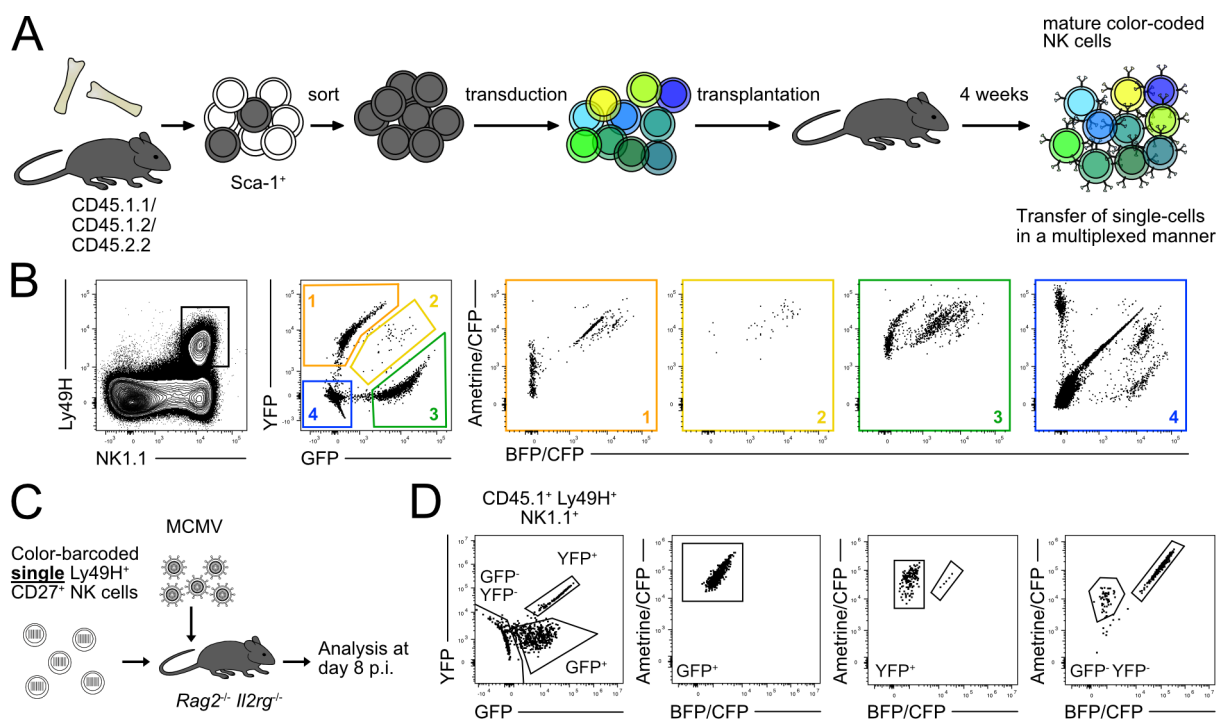


Figure 10: Retrogenic color-barcoding enables single-cell fate mapping of Ly49H⁺ NK cells.

(A) Schematic shows generation of color-barcoded NK cells. Sca-1⁺ HSCs were sorted from the bone marrow of C57BL/6 mice with distinct congenic markers and transduced with retroviruses carrying distinct fluorescent proteins. After transplantation into irradiated recipients, HSCs differentiate into mature, color-barcoded immune cells within 4 weeks. (B) Representative dot plots depict color-barcoded Ly49H⁺ NK cells found in the spleens of retrogenic donor mice during single-cell sorting. Ly49H⁺ NK cells were dissected according to their combinatorial expression of GFP and YFP and then further subdivided according to their expression of Ametrine, CFP and BFP (CFP emission appears on a diagonal between the BFP (x-axis) and the Ametrine signal (y-axis) and therefore appears as a label on both axes). (C) Multiplexed adoptive transfer of single color-barcoded CD27⁺ Ly49H⁺ NK cells into *Rag2*^{-/-} *Il2rg*^{-/-} mice, followed by infection of recipients with MCMV and analysis of expanded NK cell clones in spleen at day 8 p.i. (D) Representative dot plots show color barcodes of expanded NK cell clones in *Rag2*^{-/-} *Il2rg*^{-/-} recipients at day 8 p.i.

(modified from (Flommersfeld et al., 2021))

Results

Whereas population-derived NK cell responses showed reliable expansion (meaning predictable in size), single-cell derived responses were highly variable in their size, reaching from 10 to 100.000 daughter cells (**Figure 11A**). Recovered single-cell derived progenies were uniformly positive for CD11b expression as already observed at population level (**Figure 11B, left panel**). Further phenotypic analysis of the expanded NK cell clones identified two distinct differentiation patterns: Cells following the first pattern generated a progeny that completely lacked CD62L expression but contained a relatively large fraction of CD160⁺ and CD27⁺ cells (**Figure 11B, red**). The second pattern comprised clones that generated CD62L⁺ output but lacked CD160 expression and expressed only low percentages of CD27 (**Figure 11B, blue**).

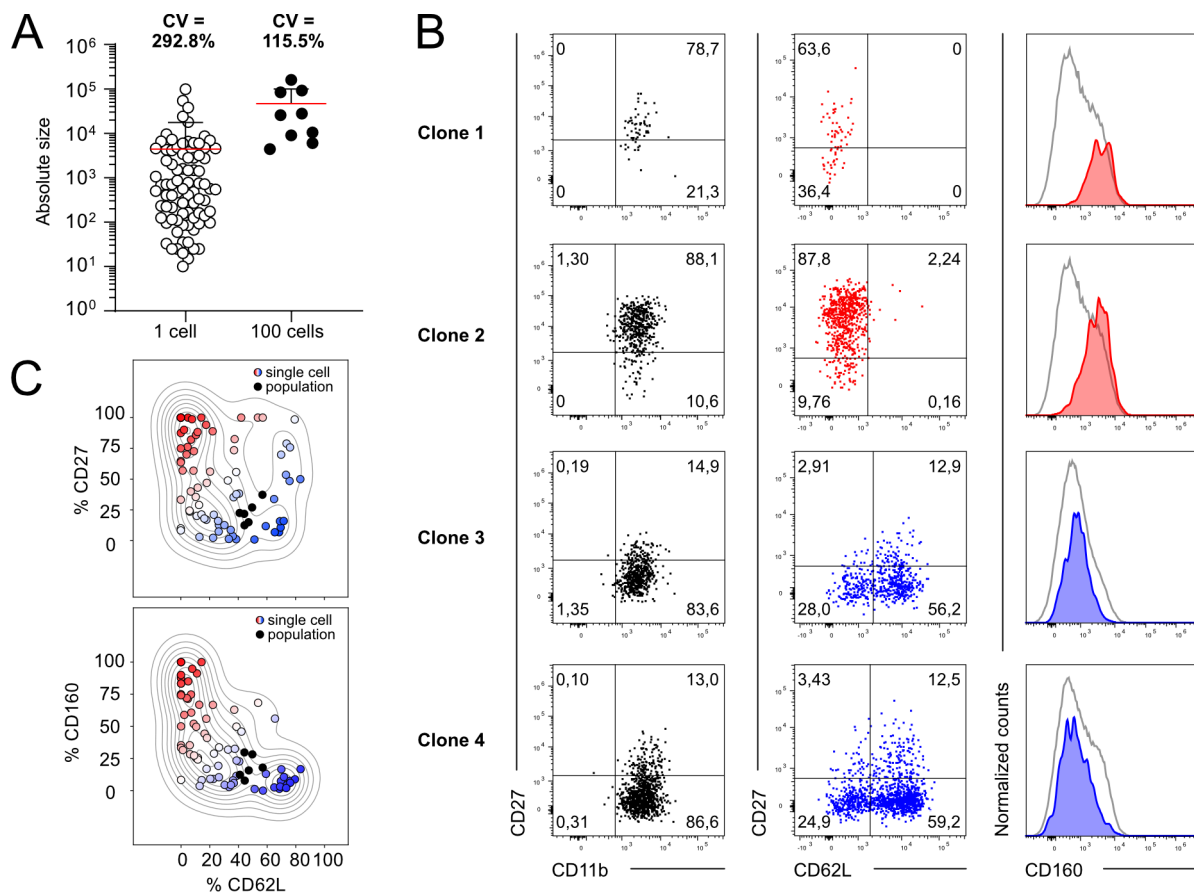


Figure 11: Single-cell fate mapping of Ly49H⁺ NK cells identifies two distinct response patterns upon MCMV infection.

(A) Absolute sizes of NK cell responses derived from single or 100 transferred cells in *Rag2^{-/-} Il2rg^{-/-}* recipients at day 8 p.i. (B) Representative dot plots and histograms depicting marker expression of NK cell clones that either lacked (red) or contained (blue) CD62L expressing cells. Gray histograms show endogenous Ly49H⁺ NK cell population. (C) Kernel density estimate (KDE) plots show expression of CD27, CD62L and CD160 within NK cell responses derived from Ly49H⁺ CD27⁺ populations (black dots) or from single cells sorted as Ly49H⁺ CD27⁺ or Ly49H⁺ CD27⁺ CD11b⁻ or Ly49H⁺ CD27⁺ CD62L⁻ (circles). Red vs. blue color-coding delineates clones containing low vs. high percentages of CD62L and high vs. low percentages of CD27 and CD160 expressing cells. Data in (A) and (C) are pooled from 7 independent, similar experiments. Data in (B) are representative of 4 independent experiments. Lines indicate mean, error bars represent SD. (modified from (Flommersfeld et al., 2021))

Results

The majority of all recovered NK cell clones adopted one of these two separate fates and were characterized by mutually exclusive expression of CD62L and CD160 (and to a lower degree also CD62L and CD27) (**Figure 11C, blue filled vs. red filled circles**). Population-derived responses in contrast showed a very reproducible phenotype resulting from the combination of individual NK cell responses (**Figure 11C, black dots**).

4.3 Distinct response patterns emerge from pre-existing NK cell subsets and are stable throughout infection

Next, we aimed to find out whether CD62L⁻ clones originate from a pre-defined subset, that already exists at steady state. As these clones expressed high levels of CD27 and therefore had a more immature phenotype compared to CD62L⁺ clones, it seemed likely that they might be derived from immature NK cells, which have been described to be CD27⁺ CD11b⁻ at steady state (Chiossone et al., 2009) (**Figure 12A, left**). However, adoptive transfer of splenic CD27⁺ CD11b⁻ Ly49H⁺ NK cell populations and single cells indicated that this subset of NK cells is still capable of forming both response patterns upon MCMV infection (**Figure 12A**). Further phenotyping of Ly49H⁺ NK cells at steady state revealed that CD27 and CD11b were not the only markers expressed in a heterogeneous manner. In particular, CD27⁺ CD11b⁻ Ly49H⁺ NK cells can be further subdivided into a CD62L⁻ and a CD62L⁺ subset (**Figure 12B**). Consequently, CD27⁺ CD62L⁻ Ly49H⁺ NK cells might be the origin of the CD62L⁻ NK cell clones at day 8 p.i.. Indeed, when transferring CD27⁺ CD62L⁻ Ly49H⁺ NK cell populations and single cells into MCMV-infected recipients, they exclusively generated CD62L⁻ response patterns (**Figure 12C**). To corroborate this finding, splenic Ly49H⁺ NK cell populations that differentially expressed the markers CD27 and CD62L at steady state, were adoptively transferred (**Figure 13A, upper left panel**): CD27⁺ CD62L⁻, CD27⁺ CD62L⁺ and CD27⁻ CD62L⁺ Ly49H⁺ NK cells were sorted and transferred into either *Rag2*^{-/-} *Il2rg*^{-/-} or *Klra8*^{-/-} recipients that were infected with MCMV. The phenotype of the expanded NK cell populations was then assessed at day 8 and 10 p.i., respectively (**Figure 13A, right and lower left panel**). Whereas bulk adoptive transfer of CD27⁺ CD62L⁻ NK cell generated response patterns that were exclusively CD62L⁻, CD62L⁺ NK cells formed response patterns that always contained CD62L⁺ cells (**Figure 13A**). Thus, transfer of defined NK cell subsets replicated the distinct response patterns emerging from single NK cells (**Figure 11B**).

Results

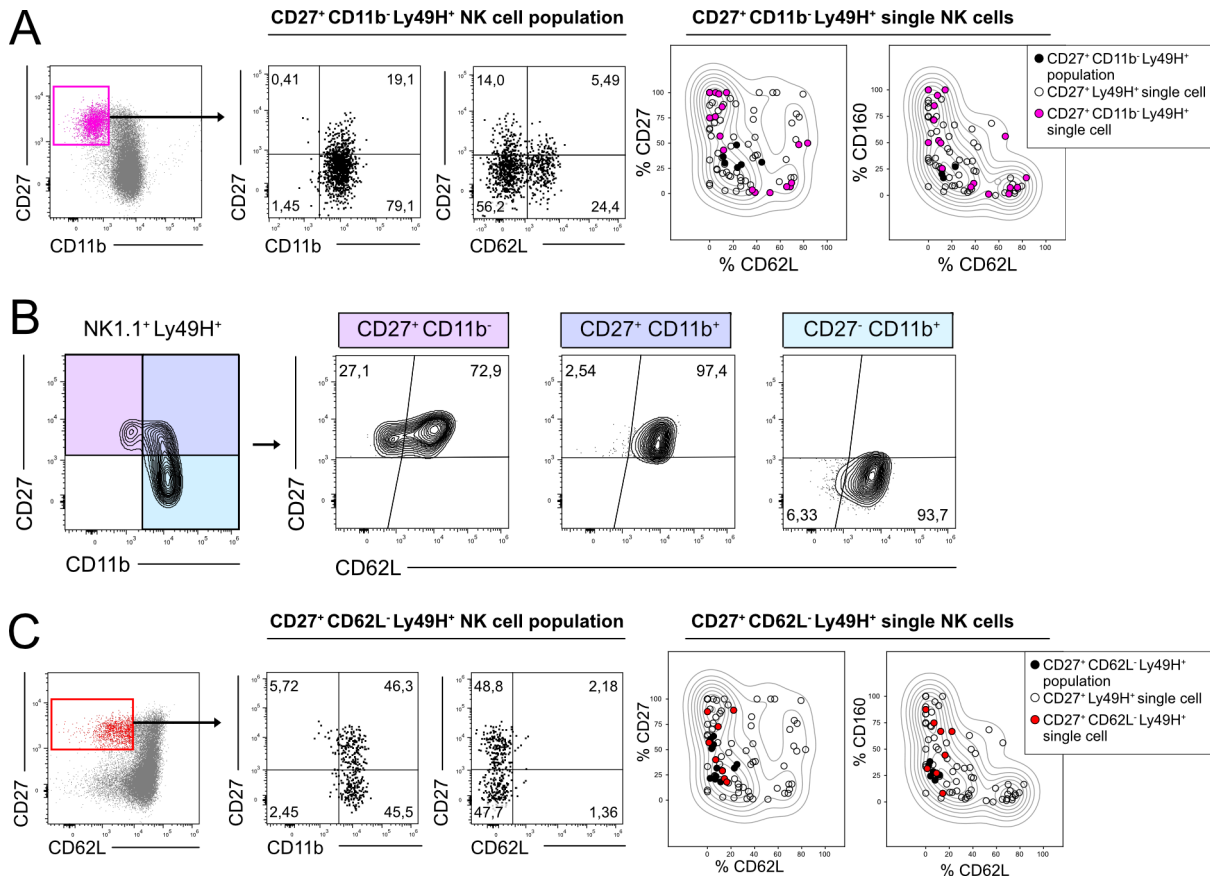


Figure 12: CD62L⁻ clones originate from CD27⁺ CD62L⁻ Ly49H⁺ NK cells in the spleen.

(A) CD27⁺ CD11b⁻ Ly49H⁺ NK cell populations and single cells were adoptively transferred into *Klra8*^{-/-} or *Rag2*^{-/-} *Il2rg*^{-/-}, respectively, subsequently infected with MCMV. Representative dot plots show phenotype of population-derived responses at day 7 p.i., KDE plots show expression of CD27, CD62L and CD160 within population and single-cell-derived progenies at day 7 or 8 p.i., respectively. (B) Contour plots show marker expression of Ly49H⁺ NK cells at steady. (C) As in (A) but adoptive transfer of Ly49H⁺ CD27⁺ CD62L⁻ NK cells. Population data in (A) and (C) are representative of at least 2 independent experiments. Single cell data in (A) and (C) are pooled from 2-3 independent experiments. (modified from (Flommersfeld et al., 2021))

To analyze whether these distinct response patterns were maintained during the memory phase of the infection, CD27⁺ CD62L⁻ and CD27⁺ CD62L⁺ Ly49H⁺ NK cells were adoptively transferred into NK cell-deficient *Nkp46*^{iCre} (Narni-Mancinelli et al., 2011) x *R26-LSL-iDTA* mice. In these mice, all Nkp46⁺ cells express Cre recombinase which mediates the excision of a *lox-stop-lox* site and consequently, constitutive expression of Diphtheria toxin (DTA), resulting in continuous depletion of developing NK cells. Whereas the expansion and contraction kinetics of the two transferred NK cell subsets were similar, they remained phenotypically distinct at least until 3 weeks p.i. (**Figure 13B**).

Finally, we aimed to assess their ability to re-expand upon re-transfer into secondary hosts and recall infection. Therefore, CD27⁺ CD62L⁻ and CD27⁺ CD62L⁺ Ly49H⁺ NK cells were adoptively transferred into *Nkp46*^{iCre} x *R26-LSL-iDTA* mice. At day 8 p.i., the expanded NK cell populations were isolated and re-transferred into *Rag2*^{-/-} *Il2rg*^{-/-} recipients. After a resting

Results

phase of 20 days, secondary recipients were infected with MCMV and recall responses were analyzed at day 8 p.i. (**Figure 13C**).

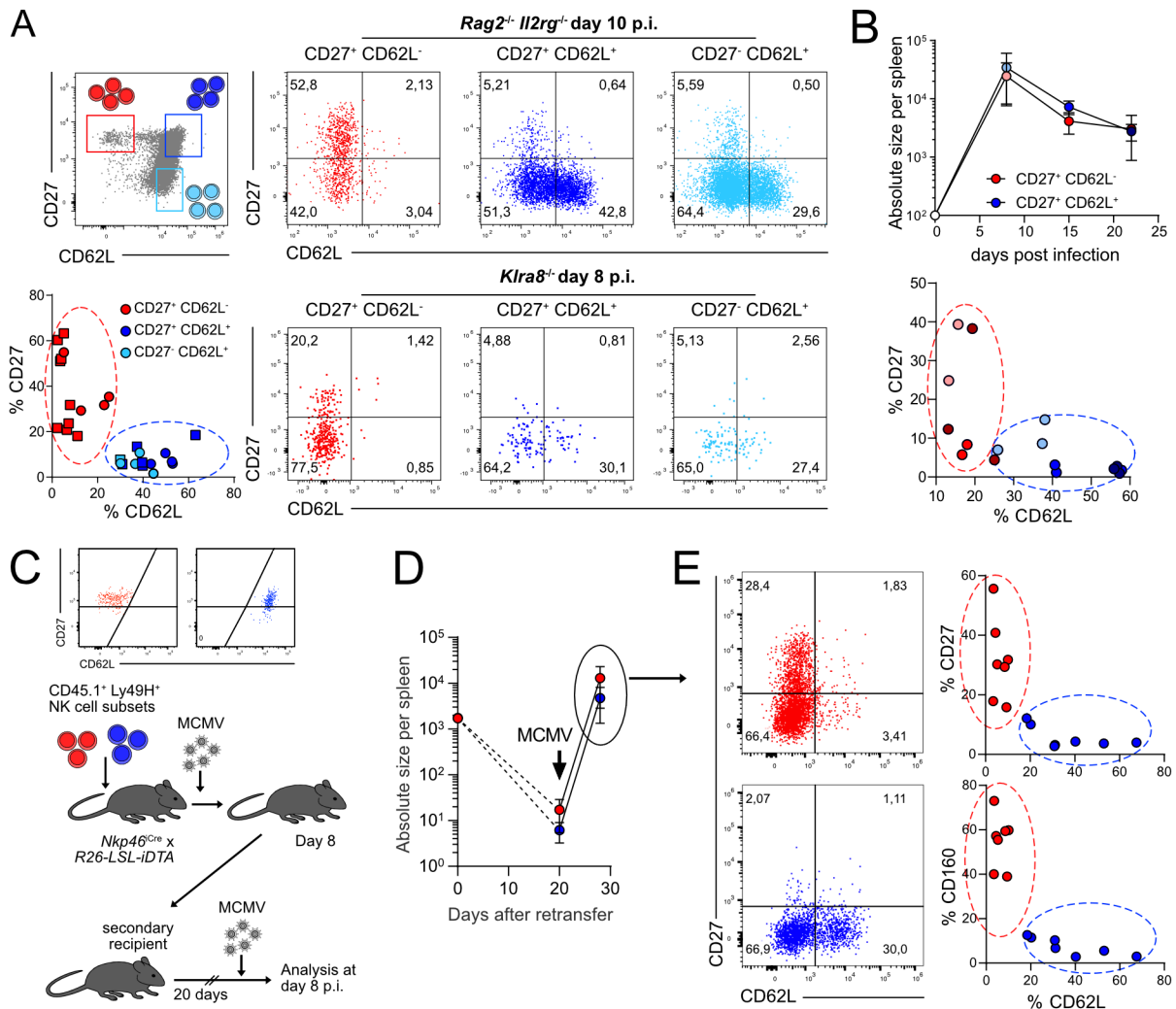


Figure 13: Distinct response patterns are maintained during memory phase and upon secondary infection.

(A) CD27⁺ CD62L⁻, CD27⁺ CD62L⁺ and CD27⁻ CD62L⁺ Ly49H⁺ NK cell populations were adoptively transferred into *Klr8^{-/-}* or *Rag2^{-/-} Il2rg^{-/-}* recipients followed by MCMV infection and analysis in spleen at day 8 or 10 p.i., respectively. Schematic dot plot depicts sort gating (upper left panel). Dot plots depict marker expression within expanded NK cell populations (right panels). Scatter plot depicts frequency of CD27 and CD62L expressing cells within expanded populations at day 8/10 p.i. in *Klr8^{-/-}* (squares) and *Rag2^{-/-} Il2rg^{-/-}* recipients (circles) (lower left panel). (B) CD27⁺ CD62L⁻ and CD27⁺ CD62L⁺ Ly49H⁺ NK cell populations were sorted and adoptively transferred into *Nkp46^{iCre} x R26-LSL-iDTA* recipients, followed by MCMV infection and analysis of expanded populations in spleen at day 8, 15 and 22 p.i. Absolute size of expanded NK cell populations at day 8 (light red/blue), 15 (bright red/blue) and 22 (dark red/blue) (upper panel). Scatter plot depicts frequency of CD27 and CD62L expressing cells within expanded populations at the respective timepoints (lower panel). (C-E) CD27⁺ CD62L⁻ and CD27⁺ CD62L⁺ Ly49H⁺ NK cell populations were sorted and adoptively transferred into *Nkp46^{iCre} x R26-LSL-iDTA* recipients. At day 8 p.i. with MCMV, 1,5-2x10³ CD45.1⁺ Ly49H⁺ NK cells derived from either subset were sorted from spleens of primary recipients, re-transferred into uninfected *Rag2^{-/-} Il2rg^{-/-}* mice, rested for 20 days and analyzed before or 8 days after secondary exposure to MCMV. (C) Initial sort purity and schematic depiction. (D) Absolute size of re-transferred NK cell populations at indicated timepoints. (E) Representative dot plots (left) and scatter plots (right) depicting frequency of marker expressing cells within expanded populations at day 8 after recall infection.

Data in (A) are pooled from 5 independent experiments. Data in (B) are representative of 3 independent experiments. Data in (D) and (E) are pooled from 2 independent experiments. Dots represent mean, error bars indicate SD. (modified from (Flommersfeld, 2018) and (Flommersfeld et al., 2021))

Results

Both subsets robustly re-expanded upon secondary infection and maintained their distinct response patterns (**Figure 13D+E**). In summary, the data showed that adaptive-like NK cell responses emerge from two NK cell subsets that are phenotypically distinct at steady state, upon acute infection, during the memory phase and upon re-infection.

4.4 The identified NK cell subsets are transcriptionally distinct

We then aimed to study whether the distinct subsets that we had identified by single-cell fate mapping, overlapped with the transcriptional composition of steady-state NK cells in the spleen. Therefore, scRNA-seq of Ly49H⁺ NK cells (**Figure 14A**) and bulk RNA-seq of the subsets defined by expression of CD27 and CD62L (**Figure 14B**) were performed and analyzed in collaboration with Michael Flossdorf. Leiden clustering of the scRNA-seq data showed the existence of three transcriptionally distinct clusters (**Figure 14A, upper right panel**). The borders of these clusters clearly matched with the gene expression of *Cd27* and *Sell* (encoding for CD62L). Whereas cells in clusters 1 and 2 showed elevated levels of *Cd27* transcripts, cells in cluster 2 lacked *Cd27* mRNA. On the other hand, *Sell* transcripts were absent from cluster 2, but high in cluster 0 and 1. (**Figure 14A, lower left panel**). Mapping the 10 best-defining genes for each of the three clusters already indicated that cluster 2 has a very unique transcriptional profile compared to clusters 0 and 1 (**Figure 14A, lower right panel**). A comparison of the expression data for the identified set of genes derived from either scRNA-seq or bulk RNA-seq, further showed that cluster 2 clearly mapped onto the transcriptional profile of CD27⁺ CD62L⁻ NK cells whereas clusters 1 and 0 overlapped with the transcriptomic data of CD27⁺ CD62L⁺ and CD27⁻ CD62L⁺ NK cells, respectively (**Figure 14A+B**). Respective mRNA levels of *Cd27* and *Sell* mirrored surface expression of CD27 and CD62L by the sorted NK cell subsets (**Figure 14C**).

Cd7, *Cd160*, *Ltb* and *Xcl1* were among the defining genes for cluster 2. On the other hand, *Gzma*, *Gzmb*, *Klf2* (the transcription factor controlling CD62L expression) and *Klrg1* were enriched in cluster 0, hinting towards an effector phenotype with strong cytotoxicity (**Figure 14D**). Indeed, by comparing normalized read counts of different functional molecules, we could show that CD27⁺ CD62L⁻ NK cells expressed lower levels of cytotoxic effector molecules and IFN- γ , but higher levels of other cytokines such as TNF- α , GM-CSF and lymphotoxin beta (*Ltb*) (**Figure 14E**).

Results

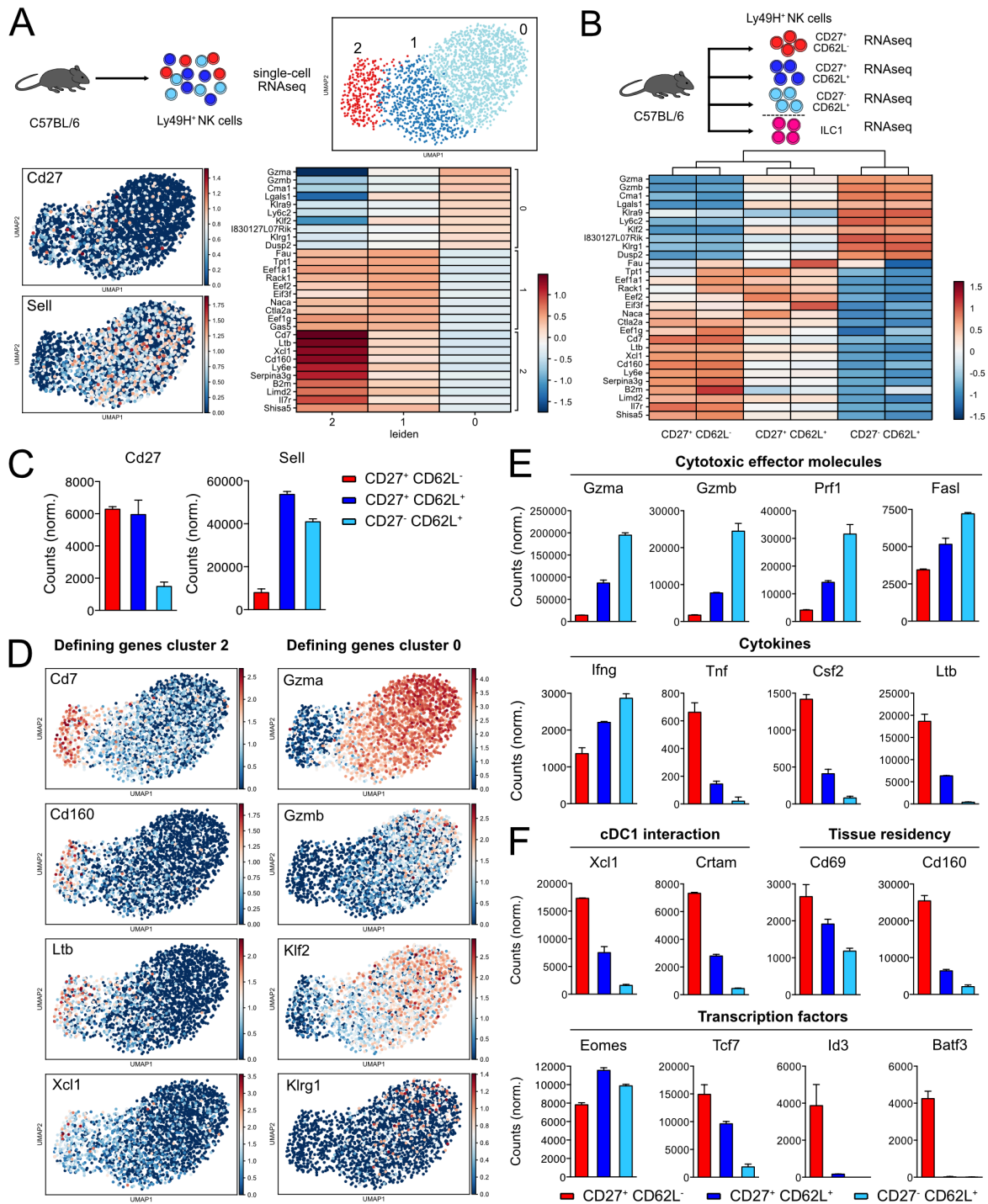


Figure 14: CD27⁺ CD62L⁻ NK cells have a unique transcriptional profile.

(A) Splenic Ly49H⁺ NK cells were sorted for transcriptome analysis by scRNA-seq. UMAP-based Leiden clustering of scRNA-seq transcriptomes shows transcriptionally distinct Ly49H⁺ NK cell subsets at steady state (upper panel). Relative expression of CD27 and CD62L in UMAP projection and depiction of the 10 best-defining genes for the three defined clusters in scRNA-seq (lower panel). (B) CD27⁺ CD62L⁻, CD27⁺ CD62L⁺ and CD27⁻ CD62L⁺ Ly49H⁺ NK cells as well as ILC1s (defined as CD19/CD3/TCR α/β NK1.1⁺ CD27⁺ CD62L⁻, Ly49A/C/D/E/F/G2/H/I negative) were sorted from spleens of C57BL/6 mice for bulk RNA-seq (upper panel). Heatmap shows relative expression of the genes depicted in (A) but in sorted NK cell populations (lower panel). (C) Normalized counts of CD27 and CD62L measured by bulk RNA-seq in sorted NK cell populations. (D) Relative expression of cluster-defining genes for putative CD27⁺ CD62L⁻ (cluster 2, left) and CD62L⁺ Ly49H⁺ NK cells (cluster 0, right) in UMAP projection. (E-F) Normalized counts of indicated genes measured by bulk RNA-seq of the NK cell populations.

Data are representative of 2 independent experiments. Bars represent mean, error bars indicate SD. (modified from (Flommersfeld et al., 2021))

Results

Furthermore, CD27⁺ CD62L⁻ NK cells showed elevated levels of transcripts encoding for the chemokine XCL1, that attracts XCR1⁺ cDC1s (Dorner et al., 2009) as well as CRTAM, that binds to Necl2 – also expressed on cDC1s (Galibert et al., 2005) (**Figure 14F, upper left panel**). These findings suggested potential interactions between CD27⁺ CD62L⁻ NK cells and cDC1s. In addition to that, CD27⁺ CD62L⁻ NK cells expressed higher levels of CD69 and CD160, markers that have been described to be expressed by tissue-resident NK cells (Sojka et al., 2014) (**Figure 14F, upper right panel**). Finally, all NK cell subsets showed similar expression of Eomes, the key transcription factor of NK cells that is commonly used to distinguish NK cells from ILC1s. CD27⁺ CD62L⁻ NK cells in addition expressed the transcription factors Id3 and Batf3 whereas CD62L⁺ NK cells lacked transcripts encoding for these two molecules (**Figure 14F, lower panel**).

To confirm that this subset composition is not restricted to Ly49H⁺ NK cells, but instead typical of the complete NK cell compartment, another scRNA-seq experiment was performed with total NK cells. To clearly separate NK cells from ILC1s, *Eomes*^{GFP} reporter mice were used to sort a highly pure population of CD19/CD3/TCRg/d⁻ NK1.1⁺ Eomes-GFP⁺ NK cells from the spleen. Cells that stained positive or negative for Ly49H were sorted from separate samples and marked with distinct hashtag antibodies carrying a barcode detectable by scRNA-seq. Both Ly49H⁺ and Ly49H⁻ NK cells consisted of two bigger clusters, that were enriched for *Sell* transcripts and a small cluster that lacked *Sell* expression and was highly enriched for transcripts encoding for Batf3 (**Figure 15A**). Consequently, the existence of transcriptionally distinct subsets (characterized by mutual exclusive expression of either CD62L or Batf3) is independent of Ly49H expression but instead conserved among all NK cells.

Finally, surface expression of the markers identified by RNA-seq was validated via antibody staining. Like CD62L⁺ NK cells, CD27⁺ CD62L⁻ NK cells lacked CD49a expression, but expressed CD49b although at lower levels compared to CD62L⁺ subsets. In accordance to transcriptomic data, CD27⁺ CD62L⁻ NK cells showed high surface expression of CD160 and CD69, but lacked the maturation markers KLRG1, CD11b and Ly6C as well as cytotoxic effector molecule granzyme B at steady state. In addition, CD27⁺ CD62L⁻ NK cells were the only subset containing a fraction of CD127 expressing cells (**Figure 15B**). No differences were observed with respect to their Ly49 receptor repertoire (**Figure 15C**). Taken together these data indicate that CD27⁺ CD62L⁻ NK cells are transcriptionally and phenotypically distinct from CD62L⁺ NK cells.

Results

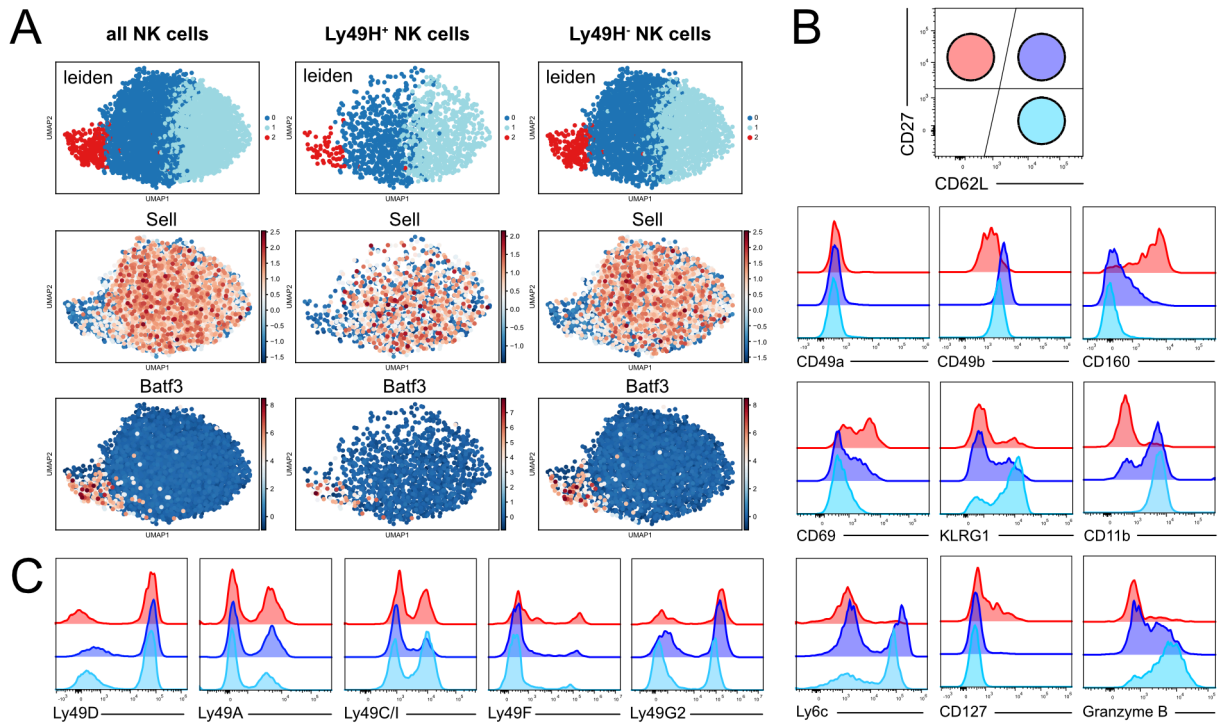


Figure 15: Distinct transcriptional signatures are conserved among Ly49H⁺ and Ly49H⁻ NK cells and mirror differences in protein levels of marker proteins.

(A) UMAP-based Leiden clustering of scRNA-seq transcriptomes and relative expression of CD62L and Batf3 in UMAP projection for all (left), Ly49H⁺ (mid) and Ly49H⁻ (right) NK cells from *Eomes*^{GFP} mice (sorted as CD19/CD3/TCRg/d⁻ NK1.1⁺ Eomes-GFP⁺). (B) Histograms show expression levels of CD49a, CD49b, CD160, CD69, KLRG1, CD11b, Ly6c, CD127 and granzyme B for CD27⁺ CD62L⁻, CD27⁺ CD62L⁺ and CD27⁻ CD62L⁺ Ly49H⁺ NK cells in spleen at steady state. (C) Histograms show expression levels of Ly49D, Ly49A, Ly49C/I, Ly49F and Ly49G2 of NK cell subsets in spleen at steady state.

(modified from (Flommersfeld et al., 2021))

4.5 CD27⁺CD62L⁻ NK cells share features with ILC1s

Overall, transcriptional analysis of the NK cell subsets suggested that CD27⁺ CD62L⁻ NK cells were less cytotoxic than conventional CD62L⁺ NK cells, but potent cytokine producers and potentially tissue-resident. As all these characteristics are also features of ILC1s, it seemed likely that CD27⁺ CD62L⁻ NK cells might be transcriptionally similar to ILC1s. Therefore, a comparison of the transcriptional profiles of all Ly49H⁺ NK cell subsets and ILC1s was done. ILC1s were sorted from the spleen defined as CD19⁻ CD3⁻ TCRα/β⁻ NK1.1⁺ CD27⁺ CD62L⁻ and Ly49A/C/D/E/F/G2/H/I⁻ and subjected to bulk RNA-seq (**Figure 14B**). As many surface markers overlap between NK cells and ILC1s, while the transcription factor *Eomes* selectively characterizes NK cells, but cannot be stained without fixation of the cells and therefore cannot be used to distinguish NK cells and ILC1s during the sort, we validated that the aforementioned surface marker combination identifies a highly pure *Eomes*⁻ and CD127⁺ population of ILC1s (**Figure 16A**). A principal component analysis (PCA) of the transcriptomic data of NK cell subsets and ILC1s showed high similarity of CD27⁺ CD62L⁻ NK cells and ILC1s in PC1, but

Results

segregation of the two cell types in PC2 (**Figure 16B**). In accordance with that, when looking at the gene expression of 40 genes that were most differentially expressed between the four populations, partial overlap of the transcriptional profiles of CD27⁺ CD62L⁻ NK cells and ILC1s was observed (**Figure 16C**). Whereas expression of several markers overlapped between CD27⁺ CD62L⁻ NK cells and ILC1s, others could be clearly attributed to one specific cell type. For example, while only ILC1s showed elevated levels of transcripts encoding for the transcription factors Id2, Hobit and Helios (encoded by *Ikzf2*) that characterize the ILC1 lineage, *Eomes* is expressed by CD27⁺ CD62L⁻ NK cells and not by ILC1s, thereby confirming their NK cell identity. Furthermore, transcripts encoding for Id3 and *Batf3* were selectively elevated in CD27⁺ CD62L⁻ NK cells (**Figure 16D**). With respect to the expression of transcripts for cytokines, similar observations were made. While CD27⁺ CD62L⁻ NK cells and ILC1s shared expression of *Ltb* and TNF- α , GM-CSF (encoded by *Csf2*) was selectively enriched in CD27⁺ CD62L⁻ NK cells (**Figure 16E**).

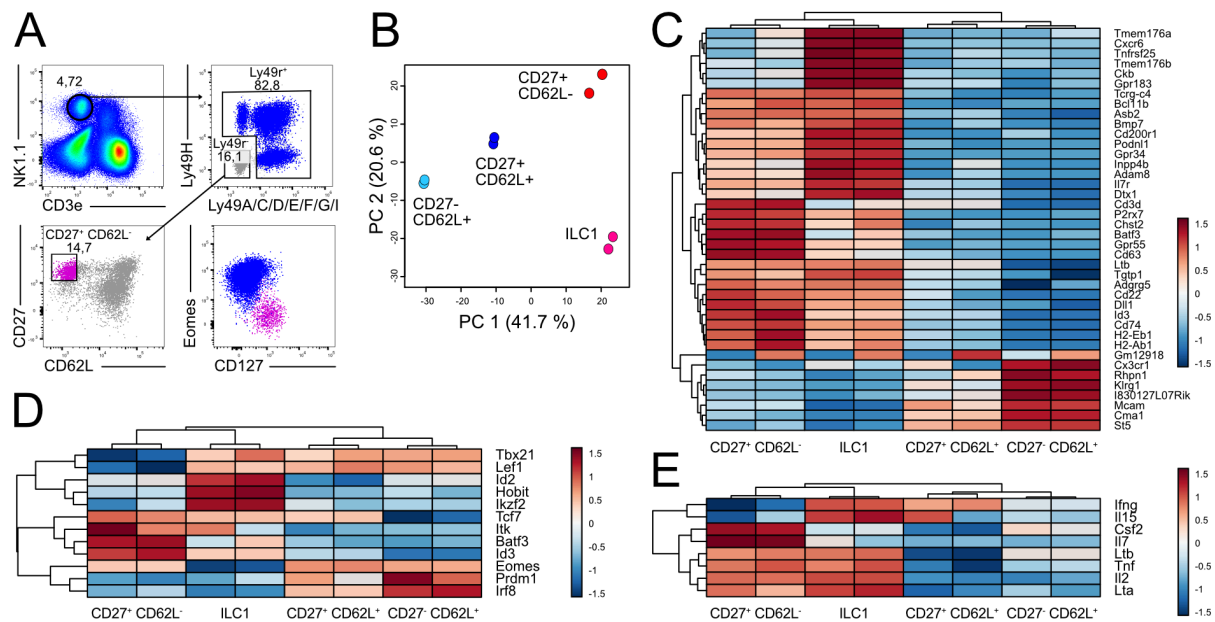


Figure 16: CD27⁺CD62L⁻ NK cells share features with ILC1s.

(A) Gating strategy for sorting ILC1s for bulk RNA-seq and expression of *Eomes* and *CD127* within the resulting population. (B) PCA of transcriptomic data from sorted NK cell subsets and ILC1. (C) Heatmap depicting 40 most variable genes in sorted NK cell subsets and ILC1. (D) Comparison of the same groups as in (C) regarding transcripts of cytokines. (E) Comparison of the same groups as in (C) regarding transcripts of transcription factors. Data in (B)-(E) are representative of 2 independent experiments. (modified from (Flommersfeld et al., 2021))

Antibody staining of *Eomes* further confirmed that CD27⁺ CD62L⁻ and CD27⁺ CD62L⁺ NK cells expressed equally high levels of the transcription factor, whereas ILC1s did not show relevant *Eomes* expression (**Figure 17, left panel**). Furthermore, absolute numbers of both subsets were similarly reduced in *Nkp46*^{iCre} x *Eomes*^{flox/flox}, in which *Eomes* is depleted in

Results

NKp46⁺ cells (**Figure 17, left panel**). This indicates that Eomes is not only expressed by both NK cell subsets, but also critical for their development. Finally, while the transcriptional profile of sorted ILC1s perfectly matched with a published dataset of ILC1-specific genes (Weizman et al., 2017), CD27⁺ CD62L⁻ NK cells clearly differed from this ILC1 signature. In conclusion, CD27⁺ CD62L⁻ NK cells show transcriptional similarity to ILC1s but also a clear NK cell signature. Therefore, this NK cell subset will be referred to as “ILC1-like NK cells” in the following.

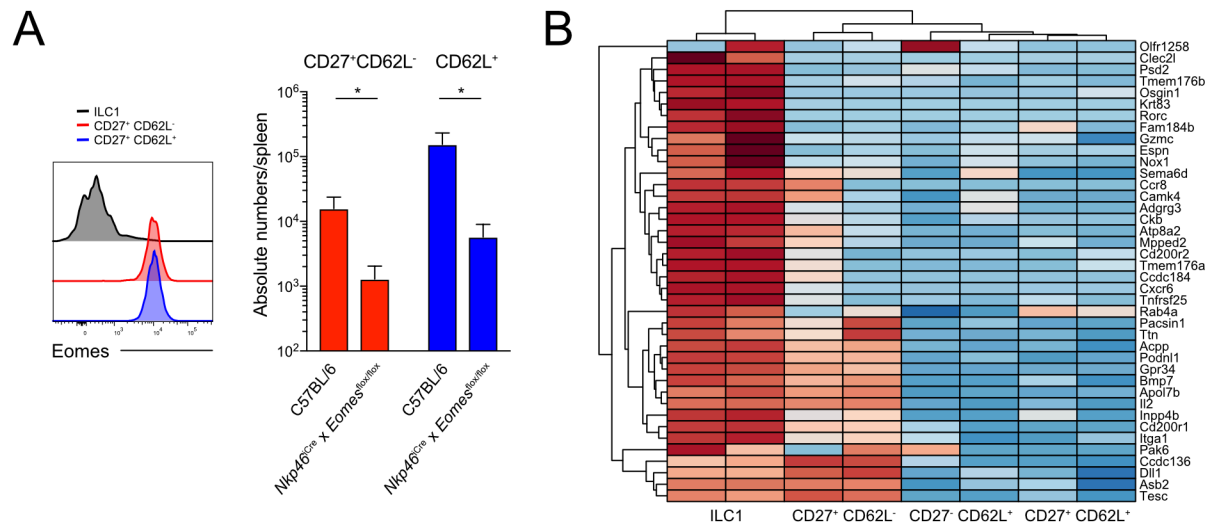


Figure 17: CD27⁺CD62L⁻ NK cells are *bona fide* NK cells.

(A) Representative histograms show Eomes expression of ILC1s, CD27⁺ CD62L⁻ and CD27⁺ CD62L⁺ Ly49H⁺ NK cells (left). Bar graph depicts absolute numbers of CD27⁺ CD62L⁻ and CD62L⁺ Ly49H⁺ NK cells in C57BL/6 and *Nkp46*^{Cre} × *Eomes*^{fllox/fllox} mice. (B) Heatmap shows relative expression of ILC1-specific genes from (Weizman et al., 2017) in sorted ILC1s and NK cell subsets.

Bars indicate mean, error bars represent SD. Significances in (A) were calculated using Mann-Whitney test. (modified from (Flommersfeld et al., 2021))

4.6 ILC1-like NK cells unite important characteristics of NK cells and ILC1s

Next, we sought to corroborate conclusions from the RNA-seq data by functional assays. To address their ability to produce cytokines, CD27⁺ CD62L⁻ (ILC1-like NK cells), CD27⁺ CD62L⁺ and CD27⁻ CD62L⁺ Ly49H⁺ NK cells were sorted, stimulated *ex vivo* with PMA and ionomycin in the presence of a protein transport inhibitor and then subjected to intracellular cytokine staining. The analysis confirmed that ILC1-like NK cells are potent cytokine producers of IFN- γ , TNF- α and GM-CSF, while conventional NK cells only produced IFN- γ (**Figure 18A+B**). Moreover, ILC1-like NK cells isolated from the spleen of C57BL/6 mice showed enhanced IFN- γ production compared to CD27⁺ CD62L⁺ NK cells at 24 hours p.i. with MCMV and after stimulation with plate-bound anti-NK1.1 antibody (**Figure 18C+D**).

Results

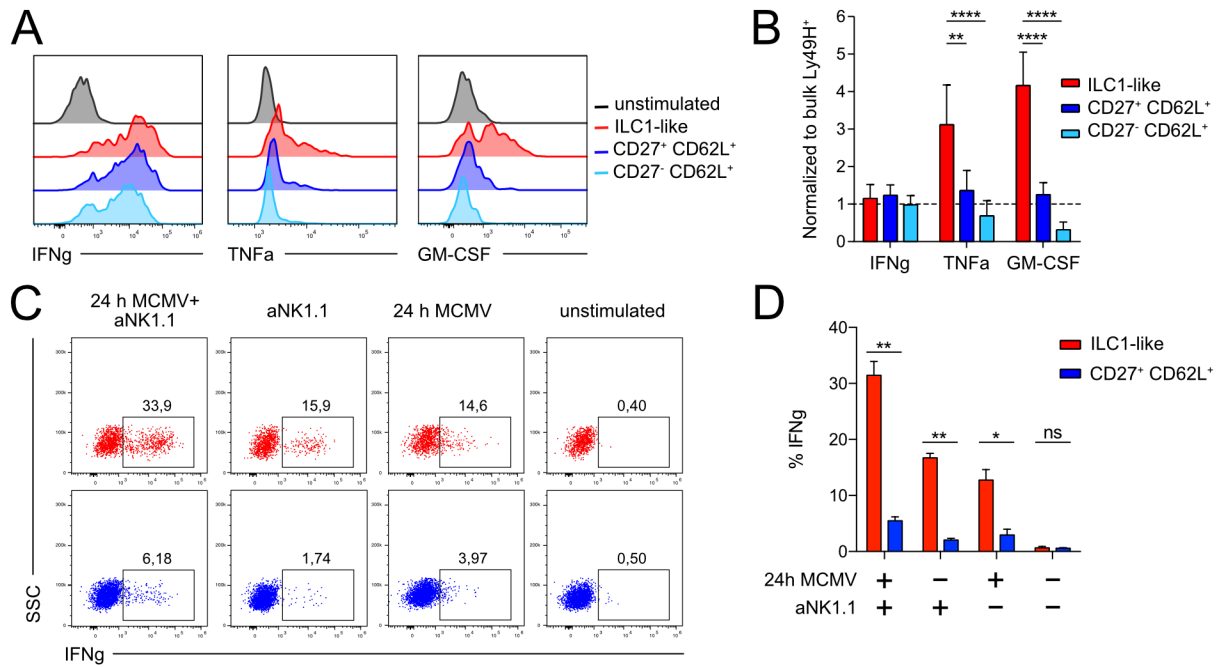


Figure 18: ILC1-like NK cells show enhanced cytokine production.

(A) Sorted CD27⁺ CD62L⁻ (ILC1-like NK cells), CD27⁺ CD62L⁺ and CD27⁻ CD62L⁺ Ly49H⁺ NK cells were stimulated with PMA and ionomycin in the presence of a protein transport inhibitor. Representative histograms show IFN- γ , TNF- α and GM-CSF expression of sorted NK cell subsets and unstimulated Ly49H⁺ NK cells as negative control. (B) Bar graph depicts cytokine production of Ly49H⁺ NK cell subsets after stimulation with PMA and ionomycin normalized to cytokine production of stimulated bulk Ly49H⁺ NK cells within the same experiment. (C+D) C57BL/6 mice were infected with MCMV or left uninfected as negative control. Splenocytes were harvested 24 h p.i. and restimulated with plate-bound aNK1.1 antibody where indicated in the presence of a protein transport inhibitor. IFN- γ production was determined by flow cytometry. (C) Representative dot plots and (D) bar graph depict IFN- γ production of ILC1-like NK cells (red) and CD27⁺ CD62L⁺ (blue) Ly49H⁺ NK cells. 24 h p.i. and after aNK1.1 restimulation.

Data in (A), (C) and (D) are representative of 2-3 independent, similar experiments. Data in (B) are pooled from 3 independent experiments. Bars indicate mean. Error bars represent SD. Significances in (B) are calculated using two-way ANOVA, followed by Tukey's multiple comparisons test. Significances in (D) are calculated using two-way ANOVA, followed by Sidak's multiple comparisons test. (modified from (Flommersfeld, 2018) and (Flommersfeld et al., 2021))

In addition to corroborating their enhanced capacity to produce cytokines, it was important to validate that ILC1-like NK cells show features specific for NK cells. Among these are activating Ly49 receptor signaling and strong target-specific cytotoxicity, which are both thought to be restricted to NK cells. To assess target recognition via the activating receptor Ly49H, ILC1-like as well as CD27⁺ CD62L⁺ Ly49H⁺ NK cells were sorted and co-incubated for 24 hours with either Ba/F3 WT or Ba/F3-m157 cells. These target cells are pro-B cell lines, the latter of which expresses m157, the ligand of Ly49H. After co-culture, we measured Ly49H geometric mean fluorescence intensity (GeoMFI) of the NK cells via antibody staining. Both subsets showed ligand-induced downregulation of the Ly49H receptor (**Figure 19A+B**).

Although we already learnt from RNA-seq analysis and antibody staining that ILC1-like NK cells show very limited granzyme B expression at steady state (**Figure 14D+E**, **Figure 15B**),

Results

to that point no conclusion could be drawn whether they express granzyme B and are able to provide target-specific cytotoxicity upon activation. Therefore, single ILC1-like as well as CD27⁺ CD62L⁺ Ly49H⁺ NK cells were adoptively transferred into *Rag2*^{-/-} *Il2rg*^{-/-} mice and at day 8 p.i. granzyme B expression of the expanded clones was assessed. NK cell clones from either subset displayed equally high levels of granzyme B expression (**Figure 19C+D**). Finally, ILC1-like NK cells that were sorted from C57BL/6 mice 24 h after infection with MCMV, killed RMA-S target cells with similar efficacy as cNK cells (**Figure 19E**). RMA-S cells – in contrast to RMA cells – lack MHC class I expression and are thereby targeted by NK cells via missing self-recognition (Ljunggren et al., 1991). In summary, ILC1-like NK cells were shown to be potent cytokine producers that receive signaling via Ly49H and show target-specific cytotoxicity. Consequently, they unite critical features of both ILC1s and NK cells.

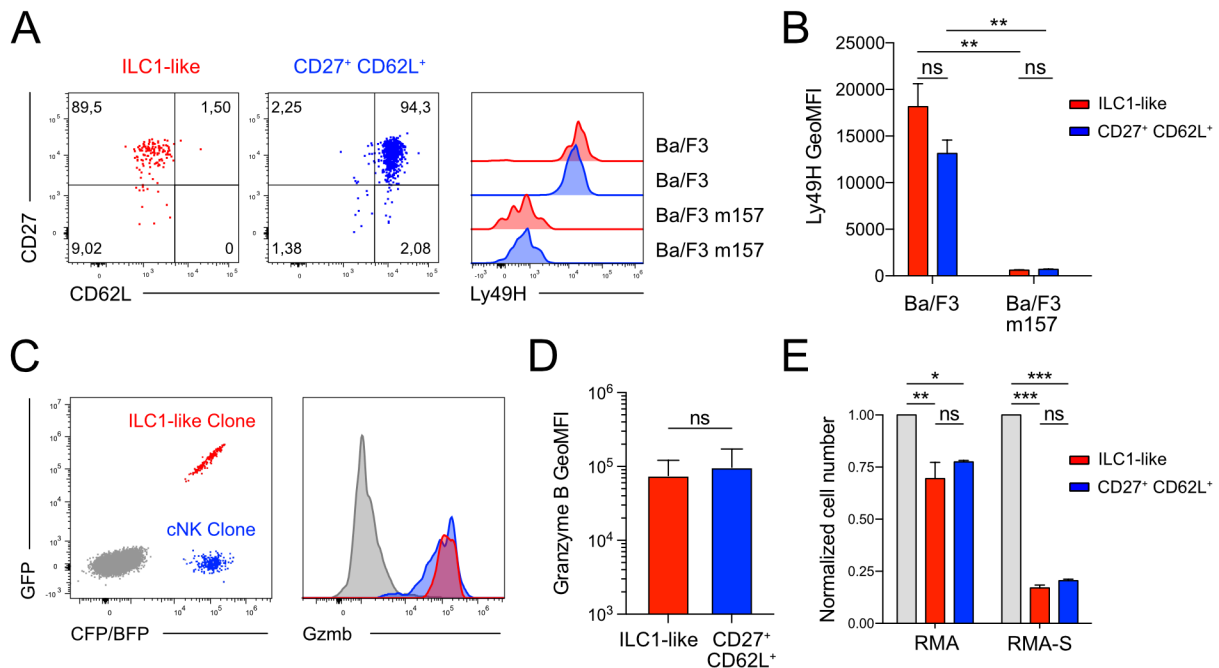


Figure 19: ILC1-like NK cells receive signaling via Ly49H and show target-specific cytotoxicity.

(A+B) Sorted Ly49H⁺ ILC1-like and CD27⁺ CD62L⁺ NK cell populations were co-incubated with Ba/F3 WT cells or Ba/F3-m157 cells for 24 h. (A) Dot plots show sort purity, histograms show the Ly49H expression. (B) Bar graph depicts Ly49H GeoMFI. (C) Granzyme B expression of single-cell-derived progenies was determined by flow cytometry. Dot plot depicts color barcode of progenies derived from a single ILC1-like NK cells (Clone 1, red) or CD27⁺ CD62L⁺ cell (Clone 2, blue). Representative histograms show granzyme B expression levels of clone 1 (red), clone 2 (blue) and endogenous non-NK cells as negative control (gray). (D) Bar graph depicts granzyme B GeoMFI of progenies derived from single ILC1-like NK cells or CD27⁺ CD62L⁺ Ly49H⁺ NK cells. (E) Ly49H⁺ ILC1-like or CD27⁺ CD62L⁺ NK cells were sorted from the spleen of C57BL/6 mice 24 hours p.i. with MCMV and incubated with equal numbers of GFP⁺ RMA and BFP⁺ RMA-S cells for 42 hours. Bar graph depicts normalized counts of RMA and RMA-S cells in the absence of NK cells (grey) and after co-incubation with Ly49H⁺ ILC1-like NK cells (red) and CD27⁺ CD62L⁺ (blue) NK cells.

Data in (A), (B), (C) and (E) are representative of 2-3 independent, similar experiments. Data in (D) are pooled from 3 independent experiments. Bars indicate mean. Error bars represent SD. Significances in (B) and (E) are calculated using two-way ANOVA, followed by Tukey's multiple comparisons test. Significances in (D) are calculated using Mann-Whitney test. (modified from (Flommersfeld et al., 2021))

Results

4.7 ILC1-like NK cells are not immature precursors of conventional NK cells

So far, the data indicated that ILC1-like NK cells represent a distinct NK cell subset that differs from conventional NK cells phenotypically – both at steady state and upon MCMV infection – and has a unique transcriptional profile as well as functional characteristics. However, NK cells undergo continuous maturation during homeostasis and therefore, it was important to analyze whether ILC1-like NK cells actually represent immature progenitors of conventional NK cells or a separate NK cell lineage that does not participate in steady state maturation (**Figure 20A**).

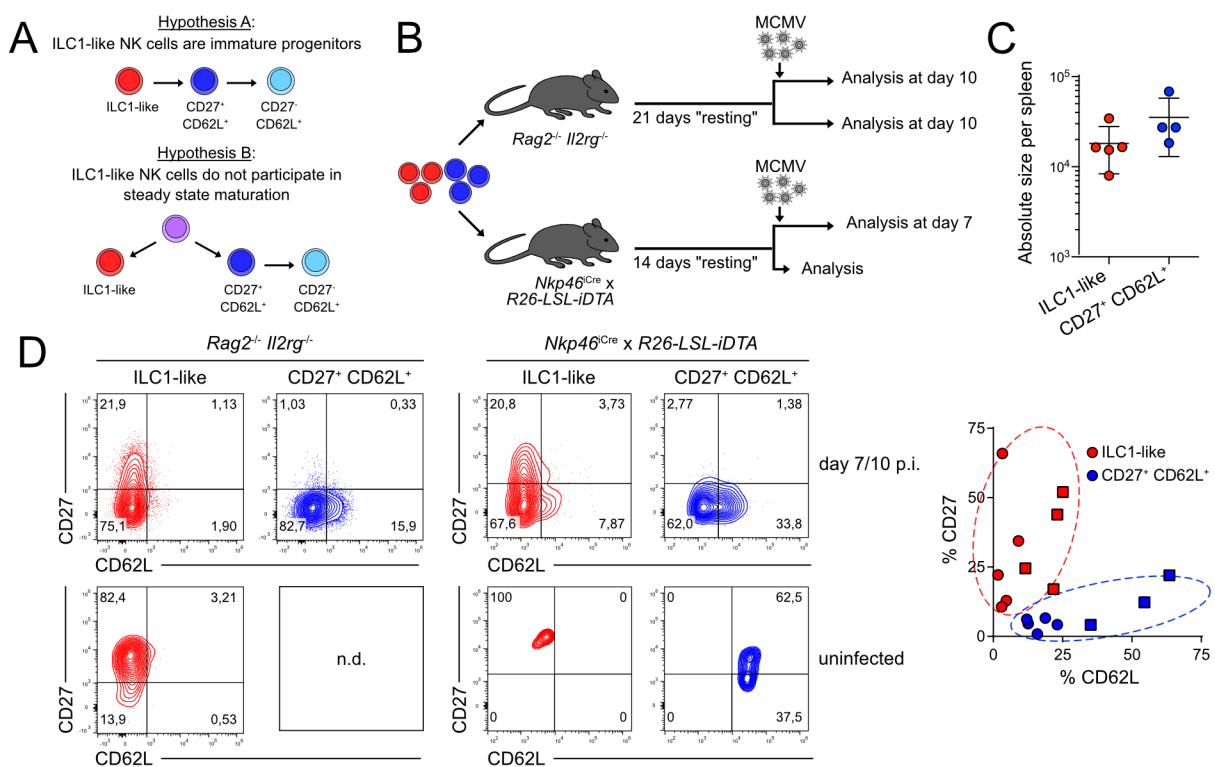


Figure 20: ILC1-like NK cells do not serve as precursors of cNK cells.

(A) Schemes depict two possible scenarios of NK cell differentiation. ILC1-like NK cells represent a transient, immature differentiation state (upper panel) or a stable subset that does not participate in steady state maturation (lower panel). (B-D) Ly49H⁺ ILC1-like NK cells and CD27⁺ CD62L⁺ NK cells were sorted and adoptively transferred into *Nkp46^{Cre} x R26-LSL-iDTA* or *Rag2^{-/-} Il2rg^{-/-}* mice. After 14 or 21 days, respectively, recipients were infected with MCMV or left uninfected and analyzed by flow cytometry. Uninfected controls were analyzed 14 (14+0) or 31 (21+10) days after initial adoptive transfer. Expanded Ly49H⁺ NK cell populations were analyzed at day 7 or 10 p.i., respectively. (B) Schematic representation. (C) Absolute size of expanded ILC1-like and CD27⁺ CD62L⁺ Ly49H⁺ NK cell populations in *Rag2^{-/-} Il2rg^{-/-}* at day 10 p.i. (D) Representative contour plots show CD27 and CD62L expression profiles of NK cell populations at day 7/10 p.i. (upper panel) and in uninfected controls (lower panel). Scatter plot depicts frequency of CD27 and CD62L expressing cells within expanded populations at day 7/10 p.i. in *Nkp46^{Cre} x R26-LSL-iDTA* (squares) and *Rag2^{-/-} Il2rg^{-/-}* (circles). Data in (C) are pooled from 2 independent, similar experiments. Data in (D) are pooled from 4 independent experiments. (modified from (Flommersfeld, 2018) and (Flommersfeld et al., 2021))

Results

To assess this question, populations of ILC1-like and CD27⁺ CD62L⁺ Ly49H⁺ NK cells were sorted and adoptively transferred into either *Nkp46*^{iCre} x *R26-LSL-iDTA* or *Rag2*^{-/-} *Il2rg*^{-/-} recipients. The cells were rested under homeostatic conditions for 2 or 3 weeks, respectively, and then either analyzed directly without infection or mice were infected and their progeny was analyzed at day 7 or 10 p.i., respectively (**Figure 20B**). Both subsets generated responses of similar size upon infection with MCMV (**Figure 20C**) and maintained their distinct response patterns (**Figure 20D, upper panel and scatter plot**). ILC1-like NK cells that were recovered from uninfected mice, appeared to stably retain their CD27⁺ CD62L⁻ phenotype and not give rise to CD62L⁺ NK cells (**Figure 20D, lower panel**).

As adoptive transfer could bias the developmental capacity of the respective NK cell subsets, RNA velocity analysis was performed to study the developmental potential of these subsets under steady-state conditions. RNA velocities provide a tool to study single cell differentiation trajectories from scRNA-seq datasets by measuring the ratio of spliced and unspliced mRNAs (La Manno et al., 2018). Thus, we generated retrogenic chimeras and performed scRNA-seq of Ly49H⁺ NK cells isolated from the spleen of these retrogenic donor mice 4 weeks after HSC transplantation (**Figure 21A**). As in these mice the immune cell compartment is newly replenished from transplanted stem cells, we suggested them to be ideal to assess the developmental relationship of ILC1-like and CD62L⁺ NK cells. Within these newly generated NK cells we could identify a cluster of cells characterized by high expression of transcripts encoding for CD160 and XCL1 as well as low granzyme B expression representing ILC1-like NK cells. However, we could not measure differentiation activity from this cluster towards conventional NK cells confirming the hypothesis that ILC1-like NK cells do not act as precursors of CD62L⁺ NK cells (**Figure 21B**). By performing RNA velocity analysis on a published scRNA-seq dataset from human spleen NK cells (Crinier et al., 2018) we found a similar bifurcation of differentiation trajectories ending up in two distinct clusters. One of them was defined by high transcript levels of *CD160* and *XCL1* and low levels of *GZMB* while the second one was enriched for *GZMB* mRNA but lacking *CD160* and *XCL1* expression – similar to our observations in murine spleen (**Figure 21C**).

Results

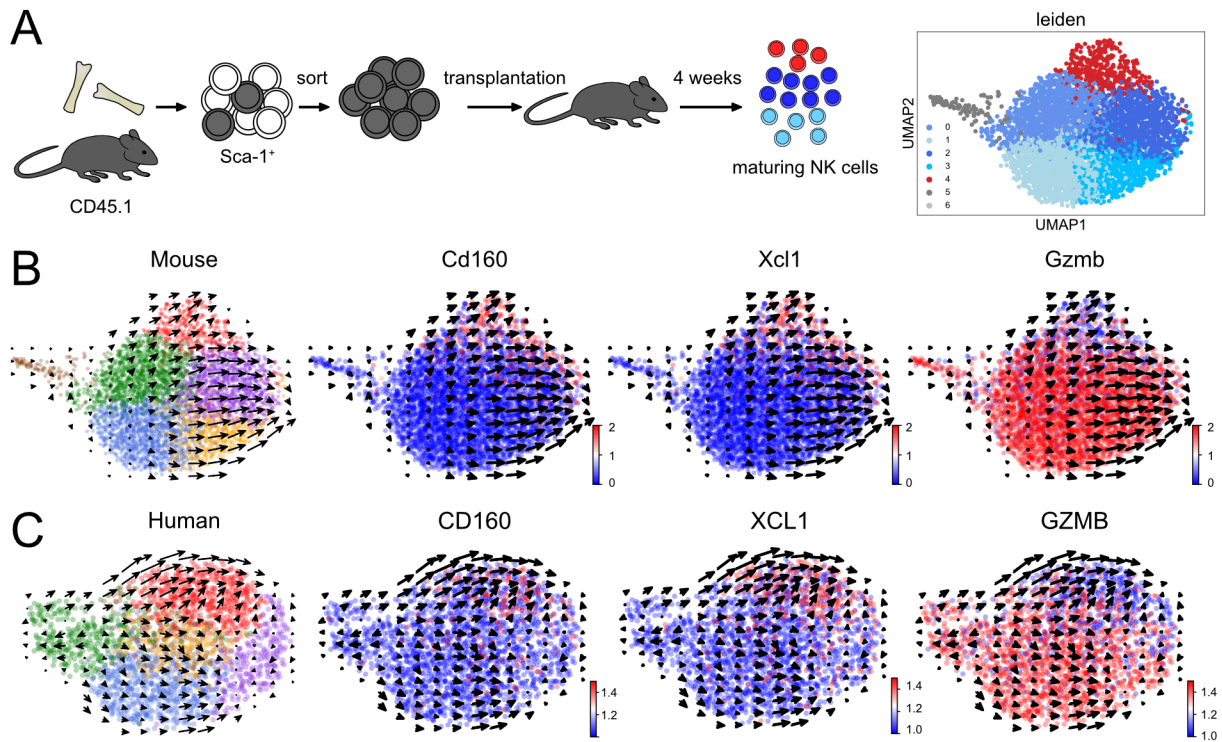


Figure 21: RNA velocities suggest no differentiation activity of ILC1-like NK cells towards cNK cells.

(A) Schematic of stem cell transfer and UMAP-based Leiden clustering of HSC-derived Ly49H⁺ NK cells. (B) RNA velocities derived from scRNA-seq of retrogenic Ly49H⁺ NK cells 4 weeks after HSC transfer. Colors indicate relative expression of the indicated genes. (C) RNA velocities in scRNA-seq data of one human donor (blood and spleen) from (Crinier et al., 2018). Colors indicate relative expression of the indicated genes. (modified from (Flommersfeld et al., 2021))

Previous experiments had already shown that both NK cell subsets generated CD27⁻ CD62L⁻ progeny upon infection with MCMV, however, it was unclear whether these terminally differentiated cells are still distinct with respect to the expression of markers other than CD27 and CD62L. Therefore, ILC1-like NK cells and CD27⁻ CD62L⁺ Ly49H⁺ cNK cells were adoptively transferred into *Rag2*^{-/-} *Il2rg*^{-/-} recipients that were infected with MCMV. At day 8 p.i., different populations were sorted from the progeny of either ILC1-like or cNK cells. In detail, CD45.1⁺ Ly49H⁺ CD27⁺ CD62L⁻ as well as CD27⁻ CD62L⁻ NK cells were sorted from ILC1-like progeny and CD45.1⁺ Ly49H⁺ CD27⁻ CD62L⁺ as well as CD27⁻ CD62L⁻ NK cells from cNK progeny (**Figure 22A**). Differential gene expression and principal component analysis of the four populations indicated that CD27⁻ CD62L⁻ cells, derived from either subset, are still transcriptionally distinct and maintain a subset-specific transcriptional signature, e.g. *Cd160* and *Cd7* expression is higher in cells originating from ILC1-like NK cells whereas cNK daughter cells retain elevated transcript levels of *Sell* and *Cx3cr1* (**Figure 22B**).

Results

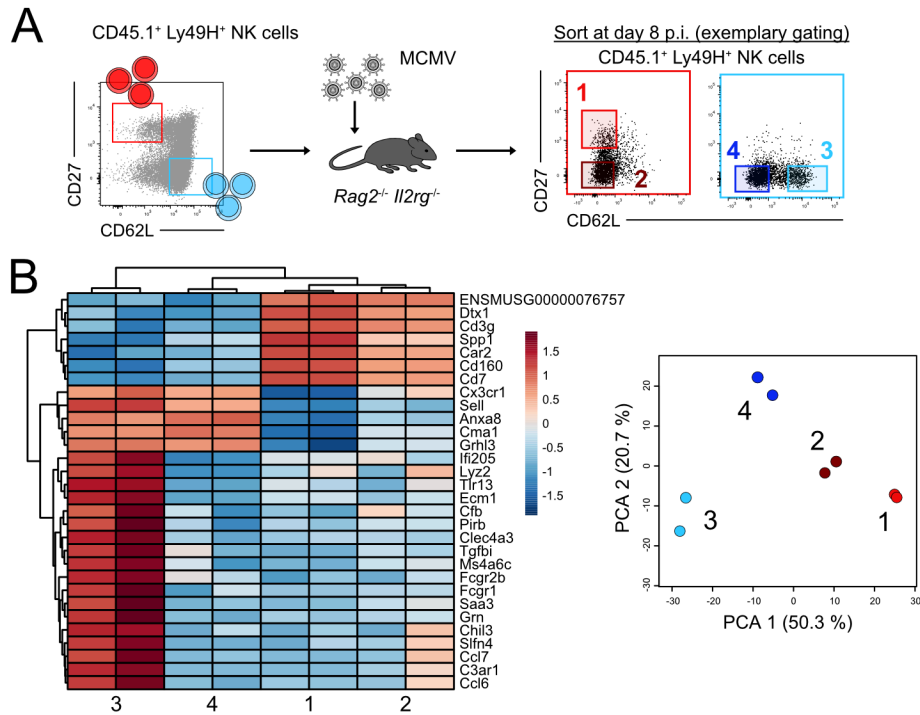


Figure 22: Transcriptional profiles of cNK and ILC1-like NK cells remain distinct upon MCMV infection.

(A+B) Ly49H⁺ ILC1-like NK cells and CD27⁻ CD62L⁺ NK cells were sorted and adoptively transferred into *Rag2*^{-/-} *Il2rg*^{-/-} recipients, followed by MCMV infection. Populations with indicated expression of CD27 and CD62L were sorted from the population-derived progenies detected in spleen at day 8 p.i. (A) Schematic depicts experimental setup and gating strategy during sort. (B) Heatmap depicting 30 most variable genes and PCA of sorted NK cell populations.

(modified from (Flommersfeld et al., 2021))

4.8 ILC1-like NK cells are restricted to lymphoid organs and tissue-resident in the spleen

Flow cytometric analysis of NK cells in spleen, mesenteric lymph nodes and blood showed that ILC1-like NK cells are restricted to lymphoid organs while largely absent from blood (Figure 23A). To further corroborate the existence of ILC1-like NK cells within the lymph nodes, Ly49H⁺ and Ly49H⁻ NK cells (distinguishable via hashtag antibody staining) were sorted from peripheral lymph nodes and subjected to scRNA-seq analysis. To identify ILC1-like NK cells based on their transcriptome, a subset score was generated from the spleen data shown in Figure 15A. Therefore, the resolution of the leiden clustering was adjusted to separate two distinct clusters representing ILC1-like and cNK cells. The top 20 defining genes for each cluster were considered for generation of the subset score. Cells that are transcriptionally similar to ILC1-like NK cells show a positive score whereas a negative value indicates similarity to cNK cells (Figure 23B). Lymph node NK cells could also be separated into two transcriptionally distinct leiden clusters. One of them (cluster 0) showed a positive subset score indicating an enrichment of genes that are overrepresented in ILC1-like NK cells within this cluster, while cluster 1 was

Results

enriched for cNK-defining transcripts (**Figure 23C**). These findings were supported by the gene expression of marker genes identified before: Cluster 0, that was assigned to ILC1-like NK cells, showed high levels of transcripts encoding for CD7 and *Ltb* as well as reduced *Gzma* and *Gzmb* expression (**Figure 23D**). Also in lymph nodes, RNA velocity analysis provided no evidence that ILC1-like NK cells might serve as precursors of cNK cells (**Figure 23E**).

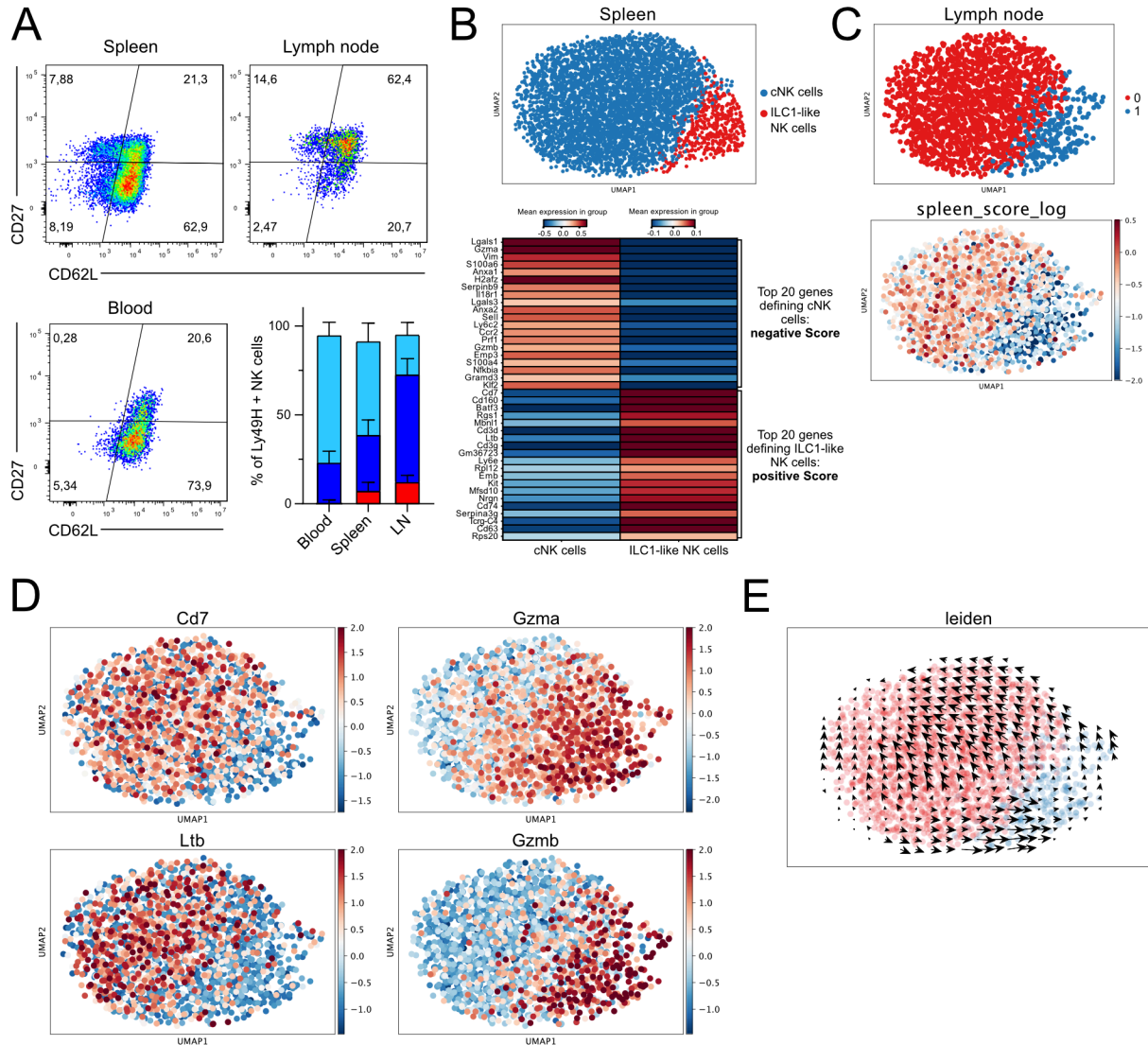


Figure 23: ILC1-like NK cells are overrepresented in lymphoid tissues.

(A) Representative pseudocolor plots show CD27 and CD62L expression of Ly49H⁺ NK cells in blood, spleen and mesenteric lymph nodes. Bar graphs show frequency of ILC1-like, CD27⁺ CD62L⁺ and CD27⁻ CD62L⁺ NK cells of Ly49H⁺ NK cells within different organs. (B) Resolution of leiden clustering from scRNA-seq of splenic NK cells was adjusted to segregate single-cell transcriptomes into two clusters representing ILC1-like NK cells and cNK cells. Top 20 defining genes of these two clusters are shown in a heatmap. (C) scRNA-seq of NK cells from inguinal, brachial and axillary lymph nodes of naïve C57BL/6 mice. UMAP projection and leiden clustering was set to a resolution that defines two clusters. A score that shows similarity to ILC1-like NK cells from the spleen was derived from the 40 defining genes in (B) and plotted in the scRNA-seq data from lymph nodes. (D) Marker gene expression in clusters found in lymph nodes. (E) RNA velocity analysis of NK cells from lymph nodes.

Lines represent mean, error bars indicate SD. (modified from (Flommersfeld et al., 2021))

Results

The finding that ILC1-like NK cells are present in lymphoid organs but do not circulate in peripheral blood as well as the observation that they express several markers for tissue-residency (Figure 14E, Figure 15B), suggested that ILC1-like NK cells might show splenic residency. To test this hypothesis, parabiosis experiments were performed by our collaborators Jonatan Ersching and Gabriel Victora at the Rockefeller University in New York. During parabiosis, two mice are joined surgically and share blood circulation. Consequently, all circulating cells are exchanged between the two parabionts while tissue-resident cells that do not enter the circulation, do not mix. The two parabionts expressed distinct congenic markers and thereby the origin of the cells could be determined by flow cytometry. Four weeks after the surgery, the frequency of endogenous and exogenous cells was measured for each NK cell subset (Figure 24A).

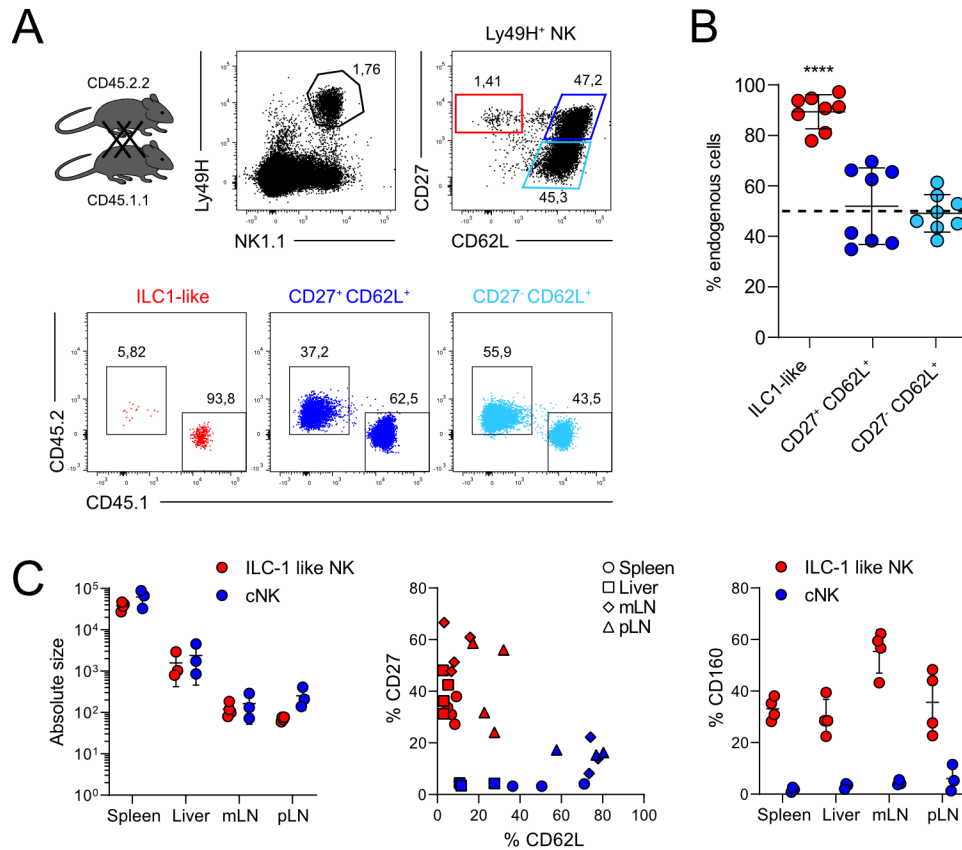


Figure 24: ILC1-like NK cells are tissue-resident in the spleen at steady state, but show a similar homing profile compared to cNK cells upon adoptive transfer.

(A) Spleens of CD45.1.1 and CD45.2.2 parabionts were analyzed 4 weeks after surgery by flow cytometry. Representative dot plots show gating of ILC1-like, CD27⁺ CD62L⁺ and CD27⁻ CD62L⁻ Ly49H⁺ NK cells and frequency of CD45.1 and CD45.2 cells within each subset. (B) Frequency of endogenous cells within Ly49H⁺ NK cell subsets after parabiosis.

Data in (A) and (C) are representative of 2 independent, similar experiments. Data in (B) are pooled from 2 independent, similar experiments. Lines represent mean, error bars indicate SD. Significances in (B) were calculated using one-sample t-test (hypothetical value = 50). (modified from (Flommersfeld et al., 2021))

Results

Indeed, whereas cNK cells had completely equilibrated between the host and the parabiont, ILC1-like NK cells were still almost completely derived from the host and thereby exhibited splenic residency at steady state (**Figure 24B**). This finding raised the question whether ILC1-like NK cells also show preferential homing to the spleen upon adoptive transfer. Therefore, Ly49H⁺ ILC1-like and CD27⁺ CD62L⁺ cNK cells were adoptively transferred into *Nkp46*^{iCre} x *R26-LSL-iDTA* recipients infected with MCMV. At day 8 p.i., spleen, liver, mesenteric and peripheral lymph nodes were harvested and analyzed by flow cytometry. Both ILC1-like and cNK cells showed similar homing profiles and were recovered from all analyzed organs while remaining phenotypically distinct with respect to CD27, CD62L and CD160 (**Figure 24C**). These data showed that upon adoptive transfer ILC1-like NK cells were not exclusively targeted to the spleen but instead homed to different organs.

4.9 ILC1-like NK cells and cDC1s form clusters early during MCMV infection

As pointed out before, ILC1-like NK cells express XCL1 and CRTAM and are thereby, at least in theory, well equipped to interact with cDC1s expressing XCR1 as well as Necl2. In collaboration with Jan Böttcher and Philippa Meiser, confocal imaging was used to assess whether resident ILC1-like NK cells indeed share a niche with cDC1s in the spleen. Therefore, spleens were isolated from both MCMV-infected *Xcr1*^{Venus/wt} mice as well as uninfected controls and spleen sections were stained with respective antibodies. In these mice, the gene encoding for the fluorescent reporter Venus is inserted into the *Xcr1* locus. Heterozygous animals show expression of Venus as a reporter for XCR1⁺ cDC1s, but still express the chemokine receptor at the cell surface. To enhance detection of the Venus signal, an anti-GFP antibody that is cross-reactive against Venus, was used. Anti-NK1.1 and anti-Ly49H antibodies were used to identify Ly49H⁺ NK cells. Of note, these antibodies were stained via intravascular injection as Ly49H staining does not work after tissue fixation. It was ensured that i.v. injection of the antibodies enabled labelling of the complete Ly49H⁺ NK cell compartment in the red pulp (data not shown). ILC1-like NK cells were discriminated from cNK cells by CD160 staining, as CD62L staining was not suitable for fixed samples and in addition, the marker is also expressed by many other cell types, e.g. T cells, in the spleen and consequently, high staining density and cellular overlap would make it very difficult to identify CD62L⁻ NK cells. Surfaces of NK cell subsets and cDC1s were reconstructed from confocal immunofluorescence images and used to measure the distances between the respective cell types. In uninfected mice,

Results

ILC1-like NK cells were already located significantly closer to cDC1s compared to cNK cells. Intriguingly, at 24 hours p.i. with MCMV, clustering of cDC1s and NK cells was observed in the red pulp. Within these clusters, ILC1-like NK cells were largely overrepresented resulting in a clear co-localization of cDC1s and ILC1-like NK cells (**Figure 25A**). This co-localization was almost abrogated in *Xcr1*^{Venus/Venus} mice which are XCR1-deficient, due to the double knock-in of the *Venus* gene into the *Xcr1* locus (**Figure 25B**). This showed that the interaction between ILC1-like NK cells and cDC1s was mediated, at least in part, by the XCL1/XCR1 axis.

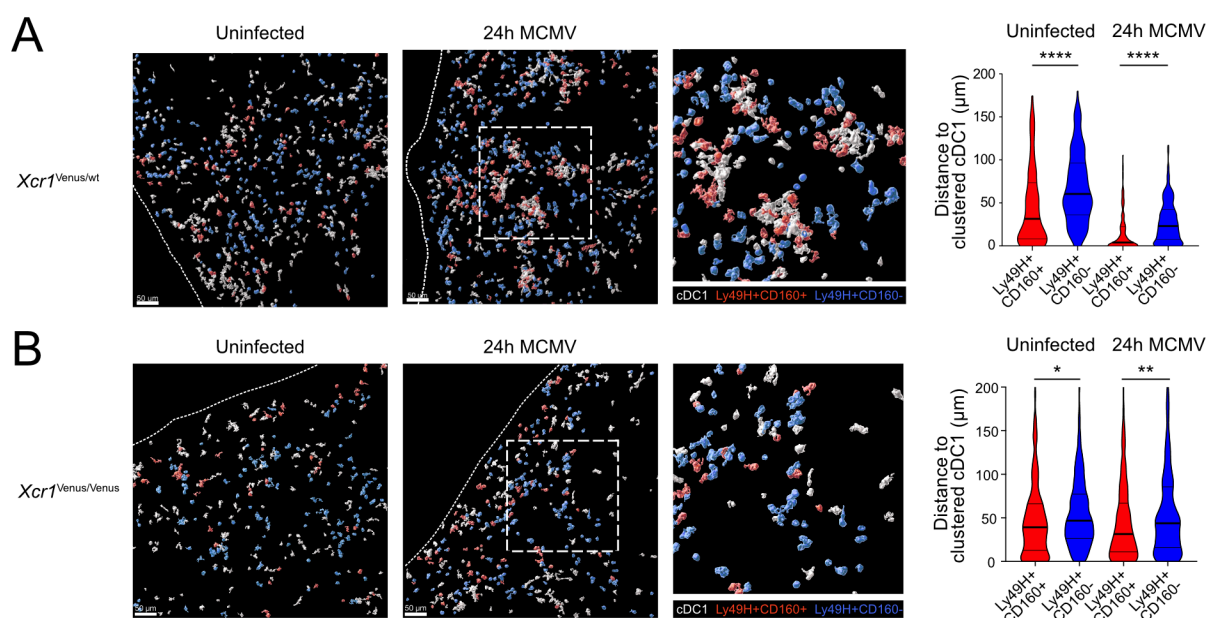


Figure 25: ILC1-like NK cells cluster with cDC1s early during MCMV infection in an XCR1-dependant manner.

(A) Visualization of cDC1s, Ly49H⁺ CD160⁺ NK cells and Ly49H⁺ CD160⁻ NK cells in MCMV-infected spleens of *Xcr1*^{Venus/wt} or uninfected controls by confocal microscopy. Depicted are three-dimensional cell objects of individual cells identified via histo-cytometry. Staining for NK1.1, Ly49H and CD160 was used to identify NK cell subsets, anti-GFP (cross reactive with XCR1-Venus) was used for identification of splenic cDC1s. Violin plot shows quantification of distances between CD160⁺ or CD160⁻ Ly49H⁺ NK cells and clustered cDC1 with and without MCMV infection. A cDC1 cluster was defined as at least three cDC1 within a distance of $\leq 5\mu\text{m}$. (B) as in (A) but in *Xcr1*^{Venus/Venus} (= XCR1-deficient) mice.

Data in (A) are representative of 2 independent experiments. Lines represent mean, error bars indicate SD. Significances in (A) and (B) were calculated using Kruskal-Wallis test, followed by Dunn's multiple comparisons analysis. Dotted lines represent spleen borders, dashed squares represent zoomed areas. (modified from (Flommersfeld et al., 2021))

Distance measurements between Ly49H⁺ or Ly49H⁻ NK cells and cDC1s indicated that Ly49H⁺ NK cells are enriched relative to Ly49H⁻ NK cells within cDC1 clusters (**Figure 26A**). This observation suggested that cluster formation requires MCMV recognition of NK cells via Ly49H. In line with that, both the fraction of cDC1s in clusters as well as cluster size were largely reduced in Ly49H-deficient *Klra8*^{-/-} mice (**Figure 26B+C**). Combining the two observations that ILC1-like NK cells are enriched in cDC1 clusters and that Ly49H is actively

Results

involved in this cluster formation, suggested that ILC1-like NK cells might be the drivers of this early clustering.

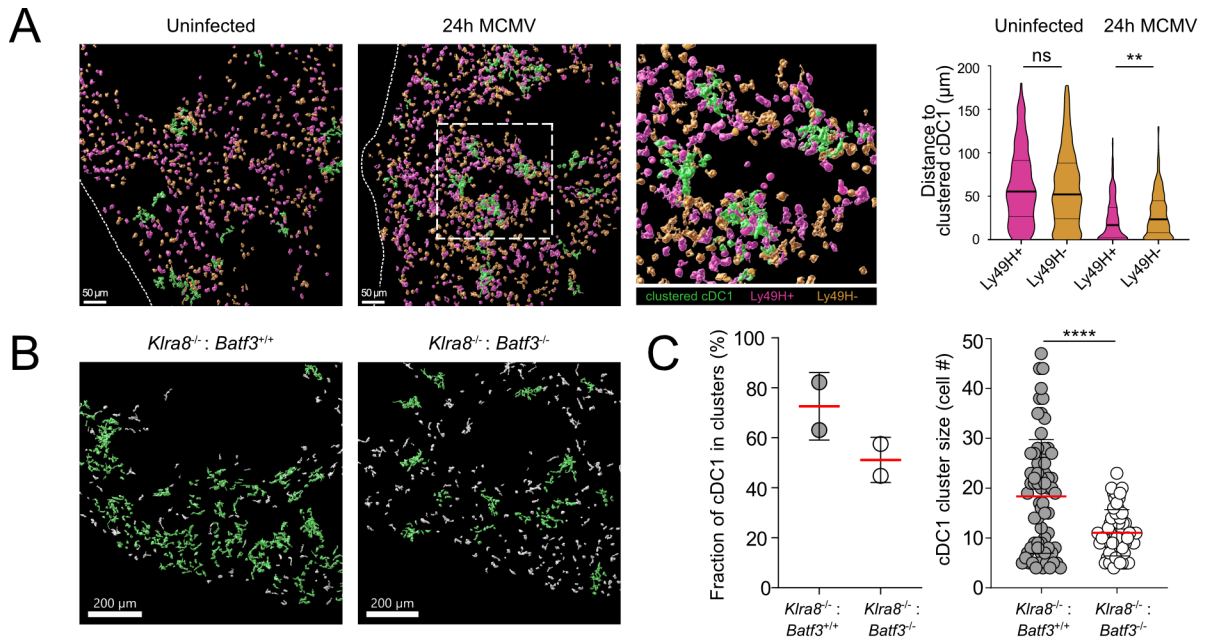


Figure 26: Clustering of ILC1-like NK cells and cDC1s requires Ly49H.

(A) Visualization of cDC1s, Ly49H⁺ and Ly49H⁻ NK cells in MCMV-infected spleens of *Xcr1*^{Venus/wt} or uninfected controls by confocal microscopy. Depicted are three-dimensional cell objects of individual cells identified via histo-cytometry. Staining for NK1.1 and Ly49H was used to identify NK cells, anti-GFP (cross reactive with XCR1-Venus) was used for identification of splenic cDC1. Violin plot shows quantification of distances between Ly49H⁺ or Ly49H⁻ NK cells and clustered cDC1s with and without MCMV infection. (B) Visualization of cDC1s (identified by intravascular staining for XCR1) in spleens of *Klra8*^{+/+} and *Klra8*^{-/-} littermates 24 hours p.i. Clustered cDC1 are indicated in green. (C) Comparison of fraction of cDC1 in clusters (left, each dot represents data for one spleen section) and cDC1 cluster sizes (right) in *Klra8*^{+/+} and *Klra8*^{-/-} mice.

Data in (B) and (C) are representative of 2 similar, independent experiments. Significances in (A) were calculated using Kruskal-Wallis test, followed by Dunn's multiple comparisons analysis. Significances in (C) are calculated using Mann-Whitney test. Lines represent mean, error bars indicate SD. Dotted lines represent spleen borders, dashed square in A represents zoomed area. (modified from (Flommersfeld et al., 2021))

Confirmation of this hypothesis required a mouse model, in which ILC1-like NK cells were specifically depleted or at least functionally impaired. Transcriptomic analysis of the NK cell subsets had shown that the transcription factor *Batf3* is exclusively expressed by ILC1-like NK cells and not by cNK cells (Figure 14E, Figure 15A) and therefore appeared as a promising candidate for a knockout model. However, comparison of the subset composition of the Ly49H⁺ NK cell compartment in *Batf3*^{-/-} versus *Batf3*^{+/+} mice showed no significant differences (Figure 27A, upper panel). Consequently, *Batf3* expression appeared not to be critical for the development of ILC1-like NK cells but still might be functionally relevant. Of note, *Batf3* expression had been described to be critical in cDC1 development and *Batf3*^{-/-} mice lack cDC1s (Hildner et al., 2008). This meant that these gene-deficient mice were not suitable to study whether a lack of *Batf3* leads to a reduction of cDC1 and NK cell clustering. This issue would

Results

be solved in a model in which specifically only Ly49H⁺ NK cells lack Batf3 expression. To this end, mixed bone marrow chimeras were generated by reconstituting irradiated *Klra8*^{-/-} mice with equal numbers of *Klra8*^{-/-} and either *Batf3*^{-/-} or *Batf3*^{+/+} bone marrow cells. In these chimeras, *Klra8*^{-/-} bone marrow cells reconstitute a fully functional immune system including cDC1s but lacking Ly49H⁺ NK cells. These instead originate exclusively from the Batf3-deficient or Batf3-competent bone marrow component. Ly49H⁺ subset composition was not altered in *Klra8*^{-/-} : *Batf3*^{-/-} chimeras in comparison to *Klra8*^{-/-} : *Batf3*^{+/+} mice (**Figure 27A, lower panel**). However, cDC1 cluster formation in *Klra8*^{-/-} : *Batf3*^{-/-} chimeras (**Figure 27B**) was similarly reduced as observed before in *Klra8*^{-/-} mice (**Figure 26B+C**). This meant, that a lack of Batf3 expression within the Ly49H⁺ NK cell compartment was sufficient to phenocopy the effects of total Ly49H-deficiency on early cDC1 clustering upon MCMV infection. This finding strongly suggested that ILC1-like NK cells are driving this early co-localization with cDC1s in the red pulp.

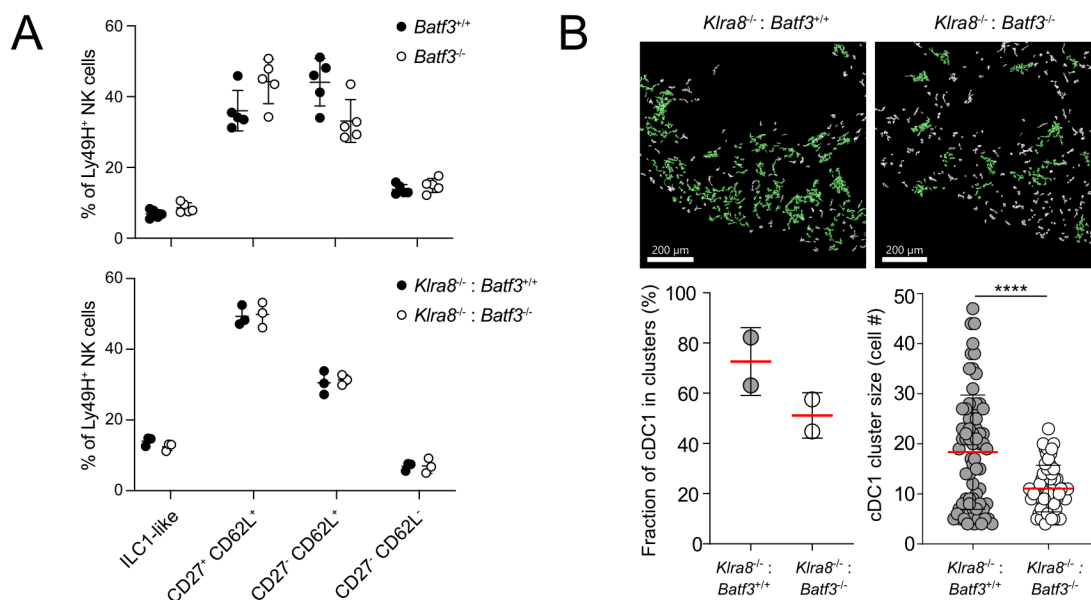


Figure 27: Clustering of ILC1-like NK cells and cDC1s requires NK-cell intrinsic expression of Batf3.

(A) Quantification of NK cell subset composition in *Batf3*^{+/+} and *Batf3*^{-/-} mice (upper panel) and *Klra8*^{-/-} : *Batf3*^{+/+} and *Klra8*^{-/-} : *Batf3*^{-/-} mixed bone marrow chimeras. (B) Visualization of cDC1s (identified by intravascular staining for XCR1) in spleens of *Klra8*^{-/-} : *Batf3*^{+/+} and *Klra8*^{-/-} : *Batf3*^{-/-} mixed bone marrow chimeras 24 hours p.i. Clustered cDC1 are indicated in green. Comparison of fraction of cDC1 in clusters (left, each dot represents data for one spleen section) and cDC1 cluster sizes (right) in *Klra8*^{-/-} : *Batf3*^{+/+} and *Klra8*^{-/-} : *Batf3*^{-/-} mice. Significances in (B) are calculated using Mann-Whitney test. Lines represent mean, error bars indicate SD. (modified from (Flommersfeld et al., 2021))

Results

4.10 Clustering of ILC1-like NK cells and cDC1s is critical for optimal priming of CD8 T cells early during MCMV infection

Finally, we wanted to assess whether the observed clusters of ILC1-like NK cells and cDC1s co-localize with infected cells and whether their formation is critical to achieve optimal priming of adaptive immune cells. cDC1s represent a subset of dendritic cells that is specialized in the cross-presentation of antigens from intracellular pathogens (den Haan et al., 2000, Schulz and Reis e Sousa, 2002, Iyoda et al., 2002). Cross-presentation plays an important role in the immune response to MCMV (Busche et al., 2013) as the virus induces downregulation of cell-surface MHC class I molecules in infected cells (Campbell and Slater, 1994, Ziegler et al., 1997, Reusch et al., 1999). Thereby, directly infected cells are weak in antigen presentation to CD8⁺ T cells.

Indeed, confocal imaging of *Klra8*^{+/+} and *Klra8*^{-/-} littermates that were infected with a GFP-expressing MCMV strain, showed that cDC1 clusters observed in wildtype mice at 24 hours p.i. co-localized with infected cells (**Figure 28A**). In *Klra8*^{-/-} mice, cluster formation was impaired resulting in increased distances between cDC1s and infected cells as well as a reduction in the fraction of cDC1s that were in direct contact to MCMV-infected cells (**Figure 28A+B**). This reduced co-localization of cDC1s and infected cells suggested less efficient uptake of cell debris or apoptotic cells and consequently less effective cross-priming of CD8⁺ T cells.

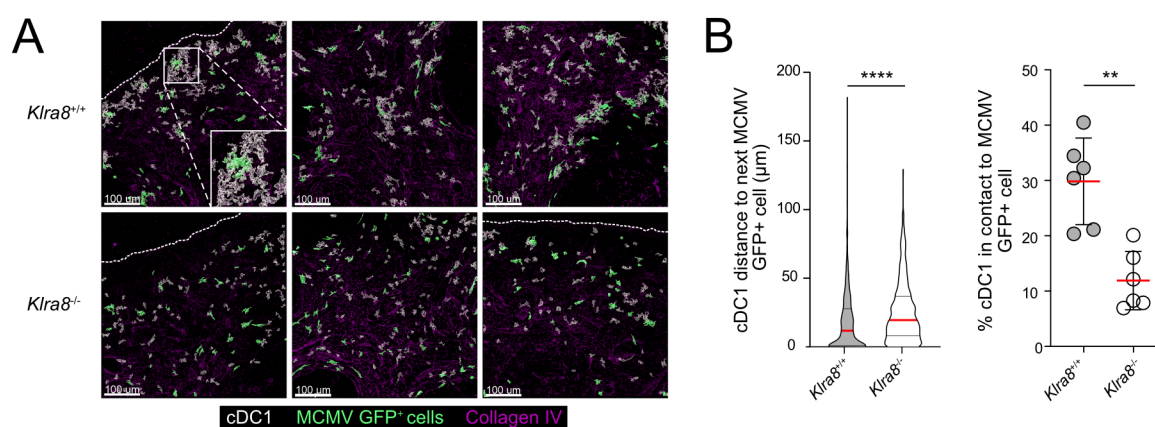


Figure 28: Co-localization of cDC1s and MCMV-infected cells is impaired in *Klra8*^{-/-} mice at 24 hours p.i.

(A) Representative images of *Klra8*^{+/+} and *Klra8*^{-/-} spleens 24 hours after infection with MCMV-*ie2*-SIINFEKL-GFP. (B) Quantification of distances between cDC1s and MCMV-infected cells in *Klra8*^{+/+} and *Klra8*^{-/-} spleens and percentage of cDC1s in contact with infected cells.

Significances in (B) are calculated using Mann-Whitney test. Lines represent mean, error bars indicate SD. Dotted lines represent spleen borders. In (B), each circle represents data for one spleen section. (modified from (Flommersfeld et al., 2021))

Results

To assess priming efficacy of CD8⁺ T cells, *Klra8^{+/+}* and *Klra8^{-/-}* littermates were infected with a recombinant MCMV strain that encodes the experimental antigen SIINFEKL under the control of the viral *ie2* promoter (MCMV-*ie2*-SIINFEKL). At 24, 48, 72 or 96 hours p.i., respectively, naïve OT-1 T cells harboring a transgenic T cell receptor (TCR) specific for SIINFEKL presented on MHC class I were injected into the infected mice. The activation status of these OT-1 T cells was analyzed 21 hours later by flow cytometry (**Figure 29A**). Importantly, MCMV titers in the spleen were elevated in *Klra8^{-/-}* mice compared to *Klra8^{+/+}* littermates at these timepoints (**Figure 29B**) due to inefficient control of the virus by NK cells. Therefore, one might expect enhanced T cell priming in *Klra8^{-/-}* mice resulting from higher antigen availability. Strikingly, the percentage of activated OT-1 T cells – identified by upregulation of CD69 and shedding of CD62L – was instead significantly reduced in *Klra8^{-/-}* mice at day 2 and 3 p.i. (**Figure 29C+D**). These findings confirmed that cross-priming of CD8⁺ T cells was reduced in the absence of Ly49H⁺ NK cells early upon MCMV infection as a consequence of the impaired co-localization of ILC1-like NK cells, cDC1s and infected cells.

To analyze whether this impaired T cell priming in *Klra8^{-/-}* mice also results in less expansion capacity of these cells throughout the course of infection, OT-1 T cells expressing distinct congenic marker combinations were adoptively transferred into *Klra8^{+/+}* or *Klra8^{-/-}* littermates, respectively, that were infected with MCMV-*ie2*-SIINFEKL. At day 2 p.i., transferred cells were isolated from the spleen of the primary recipients. These OT-1 T cells, primed in either *Klra8^{+/+}* or *Klra8^{-/-}* mice, were then co-transferred at equal numbers into infection-matched secondary wildtype recipients (**Figure 29E**). This re-transfer setup provides a possibility to compare the expansion of those two populations of OT-1 T cells longitudinally within the same environment. This is necessary as in the long run, reduced MCMV control by NK cells results in stronger T cell activation due to increased antigen load and innate cytokine levels (Mitrovic et al., 2012). The aforementioned setup is able to isolate the effects of reduced early T cell priming from these later-acting mechanisms that would outcompete initial priming differences. Following the expansion of re-transferred OT-1 T cells in peripheral blood indeed showed enhanced expansion of T cells that were primed in the presence of Ly49H⁺ NK cells, both during the acute as well as during the chronic phase of MCMV infection (**Figure 29F**).

Results

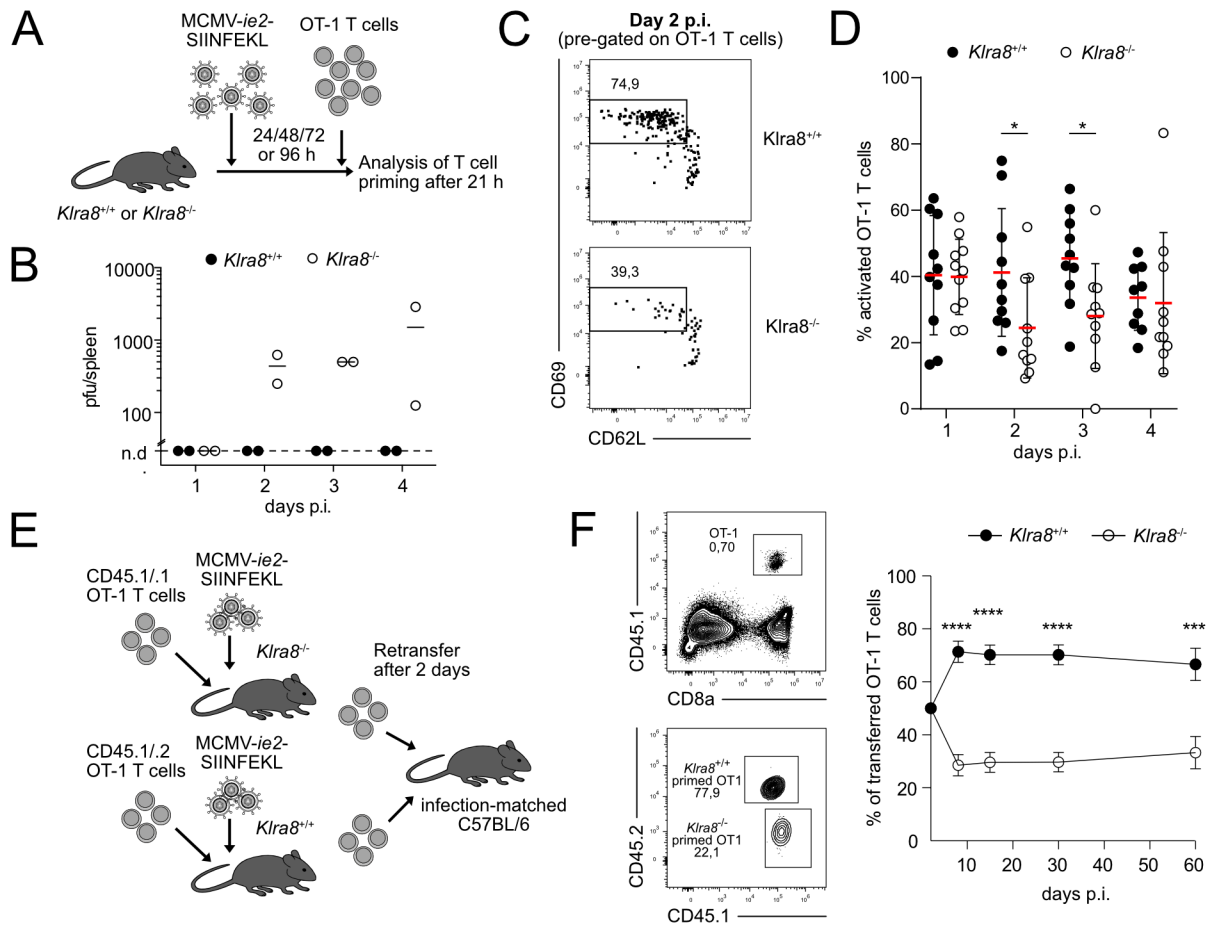


Figure 29: Optimal CD8 T cell priming upon MCMV requires expression of Ly49H.

(A) *Klra8*^{+/+} and *Klra8*^{-/-} mice were infected with MCMV-*ie2*-SIINFEKL. 1×10^6 OT-1 T cells were adoptively transferred at 24, 48, 72 and 96 h p.i., respectively. Frequency of activated OT-1 cells in the spleen was determined by flow cytometry after 21 h. (B) MCMV titers measured in the spleens of *Klra8*^{+/+} and *Klra8*^{-/-} mice infected with MCMV-*ie2*-SIINFEKL at indicated time points. (C) Representative dot plots show frequency of activated OT-1 T cells (defined as CD69⁺ CD62L⁻) in *Klra8*^{+/+} and *Klra8*^{-/-} at day 2 p.i. (D) Percentage of activated OT-1 T cells in *Klra8*^{-/-} and *Klra8*^{+/+} mice at indicated timepoints. (E) 1×10^6 CD45.1/1 and CD45.1/2 OT-1 T cells were adoptively transferred into *Klra8*^{+/+} and *Klra8*^{-/-} littermates, respectively, subsequently infected with MCMV-*ie2*-SIINFEKL. At day 2 p.i., 100 CD45.1/1 and 100 CD45.1/2 OT-1 T cells were co-transferred into infection-matched C57BL/6 recipients. (F) Expansion of CD45.1/1 and CD45.1/2 OT-1 T cells was monitored in peripheral blood. Representative contour plots show gating of CD45.1⁺ OT-1 T cells and frequency of CD45.1/1 and CD45.1/2 populations at day 30 p.i. Dot plot shows frequency of CD45.1/1 and CD45.1/2 cells among transferred OT-1 T cells in peripheral blood.

Data in (C) are representative of 5 independent, similar experiments. Data in (D) are pooled from 5 independent experiments. Lines represent mean, error bars indicate SD. Data in (F) are pooled from 4 independent experiments. Dots represent mean, error bars indicate SEM. Significances in (D) were calculated by multiple Mann-Whitney tests for each individual time point. Significances in (F) were calculated using multiple t-tests, statistical significance was determined using the Holm-Sidak method, with $\alpha=5.0\%$. (modified from (Flommersfeld et al., 2021))

To finally attribute the enhancement of early T cell priming to ILC1-like NK cells, the OT-1 priming experiment described before was repeated in *Klra8*^{-/-} : *Batf3*^{+/+} and *Klra8*^{-/-} : *Batf3*^{-/-} mixed bone marrow chimeras. The frequency of activated OT-1 T cells was significantly reduced in *Klra8*^{-/-} : *Batf3*^{-/-} mixed bone marrow chimeras at day 2 p.i. in comparison to their wildtype counterparts (Figure 30A). This indicated that NK-cell intrinsic *Batf3* expression is

Results

critical to achieve optimal priming of CD8⁺ T cells early during MCMV infection. To ensure that this reduction in T cell priming efficacy was not the result of lower cDC1 numbers in *Klra8*^{-/-} : *Batf3*^{-/-} mice, absolute numbers of cDC1s were determined in the spleen along with the priming analysis. cDC1 numbers were slightly, but not significantly reduced in *Klra8*^{-/-} : *Batf3*^{-/-} chimeras (**Figure 30B**), however, no correlation was observed between cDC1 numbers and the frequency of activated OT-1 cells (**Figure 30C**). These findings made it unlikely that priming differences result from altered cDC1 numbers.

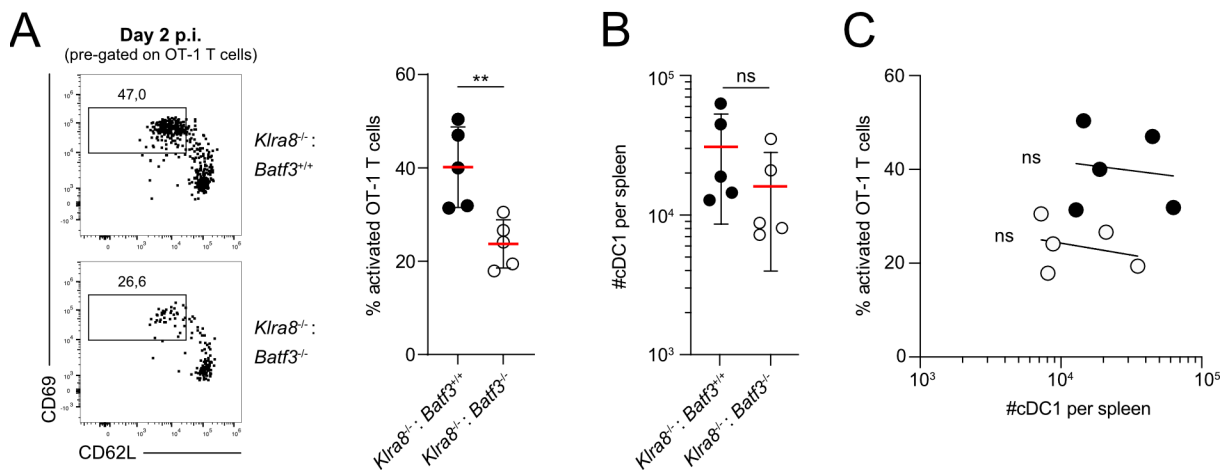


Figure 30: NK-cell intrinsic expression of Batf3 is critical to achieve optimal CD8 T cell priming upon infection.

(A) *Klra8*^{-/-} : *Batf3*^{+/+} and *Klra8*^{-/-} : *Batf3*^{-/-} mixed bone marrow chimeras were infected with MCMV-*ie2*-SIINFEKL. 1x10⁶ OT-1 T cells were adoptively transferred at day 2 p.i. and T cell priming was analyzed by flow cytometry after 21 h. Representative dot plots and scatter dot plot show frequency of activated OT-1 cells in the spleen. (B) Quantification of cDC1 cell numbers in spleens of *Klra8*^{-/-} : *Batf3*^{+/+} and *Klra8*^{-/-} : *Batf3*^{-/-} mixed bone marrow chimeras. (C) Correlation of OT-1 T cell priming (from A) and cDC1 numbers (from B).

Data in (A)-(C) are pooled from 2 independent, similar experiments. Lines represent mean, error bars indicate SD. Significances in (A) and (B) were calculated by Mann-Whitney test. Correlation in (C) was measured as Spearman correlation. Line indicates non-linear fit. (modified from (Flommersfeld et al., 2021))

5 Discussion

5.1 Individual Ly49H⁺ NK cells can adopt separate fates upon MCMV infection

Naïve Ly49H⁺ NK cells expand 100- to 1000-fold upon adoptive transfer into MCMV-infected recipients that lack endogenous expression of the receptor Ly49H (Sun et al., 2009). Upon expansion, these Ly49H⁺ NK cells mature into terminally differentiated effector cells showing increased expression of CD11b, KLRG1, CD69 and granzyme B, while CD27 is expressed at much lower levels in comparison to naïve NK cells (Min-Oo et al., 2014). This is in parallel to antigen-specific T cells which also undergo vigorous expansion upon pathogen encounter, accompanied by progressive differentiation into effector and memory subsets (Buchholz et al., 2013). A number of different T effector and memory subsets with highly specialized functions have been described (Buchholz et al., 2012, Kallies et al., 2020). Similarly, also expanded NK cells show a certain phenotypic heterogeneity. As an example, while most NK cells are CD27⁻ at day 8 p.i., a fraction of NK cells still expresses high levels of CD27 during acute infection (Min-Oo et al., 2014, Grassmann et al., 2019).

In this study, we showed that Ly49H⁺ NK cells indeed generated quite heterogenous output upon adoptive transfer into MCMV-infected *Klra8*^{-/-} or *Rag2*^{-/-} *Il2rg*^{-/-} mice, respectively. Besides CD27, the markers CD62L and CD160 were also expressed by only a fraction of activated NK cells during acute infection indicating phenotypic heterogeneity of these cells. Other markers, such as CD11b, KLRG1 or granzyme B were uniformly expressed by all activated NK cells at this respective timepoint. To analyze, how this heterogeneity is composed starting out from single Ly49H⁺ NK cells, we used retroviral fluorescent barcoding and single-cell fate mapping to study individual NK cell responses *in vivo*. Here we found, that single Ly49H⁺ NK cells followed two distinct paths of differentiation: Some of the recovered NK cell clones displayed expression of CD62L in a fraction of cells, but lacked expression of CD160 and showed low expression of CD27; the other clones instead were characterized by high expression of the markers CD160 and CD27, but completely lacked expression of CD62L. These findings suggested that Ly49H⁺ NK cells can adopt two separate fates upon activation and expansion (“one cell, one fate”) which is in contrast to T cells that undergo phenotypic diversification upon expansion and give rise to a heterogenous progeny with variable subset

Discussion

composition, but within a common differentiation framework (“one cell, multiple fates”) (Buchholz et al., 2013, Cho et al., 2017).

Peripheral NK cells are thought to continuously mature from CD11b^{low} CD27⁺ into CD11b⁺ CD27⁺ and finally into CD11b⁺ CD27⁻ cells (Chiossone et al., 2009). To make sure that it was not just immature NK cells that generated CD27^{high} CD160^{high} responses whereas CD62L^{high} patterns originated from mature CD11b⁺ NK cells, we also transferred single Ly49H⁺ NK cells that came exclusively from the most immature NK cell subset, namely CD11b^{low} CD27⁺ NK cells. However, even these immature NK cells were capable of generating the two described response patterns upon infection.

Further phenotyping of the steady-state NK cell compartment in the spleen showed that CD11b^{low} CD27⁺ NK cells could be further subdivided into two subsets based on differential expression of CD62L which is in accordance with previous studies (Peng et al., 2013b). Bulk transfers of these different NK cell subsets revealed that CD27⁺ CD62L⁻ NK cells exclusively generated CD27^{high} CD160^{high} progeny while CD62L⁺ cNK cells gave rise to CD62L^{high} progeny. In line with that, CD27⁺ CD62L⁻ single cells exclusively generated CD27^{high} CD160^{high} offspring. Consequently, these two distinct NK cell fates resulted from a pre-existing heterogeneity within the naïve NK cell compartment. This strongly indicated the existence of two distinct NK cell lineages. Both NK cell subsets showed comparable kinetics upon MCMV infection comprising expansion, contraction and transition into the memory phase as well as the capability to undergo secondary expansion upon re-transfer into secondary recipients, but remained phenotypically distinct. Moreover, global transcriptomic analysis and unbiased clustering indicated that NK cells could be subdivided into distinct cell clusters at steady state that could clearly be assigned to these subsets. Although it was proposed that CD62L⁻ NK cells can differentiate into CD62L⁺ NK cells after adoptive transfer into irradiated wildtype recipients (Peng et al., 2013b), our results did not indicate that CD62L⁻ NK cells act as progenitors of CD62L⁺ NK cells. Both subsets stably retained their identity under homeostatic conditions after adoptive transfer into either *Rag2*^{-/-} *Il2rg*^{-/-} or *Nkp46*^{iCre} x *R26-LSL-iDTA* mice, respectively, for up to 4 weeks. Additionally, the RNA velocities of steady-state NK cells confirmed the existence of two developmental branches within the NK cell compartment ending up in either the CD27⁺ CD62L⁻ or CD62L⁺ cluster. Of note, also in the mentioned study by Peng et al. the majority of NK cells that were sorted CD62L⁻, remained negative. In summary, our data showed that CD62L⁻ NK cells do not serve as progenitors for CD62L⁺ NK cells under homeostatic conditions and upon MCMV infection, but we do not know whether this might be different in other infections or during development.

Discussion

So far, we do not know at which point of NK cell development the CD27⁺ CD62L⁻ NK cell subset (termed ILC1-like NK cells) diverges from common NK cell maturation, which requirements are necessary and from which progenitor the subsets originate. Our transcriptomic data showed that the transcription factors Id3 and Batf3 were exclusively expressed by ILC1-like NK cells. However, both of them appeared not to be critical for the development of the subset. Therefore, deciphering the origin of these two distinct NK cell lineages requires further investigation. Still, single-cell fate mapping in this study enabled the identification of two distinct NK cell lineages that follow different paths of differentiation upon MCMV infection and helped to understand the underlying processes that generate the observed heterogeneity within the NK cell compartment.

5.2 Classification of ILC1-like NK cells within the growing family of innate lymphocytes

Whereas NK cells are historically defined by their ability to directly kill infected or malignant cells (Herberman et al., 1975), ILC1s are characterized by poor cytotoxicity and strong cytokine production (Vivier et al., 2018). Further features that set NK cells apart from ILC1s, are the expression of MHC class I-specific receptors that allow direct recognition of target cells and the expression of the surface marker CD49b as well as the transcription factor Eomes (Diefenbach et al., 2014, Vivier et al., 2018). Instead, ILC1s are mainly activated indirectly via proinflammatory cytokines such as cDC1-derived IL-12 (Weizman et al., 2017), they show surface expression of CD49a and CD127 and depend on the transcription factors Id2, T-bet and Hobit (Vivier et al., 2018, Mackay et al., 2016). Finally, NK cells are characterized as circulating lymphocytes while ILC1s were reported to be tissue-resident (Gasteiger et al., 2015).

Here we could show that ILC1-like NK cells unite features of both NK cells and ILC1s, however can be assigned to the NK cell lineage. Our gene expression data suggested that CD62L⁺ cNK cells might be more cytotoxic than ILC1-like NK cells due to higher mRNA levels of the cytotoxic effector molecules granzyme B and perforin. In contrast, ILC1-like NK cells showed higher transcript levels for genes encoding for cytokines such as TNF- α , GM-CSF or Ltb. This enhanced capacity to produce cytokines was confirmed by *ex vivo* stimulation of the subsets and cytokine staining. Furthermore, we could show that ILC1-like NK cells were the main producers of NK-cell-derived IFN- γ early during MCMV infection (24 hours p.i.). Interestingly, a study by Weizman et al. showed that tissue-resident ILC1s at the primary site

Discussion

of the infection are the major source of IFN- γ at day 1 after infection. However, these ILC1s do not recognize MCMV infection directly as they do not express Ly49H, but instead are activated by cDC1-derived cytokines (Weizman et al., 2017). We could show in this study that ILC1-like NK cells are also tissue-resident in the spleen and therefore might similarly act as early sentinels of viral infection. In contrast to ILC1s, they are able to specifically recognize MCMV infection via Ly49H proposing a distinct role for this NK cell subset during the immune response. A more recent study from the same group proposed that ILC1s might also directly sense MCMV infection by engagement of NK1.1 to the viral ligand m12 (Weizman et al., 2019). However, recognition via NK1.1 is rather unspecific, as it also binds to at least one other (self) ligand and is involved in the recognition of many infections and malignancies (Carlyle et al., 2004, Williams et al., 2012, Aguilar et al., 2015). Furthermore, the expression of this receptor is not specific to ILC1s, as it is also expressed by NK cells and NKT cells.

Regarding cytotoxicity, ILC1-like NK cells indeed displayed much lower expression of granzyme B in comparison to cNK cells at steady state. However, upon activation both subsets showed similar expression of granzyme B and killed “missing-self” targets with the same efficacy. These findings corroborated that ILC1-like NK cells are highly cytotoxic and can kill target cells very efficiently upon infection which is a key feature of *bona fide* NK cells. The capability to recognize “missing-self” targets (defined by absent or reduced MHC class I expression) relies on the expression of MHC class I-specific receptors by ILC1-like NK cells, e.g. Ly49 receptors. We found that both subsets had a very similar Ly49 repertoire. Moreover, cNK as well as ILC1-like NK cells received signaling via Ly49H, as both reacted and mounted adaptive-like responses upon MCMV infection. In addition, a co-culture of either NK cell subset with Ba/F3 wildtype cells or Ba/F3 cells expressing m157 led to similar ligand-specific down-regulation of the Ly49H receptor.

Finally, the phenotypic characteristics of ILC1-like NK cells also underlined their NK cell identity although to a certain degree they also showed expression of some ILC1-specific markers. First of all, ILC1-like NK cells showed as high expression of *Eomes* as cNK cells and their development was similarly impaired in the absence of *Eomes* expression. Additionally, ILC1-like NK cells expressed CD49b, albeit at lower levels than cNK cells, but not CD49a at the surface. A comparison of the transcriptomic data from sorted cNK cells, ILC1-like NK cells and ILC1s showed that ILC1-like NK cells and ILC1s had distinct transcriptional profiles with only partial overlap. RNA sequencing could confirm that transcripts of *Eomes* are high in ILC1-like NK cells but absent from ILC1s. In contrast, ILC1s showed high transcript levels of genes encoding for ILC1-specific transcription factors, such as *Id2* and *Hobit*. Furthermore, we could

Discussion

identify Batf3 and Id3 as transcription factors that set ILC1-like NK cells apart from both ILC1s and cNK cells. Transcript levels of genes encoding for the prototypic ILC1 markers CD49a, CD200R, CXCR6 and CD127 were high in ILC1s and much lower in ILC1-like NK cells, although they were slightly elevated in comparison to cNK cells. For CD127, we could confirm surface expression by a small fraction of ILC1-like NK cells. Markers that were shared between ILC1s and ILC1-like NK cells comprised for example CD160, CD69 and TCF-1 as well as the cytokines TNF- α and Ltb.

In summary, ILC1-like NK cells shared some characteristics with ILC1s, such as splenic residency and enhanced cytokine production, but also had key features of NK cells, especially pronounced cytotoxicity, the ability to directly recognize “missing-self” or virus-infected target cells via MHC class I-specific receptors or Ly49H, respectively, and the requirement of Eomes for development. Consequently, they constitute a hitherto undescribed NK cell subset with some similarities to ILC1s, prompting us to the term “ILC1-like” NK cells. Recently, some studies indicated a certain plasticity within the innate lymphocyte population. It was shown that ILC1-like cells can arise by conversion from ILC3s (Cella et al., 2019) or tumor-infiltrating NK cells (Gao et al., 2017). Whether these putatively NK-cell-derived ILC1-like cells in the tumor, for example, are generated from ILC1-like NK cells has to be elucidated.

Finally, ILC1-like NK cells are also distinct from tissue-resident NK cell subsets that have been described in other tissues, such as uterus, thymus or salivary glands. All of these subsets have unique tissue-specific phenotypes and functionalities that differ from that of ILC1-like NK cells for instance by pronounced expression of CD49a or CD103 (Diefenbach et al., 2014), limited Ly49 receptor repertoire (Vosshenrich et al., 2006) or weak cytotoxicity (Tessmer et al., 2011, Vosshenrich et al., 2006).

5.3 ILC1-like NK cells play a unique role in bridging innate and adaptive immunity

Functional interactions between NK cells, dendritic cells and T cells are critical to mount effective immune responses against MCMV infection. Efficient activation and expansion of Ly49H⁺ NK cells require cDC1-derived cytokines such as IL-12, IL-15 or IL-18 (Andrews et al., 2003). Furthermore, it has been reported that interactions between cDC1s and Ly49H⁺ NK cells are important for the maintenance of these two cell types in the spleen early during infection (day 2-4) (Andrews et al., 2003, Robbins et al., 2007). In addition, Ly49H⁺ NK cells were shown to be essential to promote CD8⁺ T cell responses and control virus burden during

Discussion

the first days of MCMV infection and thereby represent a link between innate and adaptive immunity (Robbins et al., 2007).

In this study, we demonstrated that ILC1-like NK cells exclusively expressed markers which enable direct interactions with cDC1s, such as XCL1 (Dorner et al., 2009), CRTAM (Galibert et al., 2005) and GM-CSF (Sallusto and Lanzavecchia, 1994). By performing confocal immunofluorescence imaging of spleen sections from MCMV-infected hosts, we could show that Ly49H⁺ NK cells and cDC1s formed clusters in the red pulp at 24 hours p.i. This clustering was dependent on XCR1 on the side of the cDC1s and on Ly49H on the part of the NK cells. These findings were validated independently by another group that also reported XCR1-dependent clustering of cDC1s and NK cells in the spleen during the first hours of MCMV infection (Ghilas et al., 2021). Furthermore, we could show that ILC1-like NK cells were significantly enriched within these clusters. Most of the clusters co-localized with MCMV-infected cells indicating that spleen-resident ILC1-like NK cells might sense MCMV infection via Ly49H-m157 interactions and recruit cDC1s to the site of the infection. As XCR1 was required for the cluster formation, XCL1 represented a promising candidate to be involved in this recruitment. Ghilas et al. showed that NK cells are indeed major producers of XCL1 upon MCMV infection, however NK-cell-derived XCL1 was dispensable for the crosstalk with cDC1s (meaning no reduction in NK cell activation) suggesting that other cell types, such as T cells, NKT cells or ILC1s, might compensate for defective XCL1 production on the part of NK cells (Ghilas et al., 2021). Besides MCMV, it was shown that in certain tumor models NK cells are as well a major source of XCL1 and necessary to recruit XCR1⁺ cDC1s into the tumor and to mount efficient anti-tumor immunity (Böttcher et al., 2018) – highlighting the importance of the interplay between these two cell types.

We found that the transcription factor Batf3, which is critical for cDC1 development (Hildner et al., 2008), was exclusively expressed by ILC1-like NK cells. Furthermore, mice that lacked expression of Batf3 in Ly49H⁺ NK cells, showed significantly reduced clustering of NK cells and cDC1s at 24 hours p.i. These data indicated that, although Batf3 was not required for the development of ILC1-like NK cells, it appeared to be functionally relevant for the interaction with cDC1s. Moreover, these findings further supported the hypothesis that ILC1-like NK cells were indeed drivers of this early clustering with cDC1s. However, little is known about the role of Batf3 in immune cell types other than cDC1s. A recent study revealed that Batf3 also plays a role in CD8⁺ T cells, where it promotes survival and memory formation upon infection (Ataide et al., 2020). Consequently, cDC1s as well as ILC1-like NK cells and CD8⁺ T cells, all of which collaborate during the immune response to MCMV, are dependent on Batf3 expression, either

Discussion

for development or optimal functionality. Still, the underlying mechanisms by which Batf3 promotes the function of ILC1-like NK cells, are so far unknown.

It has been previously established that both cross-presenting cDC1s (Busche et al., 2013) and Ly49H⁺ NK cells (Robbins et al., 2007) are necessary to rapidly induce effective CD8⁺ T cell responses against MCMV. Antigen cross-presentation is especially important upon MCMV infection, as directly infected dendritic cells cannot efficiently prime CD8⁺ T cells due to MCMV-induced functional impairment (Andrews et al., 2001). To cross-present viral antigens, cDC1s have to take up extracellular antigens from infected, apoptotic cells. Here, we showed that cDC1s clustered with ILC1-like NK cells in close proximity to infected cells as early as 24 hours p.i. It was reported that MCMV-infected cells in the red pulp are first detectable at 17 h p.i. and mainly comprise stromal cells (Hsu et al., 2009). Leukocytes, especially dendritic cells, are infected by 48 h p.i. (Hsu et al., 2009). Another study reported that small numbers of splenic DCs are already infected by 24 h p.i., but still the majority of DCs remain uninfected until 2 days p.i. (Andrews et al., 2001). Thus, cDC1s were redistributed towards infected cells a few hours after MCMV infection reached the spleen, but several hours before the virus directly infected DCs, in a process that depended on ILC1-like NK cells. We assessed early priming of antigen-specific CD8⁺ T cells in wildtype and Ly49H-deficient animals. Indeed, priming efficacy was significantly reduced at day 2 and 3 p.i. in the absence of Ly49H⁺ NK cells. This effect could be reproduced in mice that lacked Batf3 expression in Ly49H⁺ NK cells. These findings highlight that ILC1-like NK cells are indispensable for optimal T cell priming. Accelerated T cell responses in the presence of Ly49H⁺ NK cells have been described previously (Robbins et al., 2007). However, Robbins et al. proposed that this mainly relies on indirect effects. Ly49H⁺ NK cells are essential for early virus control. Consequently, virus load as well as innate cytokine levels, especially pDC-derived IFN- α , are reduced in Ly49H-competent mice (Robbins et al., 2007). The authors suggest that these factors ensure maintenance of cDC1s in the spleen which in return mediate enhanced T cell priming early during infection (Robbins et al., 2007). In this study we could show for the first time that the enhancement of T cell activation i) can be assigned to a specialized subset of NK cells and ii) is the result of direct interactions between these NK cells and cDC1s. Our data indicate that spleen-resident ILC1-like NK cells can rapidly sense MCMV infection and recruit cross-presenting cDC1s to the site of the infection. Within these clusters, ILC1-like NK cells and cDC1s can further activate each other and enable migration of cDC1s into the T cell zone where they can then efficiently prime antigen-specific CD8⁺ T cells. An independent study by Ghilas et al. confirmed our finding that NK cells and cDC1s directly act on each other and provided

Discussion

further insights into mechanistic details of this crosstalk. They demonstrated that cDC1s can activate NK cells within the observed clusters by direct delivery of IL-12 and trans-presentation of IL-15 via IL-15R α (Ghilas et al., 2021). In return, the activated NK cells produce GM-CSF that stimulates the upregulation of the chemokine receptor CCR7 on cDC1s and thereby enable migration of cDC1s into the T cell zone and accelerate the CD8⁺ T cell response against MCMV (Ghilas et al., 2021). In summary, our data showed that ILC1-like NK cells play a unique role in bridging innate and adaptive immunity. In how far these findings can be translated into infection models other than MCMV, has to be elucidated in the future.

5.4 From murine to human NK cell subsets

Human NK cells also consist of two major subsets: CD56^{dim} CD16⁺ and CD56^{bright} CD16^{dim/-} NK cells (Lanier et al., 1983, Lanier et al., 1986). CD56^{dim} NK cells constitute the majority of circulating cells and are highly cytotoxic, whereas CD56^{bright} NK cells represent the predominant population in secondary lymphoid organs and are less cytotoxic, but potent cytokine producers (Nagler et al., 1989, Cooper et al., 2001). Thus, CD56^{bright} NK cells have some features in common with ILC1-like NK cells that are potent cytokine producers as well and restricted to lymphoid organs, whereas cNK cells in the mouse resemble CD56^{dim} NK cells in humans. Tissue-resident NK cells in human liver were described as CD56^{bright} NK cells that express high levels of Eomes and low levels of T-bet (Harmon et al., 2016), a transcription factor profile that is similar to that of ILC1-like NK cells. Recently, Crinier et al. published a scRNA-seq dataset from human and murine blood and spleen samples demonstrating that, besides the functional aspect, CD56^{bright} NK cells also share several phenotypic markers with ILC1-like NK cells. Clusters that are assigned to CD56^{bright} NK cells display higher transcript levels of *XCL1*, *LTB*, *CD160*, *CD7* and *IL7R* (Crinier et al., 2018), genes that are also upregulated in ILC1-like NK cells. In contrast, clusters representing CD56^{dim} NK cells show increased transcript levels of *GZMA*, *GZMB*, *PRF1* and *CX3CR1* (Crinier et al., 2018), as do cNK cells. However, murine and human NK cell subsets also differ in the expression of some markers. For example, CD62L was shown to be expressed by CD56^{bright} NK cells, but not CD56^{dim} (Poli et al., 2009, Crinier et al., 2018). Of note, tissue-resident CD56^{bright} NK cells instead do not express CD62L (Melsen et al., 2016).

While we could show that in our model ILC1-like NK cells did not develop into cNK cells, CD56^{bright} NK cells are commonly described as precursors of CD56^{dim} NK cells (Chan et al., 2007, Romagnani et al., 2007). In this study, we reanalyzed a published dataset from one human

Discussion

spleen donor from Crinier et al., 2018, and performed RNA velocity analysis. This indicated that – in contrast to the established paradigm – human NK cells as well as murine NK cells differentiated along two different pathways that ended up in distinct clusters that were characterized by mutually exclusive expression of either *CD160/XCL1* or *GZMB*. Further evidence for this model comes from a recent study in rhesus macaques that were transplanted with barcoded hematopoietic stem cells. The authors demonstrated that the clonal composition of CD56⁺ and CD56⁻ NK cells differed and furthermore remained distinct under homeostatic conditions over several years potentially suggesting distinct lineage origins of the two subsets (Wu et al., 2018). However, while both RNA velocities and studies in rhesus macaques examined NK cell differentiation at steady state, the aforementioned studies by Chan et al. and Romagnani et al. showed that CD56^{bright} NK cells can gain features of CD56^{dim} NK cells, but they require additional signals such as direct contact to fibroblasts or an inflammatory environment (Chan et al., 2007, Romagnani et al., 2007).

All these data demonstrate that there are many parallels between ILC1-like NK cells in mice and CD56^{bright} NK cells in humans. However, a further in-depth analysis of the subset will be necessary to evaluate, in how far CD56^{bright} NK cells might represent a human equivalent to the subset described in this study. It will be important to understand whether CD56^{bright} NK cells play a similar role in human CMV and other viral infections and will help to improve our understanding about how individual innate lymphocytes contribute to a host's immune response against infections and cancer.

6 Summary

NK cells are key players of cellular innate immunity and represent a first line of defense against viral pathogens and cancer. Their reactivity is controlled by numerous activating and inhibitory receptors that enable recognition of infected or malignant cells. Effector mechanisms of NK cells comprise direct cytotoxicity as well as the production of proinflammatory cytokines. Recently, it has been shown that, under certain conditions, NK cells are able to mount adaptive-like immune responses. In particular, NK cells expressing the activating receptor Ly49H, that binds directly to an MCMV-encoded glycoprotein, respond to MCMV infection in an adaptive-like manner, comprising antigen-specific expansion, contraction and the formation of long-lived immunological memory (Sun et al., 2009). Several phenotypically and functionally distinct subsets of NK cells have been described. How these different subsets contribute to adaptive-like immune responses is only partly understood.

In this study, we used retrogenic color-barcoding to study infection-driven NK cell differentiation on a single-cell level and to decipher the heterogeneity of the NK cell response *in vivo*. We could show that individual Ly49H⁺ NK cells adopted separate fates upon MCMV infections and differentiated along two distinct pathways. Whereas one of these response patterns originated from conventional NK cells, the other one was generated from a phenotypically and transcriptionally distinct NK cell subset that shared features with ILC1s such as enhanced cytokine production and splenic residency. On the other hand, these cells also displayed key characteristics of *bona fide* NK cells, in particular direct recognition of MCMV-infected cells and pronounced cytotoxicity, guided by signals received from the activating receptor Ly49H. Furthermore, we could show that these ILC1-like NK cells formed clusters with XCR1⁺ cDC1s early upon MCMV infection and thereby enabled optimal priming of antigen-specific T cells. This interaction was dependent on both Ly49H and NK-intrinsic expression of the transcription factor Batf3. Taken together, these results indicate that ILC1-like NK cells unite critical features of both ILC1s and NK cells and orchestrate innate and adaptive immune responses to ensure effective host protection. These findings will help to further understand NK cell diversity and how individual components of NK-cell-mediated immunity collaborate to facilitate optimized immune responses to viral pathogens.

7 Bibliography

- ABDUL-CAREEM, M. F., LEE, A. J., PEK, E. A., GILL, N., GILLGRASS, A. E., CHEW, M. V., REID, S. & ASHKAR, A. A. 2012. Genital HSV-2 infection induces short-term NK cell memory. *PLoS One*, 7, e32821.
- ABT, M. C., LEWIS, B. B., CABALLERO, S., XIONG, H., CARTER, R. A., SUSAC, B., LING, L., LEINER, I. & PAMER, E. G. 2015. Innate Immune Defenses Mediated by Two ILC Subsets Are Critical for Protection against Acute *Clostridium difficile* Infection. *Cell Host Microbe*, 18, 27-37.
- ADAMS, E. J., JUO, Z. S., VENOOK, R. T., BOULANGER, M. J., ARASE, H., LANIER, L. L. & GARCIA, K. C. 2007. Structural elucidation of the m157 mouse cytomegalovirus ligand for Ly49 natural killer cell receptors. *Proc Natl Acad Sci U S A*, 104, 10128-33.
- ADAMS, N. M., GEARY, C. D., SANTOSA, E. K., LUMAQUIN, D., LE LUDUEC, J. B., SOTTILE, R., VAN DER PLOEG, K., HSU, J., WHITLOCK, B. M., JACKSON, B. T., WEIZMAN, O. E., HUSE, M., HSU, K. C. & SUN, J. C. 2019. Cytomegalovirus Infection Drives Avidity Selection of Natural Killer Cells. *Immunity*, 50, 1381-1390 e5.
- ADAMS, N. M., GRASSMANN, S. & SUN, J. C. 2020. Clonal expansion of innate and adaptive lymphocytes. *Nat Rev Immunol*, 20, 694-707.
- AGUILAR, O. A., MESCI, A., MA, J., CHEN, P., KIRKHAM, C. L., HUNDRIESER, J., VOIGT, S., ALLAN, D. S. & CARLYLE, J. R. 2015. Modulation of Clr Ligand Expression and NKR-P1 Receptor Function during Murine Cytomegalovirus Infection. *J Innate Immun*, 7, 584-600.
- ALEXANDRE, Y. O., COCITA, C. D., GHILAS, S. & DALOD, M. 2014. Deciphering the role of DC subsets in MCMV infection to better understand immune protection against viral infections. *Front Microbiol*, 5, 378.
- ALTER, G., RIHN, S., WALTER, K., NOLTING, A., MARTIN, M., ROSENBERG, E. S., MILLER, J. S., CARRINGTON, M. & ALTFELD, M. 2009. HLA class I subtype-dependent expansion of KIR3DS1+ and KIR3DL1+ NK cells during acute human immunodeficiency virus type 1 infection. *J Virol*, 83, 6798-805.
- ANDREWS, D. M., ANDONIOU, C. E., GRANUCCI, F., RICCIARDI-CASTAGNOLI, P. & DEGLI-ESPOSTI, M. A. 2001. Infection of dendritic cells by murine cytomegalovirus induces functional paralysis. *Nat Immunol*, 2, 1077-84.
- ANDREWS, D. M., SCALZO, A. A., YOKOYAMA, W. M., SMYTH, M. J. & DEGLI-ESPOSTI, M. A. 2003. Functional interactions between dendritic cells and NK cells during viral infection. *Nat Immunol*, 4, 175-81.
- ANUMANTHAN, A., BENSUSSAN, A., BOUMSELL, L., CHRIST, A. D., BLUMBERG, R. S., VOSS, S. D., PATEL, A. T., ROBERTSON, M. J., NADLER, L. M. & FREEMAN, G. J. 1998. Cloning of BY55, a novel Ig superfamily member expressed on NK cells, CTL, and intestinal intraepithelial lymphocytes. *J Immunol*, 161, 2780-90.

Bibliography

- ARASE, H., MOCARSKI, E. S., CAMPBELL, A. E., HILL, A. B. & LANIER, L. L. 2002. Direct recognition of cytomegalovirus by activating and inhibitory NK cell receptors. *Science*, 296, 1323-6.
- ARASE, H., SAITO, T., PHILLIPS, J. H. & LANIER, L. L. 2001. Cutting edge: the mouse NK cell-associated antigen recognized by DX5 monoclonal antibody is CD49b (alpha 2 integrin, very late antigen-2). *J Immunol*, 167, 1141-4.
- ASHKAR, A. A., DI SANTO, J. P. & CROY, B. A. 2000. Interferon gamma contributes to initiation of uterine vascular modification, decidual integrity, and uterine natural killer cell maturation during normal murine pregnancy. *J Exp Med*, 192, 259-70.
- ATAIDE, M. A., KOMANDER, K., KNOPPER, K., PETERS, A. E., WU, H., EICKHOFF, S., GOGISHVILI, T., WEBER, J., GRAFEN, A., KALLIES, A., GARBI, N., EINSELE, H., HUDECEK, M., GASTEIGER, G., HOLZEL, M., VAETH, M. & KASTENMULLER, W. 2020. BATF3 programs CD8(+) T cell memory. *Nat Immunol*, 21, 1397-1407.
- AZZI, T., LUNEMANN, A., MURER, A., UEDA, S., BEZIAT, V., MALMBERG, K. J., STAUBLI, G., GYSIN, C., BERGER, C., MUNZ, C., CHIJIJOKE, O. & NADAL, D. 2014. Role for early-differentiated natural killer cells in infectious mononucleosis. *Blood*, 124, 2533-43.
- BEAULIEU, A. M., ZAWISLAK, C. L., NAKAYAMA, T. & SUN, J. C. 2014. The transcription factor Zbtb32 controls the proliferative burst of virus-specific natural killer cells responding to infection. *Nat Immunol*, 15, 546-53.
- BELANGER, S., TU, M. M., RAHIM, M. M., MAHMOUD, A. B., PATEL, R., TAI, L. H., TROKE, A. D., WILHELM, B. T., LANDRY, J. R., ZHU, Q., TUNG, K. S., RAULET, D. H. & MAKRIGIANNIS, A. P. 2012. Impaired natural killer cell self-education and "missing-self" responses in Ly49-deficient mice. *Blood*, 120, 592-602.
- BEZMAN, N. A., KIM, C. C., SUN, J. C., MIN-OO, G., HENDRICKS, D. W., KAMIMURA, Y., BEST, J. A., GOLDRATH, A. W., LANIER, L. L. & IMMUNOLOGICAL GENOME PROJECT, C. 2012. Molecular definition of the identity and activation of natural killer cells. *Nat Immunol*, 13, 1000-9.
- BIRON, C. A., BYRON, K. S. & SULLIVAN, J. L. 1989. Severe herpesvirus infections in an adolescent without natural killer cells. *N Engl J Med*, 320, 1731-5.
- BOIERI, M., ULVMOEN, A., SUDWORTH, A., LENDREM, C., COLLIN, M., DICKINSON, A. M., KVEBERG, L. & INNGJERDINGEN, M. 2017. IL-12, IL-15, and IL-18 pre-activated NK cells target resistant T cell acute lymphoblastic leukemia and delay leukemia development in vivo. *Oncoimmunology*, 6, e1274478.
- BÖTTCHER, J. P., BONAVIDA, E., CHAKRAVARTY, P., BLEES, H., CABEZA-CABRERIZO, M., SAMMICHELI, S., ROGERS, N. C., SAHAI, E., ZELENAY, S. & REIS E SOUSA, C. 2018. NK Cells Stimulate Recruitment of cDC1 into the Tumor Microenvironment Promoting Cancer Immune Control. *Cell*, 172, 1022-1037 e14.
- BRAUD, V. M., ALLAN, D. S., O'CALLAGHAN, C. A., SODERSTROM, K., D'ANDREA, A., OGG, G. S., LAZETIC, S., YOUNG, N. T., BELL, J. I., PHILLIPS, J. H., LANIER,

Bibliography

- L. L. & MCMICHAEL, A. J. 1998. HLA-E binds to natural killer cell receptors CD94/NKG2A, B and C. *Nature*, 391, 795-9.
- BROWN, M. G., DOKUN, A. O., HEUSEL, J. W., SMITH, H. R., BECKMAN, D. L., BLATTENBERGER, E. A., DUBBELDE, C. E., STONE, L. R., SCALZO, A. A. & YOKOYAMA, W. M. 2001. Vital involvement of a natural killer cell activation receptor in resistance to viral infection. *Science*, 292, 934-7.
- BUBIC, I., WAGNER, M., KRMPOTIC, A., SAULIG, T., KIM, S., YOKOYAMA, W. M., JONJIC, S. & KOSZINOWSKI, U. H. 2004. Gain of virulence caused by loss of a gene in murine cytomegalovirus. *J Virol*, 78, 7536-44.
- BUCHHOLZ, V. R. & FLOSSDORF, M. 2018. Single-Cell Resolution of T Cell Immune Responses. *Adv Immunol*, 137, 1-41.
- BUCHHOLZ, V. R., FLOSSDORF, M., HENSEL, I., KRETSCHMER, L., WEISSBRICH, B., GRAF, P., VERSCHOOR, A., SCHIEMANN, M., HOFER, T. & BUSCH, D. H. 2013. Disparate individual fates compose robust CD8+ T cell immunity. *Science*, 340, 630-5.
- BUCHHOLZ, V. R., GRAF, P. & BUSCH, D. H. 2012. The origin of diversity: studying the evolution of multi-faceted CD8+ T cell responses. *Cell Mol Life Sci*, 69, 1585-95.
- BUCHHOLZ, V. R., SCHUMACHER, T. N. & BUSCH, D. H. 2016. T Cell Fate at the Single-Cell Level. *Annu Rev Immunol*, 34, 65-92.
- BUSCH, D. H. & PAMER, E. G. 1999. T cell affinity maturation by selective expansion during infection. *J Exp Med*, 189, 701-10.
- BUSCHE, A., JIRMO, A. C., WELTEN, S. P., ZISCHKE, J., NOACK, J., CONSTABEL, H., GATZKE, A. K., KEYSER, K. A., ARENS, R., BEHRENS, G. M. & MESSERLE, M. 2013. Priming of CD8+ T cells against cytomegalovirus-encoded antigens is dominated by cross-presentation. *J Immunol*, 190, 2767-77.
- CALIGIURI, M. A. 2008. Human natural killer cells. *Blood*, 112, 461-9.
- CAMPBELL, A. E. & SLATER, J. S. 1994. Down-regulation of major histocompatibility complex class I synthesis by murine cytomegalovirus early gene expression. *J Virol*, 68, 1805-11.
- CARLYLE, J. R., JAMIESON, A. M., GASSER, S., CLINGAN, C. S., ARASE, H. & RAULET, D. H. 2004. Missing self-recognition of Ocil/Clr-b by inhibitory NKR-P1 natural killer cell receptors. *Proc Natl Acad Sci U S A*, 101, 3527-32.
- CARLYLE, J. R., MESCI, A., LJUTIC, B., BELANGER, S., TAI, L. H., ROUSSELLE, E., TROKE, A. D., PROTEAU, M. F. & MAKRIGIANNIS, A. P. 2006. Molecular and genetic basis for strain-dependent NK1.1 alloreactivity of mouse NK cells. *J Immunol*, 176, 7511-24.
- CELLA, M., FUCHS, A., VERMI, W., FACCHETTI, F., OTERO, K., LENNERZ, J. K., DOHERTY, J. M., MILLS, J. C. & COLONNA, M. 2009. A human natural killer cell subset provides an innate source of IL-22 for mucosal immunity. *Nature*, 457, 722-5.

Bibliography

- CELLA, M., GAMINI, R., SECCA, C., COLLINS, P. L., ZHAO, S., PENG, V., ROBINETTE, M. L., SCHETTINI, J., ZAITSEV, K., GORDON, W., BANDO, J. K., YOMOGIDA, K., CORTEZ, V., FRONICK, C., FULTON, R., LIN, L. L., GILFILLAN, S., FLAVELL, R. A., SHAN, L., ARTYOMOV, M. N., BOWMAN, M., OLTZ, E. M., JELINSKY, S. A. & COLONNA, M. 2019. Subsets of ILC3-ILC1-like cells generate a diversity spectrum of innate lymphoid cells in human mucosal tissues. *Nat Immunol*, 20, 980-991.
- CHAN, A., HONG, D. L., ATZBERGER, A., KOLLNBERGER, S., FILER, A. D., BUCKLEY, C. D., MCMICHAEL, A., ENVER, T. & BOWNESS, P. 2007. CD56bright human NK cells differentiate into CD56dim cells: role of contact with peripheral fibroblasts. *J Immunol*, 179, 89-94.
- CHAUDHRY, M. Z., CASALEGNO-GARDUNO, R., SITNIK, K. M., KASMAPOUR, B., PULM, A. K., BRIZIC, I., EIZ-VESPER, B., MOOSMANN, A., JONJIC, S., MOCARSKI, E. S. & CICIN-SAIN, L. 2020. Cytomegalovirus inhibition of extrinsic apoptosis determines fitness and resistance to cytotoxic CD8 T cells. *Proc Natl Acad Sci U S A*, 117, 12961-12968.
- CHENG, T. P., FRENCH, A. R., PLOUGASTEL, B. F., PINGEL, J. T., ORIHUELA, M. M., BULLER, M. L. & YOKOYAMA, W. M. 2008. Ly49h is necessary for genetic resistance to murine cytomegalovirus. *Immunogenetics*, 60, 565-73.
- CHIOSSONE, L., CHAIX, J., FUSERI, N., ROTH, C., VIVIER, E. & WALZER, T. 2009. Maturation of mouse NK cells is a 4-stage developmental program. *Blood*, 113, 5488-96.
- CHO, Y. L., FLOSSDORF, M., KRETSCHMER, L., HOFER, T., BUSCH, D. H. & BUCHHOLZ, V. R. 2017. TCR Signal Quality Modulates Fate Decisions of Single CD4(+) T Cells in a Probabilistic Manner. *Cell Rep*, 20, 806-818.
- COLEMAN, D. L. & HUMMEL, K. P. 1969. Effects of parabiosis of normal with genetically diabetic mice. *Am J Physiol*, 217, 1298-304.
- COOPER, M. A., ELLIOTT, J. M., KEYEL, P. A., YANG, L., CARRERO, J. A. & YOKOYAMA, W. M. 2009. Cytokine-induced memory-like natural killer cells. *Proc Natl Acad Sci U S A*, 106, 1915-9.
- COOPER, M. A., FEHNIGER, T. A., TURNER, S. C., CHEN, K. S., GHAHERI, B. A., GHAYUR, T., CARSON, W. E. & CALIGIURI, M. A. 2001. Human natural killer cells: a unique innate immunoregulatory role for the CD56(bright) subset. *Blood*, 97, 3146-51.
- CORTEZ, V. S., FUCHS, A., CELLA, M., GILFILLAN, S. & COLONNA, M. 2014. Cutting edge: Salivary gland NK cells develop independently of Nfil3 in steady-state. *J Immunol*, 192, 4487-91.
- CRINIER, A., MILPIED, P., ESCALIERE, B., PIPEROGLOU, C., GALLUSO, J., BALSAMO, A., SPINELLI, L., CERVERA-MARZAL, I., EBBO, M., GIRARD-MADOUX, M., JAEGER, S., BOLLON, E., HAMED, S., HARDWIGSEN, J., UGOLINI, S., VELY, F., NARNI-MANCINELLI, E. & VIVIER, E. 2018. High-Dimensional Single-Cell Analysis Identifies Organ-Specific Signatures and Conserved NK Cell Subsets in Humans and Mice. *Immunity*, 49, 971-986.e5.

Bibliography

- DALOD, M., SALAZAR-MATHER, T. P., MALMGAARD, L., LEWIS, C., ASSELIN-PATUREL, C., BRIERE, F., TRINCHIERI, G. & BIRON, C. A. 2002. Interferon alpha/beta and interleukin 12 responses to viral infections: pathways regulating dendritic cell cytokine expression in vivo. *J Exp Med*, 195, 517-28.
- DANIELS, K. A., DEVORA, G., LAI, W. C., O'DONNELL, C. L., BENNETT, M. & WELSH, R. M. 2001. Murine cytomegalovirus is regulated by a discrete subset of natural killer cells reactive with monoclonal antibody to Ly49H. *J Exp Med*, 194, 29-44.
- DAUSSY, C., FAURE, F., MAYOL, K., VIEL, S., GASTEIGER, G., CHARRIER, E., BIENVENU, J., HENRY, T., DEBIEN, E., HASAN, U. A., MARVEL, J., YOH, K., TAKAHASHI, S., PRINZ, I., DE BERNARD, S., BUFFAT, L. & WALZER, T. 2014. T-bet and Eomes instruct the development of two distinct natural killer cell lineages in the liver and in the bone marrow. *J Exp Med*, 211, 563-77.
- DEKHTIARENKO, I., RATTS, R. B., BLATNIK, R., LEE, L. N., FISCHER, S., BORKNER, L., ODURO, J. D., MARANDU, T. F., HOPPE, S., RUZSICS, Z., SONNEMANN, J. K., MANSOURI, M., MEYER, C., LEMMERMANN, N. A., HOLTAPPELS, R., ARENS, R., KLENERMAN, P., FRUH, K., REDDEHASE, M. J., RIEMER, A. B. & CICIN-SAIN, L. 2016. Peptide Processing Is Critical for T-Cell Memory Inflation and May Be Optimized to Improve Immune Protection by CMV-Based Vaccine Vectors. *PLoS Pathog*, 12, e1006072.
- DEN HAAN, J. M., LEHAR, S. M. & BEVAN, M. J. 2000. CD8(+) but not CD8(-) dendritic cells cross-prime cytotoxic T cells in vivo. *J Exp Med*, 192, 1685-96.
- DIEFENBACH, A., COLONNA, M. & KOYASU, S. 2014. Development, differentiation, and diversity of innate lymphoid cells. *Immunity*, 41, 354-365.
- DOKUN, A. O., KIM, S., SMITH, H. R., KANG, H. S., CHU, D. T. & YOKOYAMA, W. M. 2001. Specific and nonspecific NK cell activation during virus infection. *Nat Immunol*, 2, 951-6.
- DORNER, B. G., DORNER, M. B., ZHOU, X., OPITZ, C., MORA, A., GUTTLER, S., HUTLOFF, A., MAGES, H. W., RANKE, K., SCHAEFER, M., JACK, R. S., HENN, V. & KROCZEK, R. A. 2009. Selective expression of the chemokine receptor XCR1 on cross-presenting dendritic cells determines cooperation with CD8+ T cells. *Immunity*, 31, 823-33.
- DOU, Y., FU, B., SUN, R., LI, W., HU, W., TIAN, Z. & WEI, H. 2015. Influenza vaccine induces intracellular immune memory of human NK cells. *PLoS One*, 10, e0121258.
- ERICK, T. K., ANDERSON, C. K., REILLY, E. C., WANDS, J. R. & BROSSAY, L. 2016. NFIL3 Expression Distinguishes Tissue-Resident NK Cells and Conventional NK-like Cells in the Mouse Submandibular Glands. *J Immunol*, 197, 2485-91.
- FALLON, P. G., BALLANTYNE, S. J., MANGAN, N. E., BARLOW, J. L., DASVARMA, A., HEWETT, D. R., MCILGORM, A., JOLIN, H. E. & MCKENZIE, A. N. 2006. Identification of an interleukin (IL)-25-dependent cell population that provides IL-4, IL-5, and IL-13 at the onset of helminth expulsion. *J Exp Med*, 203, 1105-16.
- FEHNIGER, T. A., COOPER, M. A., NUOVO, G. J., CELLA, M., FACCHETTI, F., COLONNA, M. & CALIGIURI, M. A. 2003. CD56bright natural killer cells are present

Bibliography

- in human lymph nodes and are activated by T cell-derived IL-2: a potential new link between adaptive and innate immunity. *Blood*, 101, 3052-7.
- FEHNIGER, T. A., SHAH, M. H., TURNER, M. J., VANDEUSEN, J. B., WHITMAN, S. P., COOPER, M. A., SUZUKI, K., WECHSER, M., GOODSAY, F. & CALIGIURI, M. A. 1999. Differential cytokine and chemokine gene expression by human NK cells following activation with IL-18 or IL-15 in combination with IL-12: implications for the innate immune response. *J Immunol*, 162, 4511-20.
- FERNANDEZ, N. C., TREINER, E., VANCE, R. E., JAMIESON, A. M., LEMIEUX, S. & RAULET, D. H. 2005. A subset of natural killer cells achieves self-tolerance without expressing inhibitory receptors specific for self-MHC molecules. *Blood*, 105, 4416-23.
- FLOMMERSFELD, S., BÖTTCHER, J. P., ERSCHING, J., FLOSSDORF, M., MEISER, P., PACHMAYR, L. O., LEUBE, J., HENSEL, I., JAROSCH, S., ZHANG, Q., CHAUDHRY, M. Z., ANDRAE, I., SCHIEMANN, M., BUSCH, D. H., CICIN-SAIN, L., SUN, J. C., GASTEIGER, G., VICTORA, G. D., HÖFER, T., BUCHHOLZ, V. R. & GRASSMANN, S. 2021. Fate mapping of single NK cells identifies a type 1 innate lymphoid-like lineage that bridges innate and adaptive recognition of viral infection. *Immunity*.
- FLOMMERSFELD, S. 2018. Two distinct Ly49H⁺ NK cell subsets react to MCMV infection (unpublished Master's thesis). *Technical University of Munich*.
- FODIL-CORNU, N., LEE, S. H., BELANGER, S., MAKRIGIANNIS, A. P., BIRON, C. A., BULLER, R. M. & VIDAL, S. M. 2008. Ly49h-deficient C57BL/6 mice: a new mouse cytomegalovirus-susceptible model remains resistant to unrelated pathogens controlled by the NK gene complex. *J Immunol*, 181, 6394-405.
- FRENCH, A. R., PINGEL, J. T., WAGNER, M., BUBIC, I., YANG, L., KIM, S., KOSZINOWSKI, U., JONJIC, S. & YOKOYAMA, W. M. 2004. Escape of mutant double-stranded DNA virus from innate immune control. *Immunity*, 20, 747-56.
- GALIBERT, L., DIEMER, G. S., LIU, Z., JOHNSON, R. S., SMITH, J. L., WALZER, T., COMEAU, M. R., RAUCH, C. T., WOLFSON, M. F., SORENSEN, R. A., VAN DER VUURST DE VRIES, A. R., BRANSTETTER, D. G., KOELLING, R. M., SCHOLLER, J., FANSLow, W. C., BAUM, P. R., DERRY, J. M. & YAN, W. 2005. Nectin-like protein 2 defines a subset of T-cell zone dendritic cells and is a ligand for class-I-restricted T-cell-associated molecule. *J Biol Chem*, 280, 21955-64.
- GAO, Y., SOUZA-FONSECA-GUIMARAES, F., BALD, T., NG, S. S., YOUNG, A., NGIOW, S. F., RAUTELA, J., STRAUBE, J., WADDELL, N., BLAKE, S. J., YAN, J., BARTHOLIN, L., LEE, J. S., VIVIER, E., TAKEDA, K., MESSAOUDENE, M., ZITVOGEL, L., TENG, M. W. L., BELZ, G. T., ENGWERDA, C. R., HUNTINGTON, N. D., NAKAMURA, K., HOLZEL, M. & SMYTH, M. J. 2017. Tumor immunoevasion by the conversion of effector NK cells into type 1 innate lymphoid cells. *Nat Immunol*, 18, 1004-1015.
- GASCOYNE, D. M., LONG, E., VEIGA-FERNANDES, H., DE BOER, J., WILLIAMS, O., SEDDON, B., COLES, M., KIOUSSIS, D. & BRADY, H. J. 2009. The basic leucine zipper transcription factor E4BP4 is essential for natural killer cell development. *Nat Immunol*, 10, 1118-24.

Bibliography

- GASTEIGER, G., FAN, X., DIKIY, S., LEE, S. Y. & RUDENSKY, A. Y. 2015. Tissue residency of innate lymphoid cells in lymphoid and nonlymphoid organs. *Science*, 350, 981-5.
- GERLACH, C., ROHR, J. C., PERIE, L., VAN ROOIJ, N., VAN HEIJST, J. W., VELDS, A., URBANUS, J., NAIK, S. H., JACOBS, H., BELTMAN, J. B., DE BOER, R. J. & SCHUMACHER, T. N. 2013. Heterogeneous differentiation patterns of individual CD8⁺ T cells. *Science*, 340, 635-9.
- GERLACH, C., VAN HEIJST, J. W., SWART, E., SIE, D., ARMSTRONG, N., KERKHOVEN, R. M., ZEHN, D., BEVAN, M. J., SCHEPERS, K. & SCHUMACHER, T. N. 2010. One naive T cell, multiple fates in CD8⁺ T cell differentiation. *J Exp Med*, 207, 1235-46.
- GEROSA, F., BALDANI-GUERRA, B., NISII, C., MARCHESINI, V., CARRA, G. & TRINCHIERI, G. 2002. Reciprocal activating interaction between natural killer cells and dendritic cells. *J Exp Med*, 195, 327-33.
- GHILAS, S., AMBROSINI, M., CANCEL, J. C., BROUSSE, C., MASSE, M., LELOUARD, H., DALOD, M. & CROZAT, K. 2021. Natural killer cells and dendritic epidermal gammadelta T cells orchestrate type 1 conventional DC spatiotemporal repositioning toward CD8(+) T cells. *iScience*, 24, 103059.
- GILLARD, G. O., BIVAS-BENITA, M., HOVAV, A. H., GRANDPRE, L. E., PANAS, M. W., SEAMAN, M. S., HAYNES, B. F. & LETVIN, N. L. 2011. Thy1⁺ NK [corrected] cells from vaccinia virus-primed mice confer protection against vaccinia virus challenge in the absence of adaptive lymphocytes. *PLoS Pathog*, 7, e1002141.
- GORDON, S. M., CHAIX, J., RUPP, L. J., WU, J., MADERA, S., SUN, J. C., LINDSTEN, T. & REINER, S. L. 2012. The transcription factors T-bet and Eomes control key checkpoints of natural killer cell maturation. *Immunity*, 36, 55-67.
- GRAEF, P., BUCHHOLZ, V. R., STEMBERGER, C., FLOSSDORF, M., HENKEL, L., SCHIEMANN, M., DREXLER, I., HOFER, T., RIDDELL, S. R. & BUSCH, D. H. 2014. Serial transfer of single-cell-derived immunocompetence reveals stemness of CD8(+) central memory T cells. *Immunity*, 41, 116-26.
- GRASSMANN, S., MIHATSCH, L., MIR, J., KAZEROONIAN, A., RAHIMI, R., FLOMMERSFELD, S., SCHOBER, K., HENSEL, I., LEUBE, J., PACHMAYR, L. O., KRETSCHMER, L., ZHANG, Q., JOLLY, A., CHAUDHRY, M. Z., SCHIEMANN, M., CICIN-SAIN, L., HOFER, T., BUSCH, D. H., FLOSSDORF, M. & BUCHHOLZ, V. R. 2020. Early emergence of T central memory precursors programs clonal dominance during chronic viral infection. *Nat Immunol*, 21, 1563-1573.
- GRASSMANN, S., PACHMAYR, L. O., LEUBE, J., MIHATSCH, L., ANDRAE, I., FLOMMERSFELD, S., ODURO, J., CICIN-SAIN, L., SCHIEMANN, M., FLOSSDORF, M. & BUCHHOLZ, V. R. 2019. Distinct Surface Expression of Activating Receptor Ly49H Drives Differential Expansion of NK Cell Clones upon Murine Cytomegalovirus Infection. *Immunity*, 50, 1391-1400 e4.
- GUMA, M., ANGULO, A., VILCHES, C., GOMEZ-LOZANO, N., MALATS, N. & LOPEZ-BOTET, M. 2004. Imprint of human cytomegalovirus infection on the NK cell receptor repertoire. *Blood*, 104, 3664-71.

Bibliography

- GUMA, M., BUDT, M., SAEZ, A., BRCKALO, T., HENGEL, H., ANGULO, A. & LOPEZ-BOTET, M. 2006. Expansion of CD94/NKG2C+ NK cells in response to human cytomegalovirus-infected fibroblasts. *Blood*, 107, 3624-31.
- HAMMER, Q., RUCKERT, T., BORST, E. M., DUNST, J., HAUBNER, A., DUREK, P., HEINRICH, F., GASPARONI, G., BABIC, M., TOMIC, A., PIETRA, G., NIENEN, M., BLAU, I. W., HOFMANN, J., NA, I. K., PRINZ, I., KOENECKE, C., HEMMATI, P., BABEL, N., ARNOLD, R., WALTER, J., THURLEY, K., MASHREGHI, M. F., MESSERLE, M. & ROMAGNANI, C. 2018. Peptide-specific recognition of human cytomegalovirus strains controls adaptive natural killer cells. *Nat Immunol*, 19, 453-463.
- HANNA, J., GOLDMAN-WOHL, D., HAMANI, Y., AVRAHAM, I., GREENFIELD, C., NATANSON-YARON, S., PRUS, D., COHEN-DANIEL, L., ARNON, T. I., MANASTER, I., GAZIT, R., YUTKIN, V., BENHARROCH, D., PORGADOR, A., KESHET, E., YAGEL, S. & MANDELBOIM, O. 2006. Decidual NK cells regulate key developmental processes at the human fetal-maternal interface. *Nat Med*, 12, 1065-74.
- HARMON, C., ROBINSON, M. W., FAHEY, R., WHELAN, S., HOULIHAN, D. D., GEOGHEGAN, J. & O'FARRELLY, C. 2016. Tissue-resident Eomes(hi) T-bet(lo) CD56(bright) NK cells with reduced proinflammatory potential are enriched in the adult human liver. *Eur J Immunol*, 46, 2111-20.
- HARRIS, R. B. 1997. Loss of body fat in lean parabiotic partners of ob/ob mice. *Am J Physiol*, 272, R1809-15.
- HASHEMI, E. & MALARKANNAN, S. 2020. Tissue-Resident NK Cells: Development, Maturation, and Clinical Relevance. *Cancers (Basel)*, 12.
- HAYAKAWA, Y. & SMYTH, M. J. 2006. CD27 dissects mature NK cells into two subsets with distinct responsiveness and migratory capacity. *J Immunol*, 176, 1517-24.
- HEISE, M. T. & VIRGIN, H. W. T. 1995. The T-cell-independent role of gamma interferon and tumor necrosis factor alpha in macrophage activation during murine cytomegalovirus and herpes simplex virus infections. *J Virol*, 69, 904-9.
- HERBERMAN, R. B., NUNN, M. E., HOLDEN, H. T. & LAVRIN, D. H. 1975. Natural cytotoxic reactivity of mouse lymphoid cells against syngeneic and allogeneic tumors. II. Characterization of effector cells. *Int J Cancer*, 16, 230-9.
- HILDNER, K., EDELSON, B. T., PURTHA, W. E., DIAMOND, M., MATSUSHITA, H., KOHYAMA, M., CALDERON, B., SCHRAML, B. U., UNANUE, E. R., DIAMOND, M. S., SCHREIBER, R. D., MURPHY, T. L. & MURPHY, K. M. 2008. Batf3 deficiency reveals a critical role for CD8alpha+ dendritic cells in cytotoxic T cell immunity. *Science*, 322, 1097-100.
- HOGLUND, P., OHLEN, C., CARBONE, E., FRANKSSON, L., LJUNGGREN, H. G., LATOUR, A., KOLLER, B. & KARRE, K. 1991. Recognition of beta 2-microglobulin-negative (beta 2m-) T-cell blasts by natural killer cells from normal but not from beta 2m- mice: nonresponsiveness controlled by beta 2m- bone marrow in chimeric mice. *Proc Natl Acad Sci U S A*, 88, 10332-6.
- HOYLER, T., KLOSE, C. S., SOUABNI, A., TURQUETI-NEVES, A., PFEIFER, D., RAWLINS, E. L., VOEHRINGER, D., BUSSLINGER, M. & DIEFENBACH, A. 2012.

Bibliography

- The transcription factor GATA-3 controls cell fate and maintenance of type 2 innate lymphoid cells. *Immunity*, 37, 634-48.
- HSU, K. M., PRATT, J. R., AKERS, W. J., ACHILEFU, S. I. & YOKOYAMA, W. M. 2009. Murine cytomegalovirus displays selective infection of cells within hours after systemic administration. *J Gen Virol*, 90, 33-43.
- IYODA, T., SHIMOYAMA, S., LIU, K., OMATSU, Y., AKIYAMA, Y., MAEDA, Y., TAKAHARA, K., STEINMAN, R. M. & INABA, K. 2002. The CD8⁺ dendritic cell subset selectively endocytoses dying cells in culture and in vivo. *J Exp Med*, 195, 1289-302.
- JAMIESON, A. M., DIEFENBACH, A., MCMAHON, C. W., XIONG, N., CARLYLE, J. R. & RAULET, D. H. 2002. The role of the NKG2D immunoreceptor in immune cell activation and natural killing. *Immunity*, 17, 19-29.
- JONCKER, N. T., FERNANDEZ, N. C., TREINER, E., VIVIER, E. & RAULET, D. H. 2009. NK cell responsiveness is tuned commensurate with the number of inhibitory receptors for self-MHC class I: the rheostat model. *J Immunol*, 182, 4572-80.
- JUELKE, K., KILLIG, M., LUETKE-EVERSLOH, M., PARENTE, E., GRUEN, J., MORANDI, B., FERLAZZO, G., THIEL, A., SCHMITT-KNOSALLA, I. & ROMAGNANI, C. 2010. CD62L expression identifies a unique subset of polyfunctional CD56dim NK cells. *Blood*, 116, 1299-307.
- KALLIES, A., ZEHN, D. & UTZSCHNEIDER, D. T. 2020. Precursor exhausted T cells: key to successful immunotherapy? *Nat Rev Immunol*, 20, 128-136.
- KAMIMURA, Y. & LANIER, L. L. 2015. Homeostatic control of memory cell progenitors in the natural killer cell lineage. *Cell Rep*, 10, 280-91.
- KARRE, K., LJUNGGREN, H. G., PIONTEK, G. & KIESSLING, R. 1986. Selective rejection of H-2-deficient lymphoma variants suggests alternative immune defence strategy. *Nature*, 319, 675-8.
- KEPPEL, M. P., YANG, L. & COOPER, M. A. 2013. Murine NK cell intrinsic cytokine-induced memory-like responses are maintained following homeostatic proliferation. *J Immunol*, 190, 4754-62.
- KIM, S., POURSIENE-LAURENT, J., TRUSCOTT, S. M., LYBARGER, L., SONG, Y. J., YANG, L., FRENCH, A. R., SUNWOO, J. B., LEMIEUX, S., HANSEN, T. H. & YOKOYAMA, W. M. 2005. Licensing of natural killer cells by host major histocompatibility complex class I molecules. *Nature*, 436, 709-13.
- KLOSE, C. S. N., FLACH, M., MOHLE, L., ROGELL, L., HOYLER, T., EBERT, K., FABIUNKE, C., PFEIFER, D., SEXL, V., FONSECA-PEREIRA, D., DOMINGUES, R. G., VEIGA-FERNANDES, H., ARNOLD, S. J., BUSSLINGER, M., DUNAY, I. R., TANRIVER, Y. & DIEFENBACH, A. 2014. Differentiation of type 1 ILCs from a common progenitor to all helper-like innate lymphoid cell lineages. *Cell*, 157, 340-356.
- KOH, C. Y., BLAZAR, B. R., GEORGE, T., WELNIAK, L. A., CAPITINI, C. M., RAZIUDDIN, A., MURPHY, W. J. & BENNETT, M. 2001. Augmentation of antitumor effects by NK cell inhibitory receptor blockade in vitro and in vivo. *Blood*, 97, 3132-7.

Bibliography

- KOO, G. C. & PEPPARD, J. R. 1984. Establishment of monoclonal anti-Nk-1.1 antibody. *Hybridoma*, 3, 301-3.
- KRETSCHMER, L., BUSCH, D. H. & BUCHHOLZ, V. R. 2021. A Single-Cell Perspective on Memory T-Cell Differentiation. *Cold Spring Harb Perspect Biol*, 13.
- KRUG, A., FRENCH, A. R., BARCHET, W., FISCHER, J. A., DZIOONEK, A., PINGEL, J. T., ORIHUELA, M. M., AKIRA, S., YOKOYAMA, W. M. & COLONNA, M. 2004. TLR9-dependent recognition of MCMV by IPC and DC generates coordinated cytokine responses that activate antiviral NK cell function. *Immunity*, 21, 107-19.
- LA MANNO, G., SOLDATOV, R., ZEISEL, A., BRAUN, E., HOCHGERNER, H., PETUKHOV, V., LIDSCHREIBER, K., KASTRITI, M. E., LONNERBERG, P., FURLAN, A., FAN, J., BORM, L. E., LIU, Z., VAN BRUGGEN, D., GUO, J., HE, X., BARKER, R., SUNDSTROM, E., CASTELO-BRANCO, G., CRAMER, P., ADAMEYKO, I., LINNARSSON, S. & KHARCHENKO, P. V. 2018. RNA velocity of single cells. *Nature*, 560, 494-498.
- LANIER, L. L. 2005. NK cell recognition. *Annu Rev Immunol*, 23, 225-74.
- LANIER, L. L. 2008. Evolutionary struggles between NK cells and viruses. *Nat Rev Immunol*, 8, 259-68.
- LANIER, L. L., LE, A. M., CIVIN, C. I., LOKEN, M. R. & PHILLIPS, J. H. 1986. The relationship of CD16 (Leu-11) and Leu-19 (NKH-1) antigen expression on human peripheral blood NK cells and cytotoxic T lymphocytes. *J Immunol*, 136, 4480-6.
- LANIER, L. L., LE, A. M., PHILLIPS, J. H., WARNER, N. L. & BABCOCK, G. F. 1983. Subpopulations of human natural killer cells defined by expression of the Leu-7 (HNK-1) and Leu-11 (NK-15) antigens. *J Immunol*, 131, 1789-96.
- LANIER, L. L., RUITENBERG, J. J. & PHILLIPS, J. H. 1988. Functional and biochemical analysis of CD16 antigen on natural killer cells and granulocytes. *J Immunol*, 141, 3478-85.
- LASH, G. E., SCHIESSL, B., KIRKLEY, M., INNES, B. A., COOPER, A., SEARLE, R. F., ROBSON, S. C. & BULMER, J. N. 2006. Expression of angiogenic growth factors by uterine natural killer cells during early pregnancy. *J Leukoc Biol*, 80, 572-80.
- LATHBURY, L. J., ALLAN, J. E., SHELLAM, G. R. & SCALZO, A. A. 1996. Effect of host genotype in determining the relative roles of natural killer cells and T cells in mediating protection against murine cytomegalovirus infection. *J Gen Virol*, 77 (Pt 10), 2605-13.
- LAU, C. M., ADAMS, N. M., GEARY, C. D., WEIZMAN, O. E., RAPP, M., PRITYKIN, Y., LESLIE, C. S. & SUN, J. C. 2018. Epigenetic control of innate and adaptive immune memory. *Nat Immunol*, 19, 963-972.
- LEE, S. H., GIRARD, S., MACINA, D., BUSA, M., ZAFER, A., BELOUCHI, A., GROS, P. & VIDAL, S. M. 2001. Susceptibility to mouse cytomegalovirus is associated with deletion of an activating natural killer cell receptor of the C-type lectin superfamily. *Nat Genet*, 28, 42-5.

Bibliography

- LEIDEN, J. M., KARPINSKI, B. A., GOTTSCHALK, L. & KORNBLUTH, J. 1989. Susceptibility to natural killer cell-mediated cytotoxicity is independent of the level of target cell class I HLA expression. *J Immunol*, 142, 2140-7.
- LI, T., WANG, J., WANG, Y., CHEN, Y., WEI, H., SUN, R. & TIAN, Z. 2017. Respiratory Influenza Virus Infection Induces Memory-like Liver NK Cells in Mice. *J Immunol*, 198, 1242-1252.
- LIAO, N. S., BIX, M., ZIJLSTRA, M., JAENISCH, R. & RAULET, D. 1991. MHC class I deficiency: susceptibility to natural killer (NK) cells and impaired NK activity. *Science*, 253, 199-202.
- LJUNGGREN, H. G., OHLEN, C., HOGLUND, P., FRANKSSON, L. & KARRE, K. 1991. The RMA-S lymphoma mutant; consequences of a peptide loading defect on immunological recognition and graft rejection. *Int J Cancer Suppl*, 6, 38-44.
- LOPEZ-VERGES, S., MILUSH, J. M., SCHWARTZ, B. S., PANDO, M. J., JARJOURA, J., YORK, V. A., HOUCHINS, J. P., MILLER, S., KANG, S. M., NORRIS, P. J., NIXON, D. F. & LANIER, L. L. 2011. Expansion of a unique CD57(+)NKG2Chi natural killer cell subset during acute human cytomegalovirus infection. *Proc Natl Acad Sci U S A*, 108, 14725-32.
- LUCIN, P., JONJIC, S., MESSERLE, M., POLIC, B., HENGEL, H. & KOSZINOWSKI, U. H. 1994. Late phase inhibition of murine cytomegalovirus replication by synergistic action of interferon-gamma and tumour necrosis factor. *J Gen Virol*, 75 (Pt 1), 101-10.
- MACKAY, L. K., MINNICH, M., KRAGTEN, N. A., LIAO, Y., NOTA, B., SEILLET, C., ZAID, A., MAN, K., PRESTON, S., FREESTONE, D., BRAUN, A., WYNNE-JONES, E., BEHR, F. M., STARK, R., PELLICCI, D. G., GODFREY, D. I., BELZ, G. T., PELLEGRINI, M., GEBHARDT, T., BUSSLINGER, M., SHI, W., CARBONE, F. R., VAN LIER, R. A., KALLIES, A. & VAN GISBERGEN, K. P. 2016. Hobit and Blimp1 instruct a universal transcriptional program of tissue residency in lymphocytes. *Science*, 352, 459-63.
- MAEDA, M., CARPENITO, C., RUSSELL, R. C., DASANJH, J., VEINOTTE, L. L., OHTA, H., YAMAMURA, T., TAN, R. & TAKEI, F. 2005. Murine CD160, Ig-like receptor on NK cells and NKT cells, recognizes classical and nonclassical MHC class I and regulates NK cell activation. *J Immunol*, 175, 4426-32.
- MAHMOUD, A. B., TU, M. M., WIGHT, A., ZEIN, H. S., RAHIM, M. M., LEE, S. H., SEKHON, H. S., BROWN, E. G. & MAKRIGIANNIS, A. P. 2016. Influenza Virus Targets Class I MHC-Educated NK Cells for Immuno-evasion. *PLoS Pathog*, 12, e1005446.
- MAIZA, H., LECA, G., MANSUR, I. G., SCHIAVON, V., BOUMSELL, L. & BENSUSSAN, A. 1993. A novel 80-kD cell surface structure identifies human circulating lymphocytes with natural killer activity. *J Exp Med*, 178, 1121-6.
- MAJEWSKA-SZCZEPANIK, M., PAUST, S., VON ANDRIAN, U. H., ASKENASE, P. W. & SZCZEPANIK, M. 2013. Natural killer cell-mediated contact sensitivity develops rapidly and depends on interferon-alpha, interferon-gamma and interleukin-12. *Immunology*, 140, 98-110.

Bibliography

- MANDELBOIM, O., LIEBERMAN, N., LEV, M., PAUL, L., ARNON, T. I., BUSHKIN, Y., DAVIS, D. M., STROMINGER, J. L., YEWDELL, J. W. & PORGADOR, A. 2001. Recognition of haemagglutinins on virus-infected cells by NKp46 activates lysis by human NK cells. *Nature*, 409, 1055-60.
- MCFARLAND, A. P., YALIN, A., WANG, S. Y., CORTEZ, V. S., LANDSBERGER, T., SUDAN, R., PENG, V., MILLER, H. L., RICCI, B., DAVID, E., FACCIO, R., AMIT, I. & COLONNA, M. 2021. Multi-tissue single-cell analysis deconstructs the complex programs of mouse natural killer and type 1 innate lymphoid cells in tissues and circulation. *Immunity*, 54, 1320-1337 e4.
- MELSEN, J. E., LUGTHART, G., LANKESTER, A. C. & SCHILHAM, M. W. 2016. Human Circulating and Tissue-Resident CD56(bright) Natural Killer Cell Populations. *Front Immunol*, 7, 262.
- MIN-OO, G., BEZMAN, N. A., MADERA, S., SUN, J. C. & LANIER, L. L. 2014. Proapoptotic Bim regulates antigen-specific NK cell contraction and the generation of the memory NK cell pool after cytomegalovirus infection. *J Exp Med*, 211, 1289-96.
- MITROVIC, M., ARAPOVIC, J., JORDAN, S., FODIL-CORNU, N., EBERT, S., VIDAL, S. M., KRMPOTIC, A., REDDEHASE, M. J. & JONJIC, S. 2012. The NK cell response to mouse cytomegalovirus infection affects the level and kinetics of the early CD8(+) T-cell response. *J Virol*, 86, 2165-75.
- MOCIKAT, R., BRAUMULLER, H., GUMY, A., EGETER, O., ZIEGLER, H., REUSCH, U., BUBECK, A., LOUIS, J., MAILHAMMER, R., RIETHMULLER, G., KOSZINOWSKI, U. & ROCKEN, M. 2003. Natural killer cells activated by MHC class I(low) targets prime dendritic cells to induce protective CD8 T cell responses. *Immunity*, 19, 561-9.
- MONTICELLI, L. A., SONNENBERG, G. F., ABT, M. C., ALENGHAT, T., ZIEGLER, C. G., DOERING, T. A., ANGELOSANTO, J. M., LAIDLAW, B. J., YANG, C. Y., SATHALIYAWALA, T., KUBOTA, M., TURNER, D., DIAMOND, J. M., GOLDRATH, A. W., FARBER, D. L., COLLMAN, R. G., WHERRY, E. J. & ARTIS, D. 2011. Innate lymphoid cells promote lung-tissue homeostasis after infection with influenza virus. *Nat Immunol*, 12, 1045-54.
- MORETTA, A., BOTTINO, C., VITALE, M., PENDE, D., BIASSONI, R., MINGARI, M. C. & MORETTA, L. 1996. Receptors for HLA class-I molecules in human natural killer cells. *Annu Rev Immunol*, 14, 619-48.
- NABEKURA, T., KANAYA, M., SHIBUYA, A., FU, G., GASCOIGNE, N. R. & LANIER, L. L. 2014. Costimulatory molecule DNAM-1 is essential for optimal differentiation of memory natural killer cells during mouse cytomegalovirus infection. *Immunity*, 40, 225-34.
- NAGLER, A., LANIER, L. L., CWIRLA, S. & PHILLIPS, J. H. 1989. Comparative studies of human FcRIII-positive and negative natural killer cells. *J Immunol*, 143, 3183-91.
- NARNI-MANCINELLI, E., CHAIX, J., FENIS, A., KERDILES, Y. M., YESSAAD, N., REYNDERS, A., GREGOIRE, C., LUCHE, H., UGOLINI, S., TOMASELLO, E., WALZER, T. & VIVIER, E. 2011. Fate mapping analysis of lymphoid cells expressing the NKp46 cell surface receptor. *Proc Natl Acad Sci U S A*, 108, 18324-9.

Bibliography

- NI, J., MILLER, M., STOJANOVIC, A., GARBI, N. & CERWENKA, A. 2012. Sustained effector function of IL-12/15/18-preactivated NK cells against established tumors. *J Exp Med*, 209, 2351-65.
- NISHIMURA, M. I., STROYNOWSKI, I., HOOD, L. & OSTRAND-ROSENBERG, S. 1988. H-2Kb antigen expression has no effect on natural killer susceptibility and tumorigenicity of a murine hepatoma. *J Immunol*, 141, 4403-9.
- O'LEARY, J. G., GOODARZI, M., DRAYTON, D. L. & VON ANDRIAN, U. H. 2006. T cell- and B cell-independent adaptive immunity mediated by natural killer cells. *Nat Immunol*, 7, 507-16.
- O'SULLIVAN, T. E., SUN, J. C. & LANIER, L. L. 2015. Natural Killer Cell Memory. *Immunity*, 43, 634-45.
- ORANGE, J. S. 2013. Natural killer cell deficiency. *J Allergy Clin Immunol*, 132, 515-25; quiz 526.
- ORANGE, J. S. & BIRON, C. A. 1996. Characterization of early IL-12, IFN- α , and TNF effects on antiviral state and NK cell responses during murine cytomegalovirus infection. *J Immunol*, 156, 4746-56.
- ORR, M. T., MURPHY, W. J. & LANIER, L. L. 2010. 'Unlicensed' natural killer cells dominate the response to cytomegalovirus infection. *Nat Immunol*, 11, 321-7.
- PAUST, S., GILL, H. S., WANG, B. Z., FLYNN, M. P., MOSEMAN, E. A., SENMAN, B., SZCZEPANIK, M., TELENTI, A., ASKENASE, P. W., COMPANS, R. W. & VON ANDRIAN, U. H. 2010. Critical role for the chemokine receptor CXCR6 in NK cell-mediated antigen-specific memory of haptens and viruses. *Nat Immunol*, 11, 1127-35.
- PEI, W., FEYERABEND, T. B., ROSSLER, J., WANG, X., POSTRACH, D., BUSCH, K., RODE, I., KLAPPROTH, K., DIETLEIN, N., QUEDENAU, C., CHEN, W., SAUER, S., WOLF, S., HOFER, T. & RODEWALD, H. R. 2017. Polylox barcoding reveals haematopoietic stem cell fates realized in vivo. *Nature*, 548, 456-460.
- PENG, H., JIANG, X., CHEN, Y., SOJKA, D. K., WEI, H., GAO, X., SUN, R., YOKOYAMA, W. M. & TIAN, Z. 2013a. Liver-resident NK cells confer adaptive immunity in skin-contact inflammation. *J Clin Invest*, 123, 1444-56.
- PENG, H., SUN, R., TANG, L., WEI, H. & TIAN, Z. 2013b. CD62L is critical for maturation and accumulation of murine hepatic NK cells in response to viral infection. *J Immunol*, 190, 4255-62.
- POLI, A., MICHEL, T., THERESINE, M., ANDRES, E., HENTGES, F. & ZIMMER, J. 2009. CD56bright natural killer (NK) cells: an important NK cell subset. *Immunology*, 126, 458-65.
- PRAGER, I. & WATZL, C. 2019. Mechanisms of natural killer cell-mediated cellular cytotoxicity. *J Leukoc Biol*, 105, 1319-1329.
- RAULET, D. H., GASSER, S., GOWEN, B. G., DENG, W. & JUNG, H. 2013. Regulation of ligands for the NKG2D activating receptor. *Annu Rev Immunol*, 31, 413-41.

Bibliography

- RAULET, D. H., HELD, W., CORREA, I., DORFMAN, J. R., WU, M. F. & CORRAL, L. 1997. Specificity, tolerance and developmental regulation of natural killer cells defined by expression of class I-specific Ly49 receptors. *Immunol Rev*, 155, 41-52.
- REEVES, R. K., LI, H., JOST, S., BLASS, E., LI, H., SCHAFER, J. L., VARNER, V., MANICKAM, C., ESLAMIZAR, L., ALTFELD, M., VON ANDRIAN, U. H. & BAROUCH, D. H. 2015. Antigen-specific NK cell memory in rhesus macaques. *Nat Immunol*, 16, 927-32.
- RESTIFO, N. P., ESQUIVEL, F., KAWAKAMI, Y., YEWDELL, J. W., MULE, J. J., ROSENBERG, S. A. & BENNINK, J. R. 1993. Identification of human cancers deficient in antigen processing. *J Exp Med*, 177, 265-72.
- REUSCH, U., MURANYI, W., LUCIN, P., BURGERT, H. G., HENGEL, H. & KOSZINOWSKI, U. H. 1999. A cytomegalovirus glycoprotein re-routes MHC class I complexes to lysosomes for degradation. *EMBO J*, 18, 1081-91.
- ROBBINS, S. H., BESSOU, G., CORNILLON, A., ZUCCHINI, N., RUPP, B., RUZSICS, Z., SACHER, T., TOMASELLO, E., VIVIER, E., KOSZINOWSKI, U. H. & DALOD, M. 2007. Natural killer cells promote early CD8 T cell responses against cytomegalovirus. *PLoS Pathog*, 3, e123.
- ROBINETTE, M. L., FUCHS, A., CORTEZ, V. S., LEE, J. S., WANG, Y., DURUM, S. K., GILFILLAN, S., COLONNA, M. & IMMUNOLOGICAL GENOME, C. 2015. Transcriptional programs define molecular characteristics of innate lymphoid cell classes and subsets. *Nat Immunol*, 16, 306-17.
- ROLLE, A., POLLMANN, J., EWEN, E. M., LE, V. T., HALENIUS, A., HENGEL, H. & CERWENKA, A. 2014. IL-12-producing monocytes and HLA-E control HCMV-driven NKG2C+ NK cell expansion. *J Clin Invest*, 124, 5305-16.
- ROMAGNANI, C., JUELKE, K., FALCO, M., MORANDI, B., D'AGOSTINO, A., COSTA, R., RATTO, G., FORTE, G., CARREGA, P., LUI, G., CONTE, R., STROWIG, T., MORETTA, A., MUNZ, C., THIEL, A., MORETTA, L. & FERLAZZO, G. 2007. CD56brightCD16- killer Ig-like receptor- NK cells display longer telomeres and acquire features of CD56dim NK cells upon activation. *J Immunol*, 178, 4947-55.
- ROME, R., ROSARIO, M., BERRIEN-ELLIOTT, M. M., WAGNER, J. A., JEWELL, B. A., SCHAPPE, T., LEONG, J. W., ABDEL-LATIF, S., SCHNEIDER, S. E., WILLEY, S., NEAL, C. C., YU, L., OH, S. T., LEE, Y. S., MULDER, A., CLAAS, F., COOPER, M. A. & FEHNIGER, T. A. 2016. Cytokine-induced memory-like natural killer cells exhibit enhanced responses against myeloid leukemia. *Sci Transl Med*, 8, 357ra123.
- ROME, R., SCHNEIDER, S. E., LEONG, J. W., CHASE, J. M., KEPPEL, C. R., SULLIVAN, R. P., COOPER, M. A. & FEHNIGER, T. A. 2012. Cytokine activation induces human memory-like NK cells. *Blood*, 120, 4751-60.
- ROSMARAKI, E. E., DOUAGI, I., ROTH, C., COLUCCI, F., CUMANO, A. & DI SANTO, J. P. 2001. Identification of committed NK cell progenitors in adult murine bone marrow. *Eur J Immunol*, 31, 1900-9.
- SALLUSTO, F. & LANZAVECCHIA, A. 1994. Efficient presentation of soluble antigen by cultured human dendritic cells is maintained by granulocyte/macrophage colony-

Bibliography

- stimulating factor plus interleukin 4 and downregulated by tumor necrosis factor alpha. *J Exp Med*, 179, 1109-18.
- SANOS, S. L., BUI, V. L., MORTHA, A., OBERLE, K., HENERS, C., JOHNER, C. & DIEFENBACH, A. 2009. ROR γ and commensal microflora are required for the differentiation of mucosal interleukin 22-producing NKp46+ cells. *Nat Immunol*, 10, 83-91.
- SATOH-TAKAYAMA, N., VOSSHENRICH, C. A., LESJEAN-POTTIER, S., SAWA, S., LOCHNER, M., RATTIS, F., MENTION, J. J., THIAM, K., CERF-BENSUSSAN, N., MANDELBOIM, O., EBERL, G. & DI SANTO, J. P. 2008. Microbial flora drives interleukin 22 production in intestinal NKp46+ cells that provide innate mucosal immune defense. *Immunity*, 29, 958-70.
- SCHEPERS, K., SWART, E., VAN HEIJST, J. W., GERLACH, C., CASTRUCCI, M., SIE, D., HEIMERIKX, M., VELDS, A., KERKHOVEN, R. M., ARENS, R. & SCHUMACHER, T. N. 2008. Dissecting T cell lineage relationships by cellular barcoding. *J Exp Med*, 205, 2309-18.
- SCHULZ, O. & REIS E SOUSA, C. 2002. Cross-presentation of cell-associated antigens by CD8 α + dendritic cells is attributable to their ability to internalize dead cells. *Immunology*, 107, 183-9.
- SHELLAM, G. R., ALLAN, J. E., PAPADIMITRIOU, J. M. & BANCROFT, G. J. 1981. Increased susceptibility to cytomegalovirus infection in beige mutant mice. *Proc Natl Acad Sci U S A*, 78, 5104-8.
- SHEN, F. W., SAGA, Y., LITMAN, G., FREEMAN, G., TUNG, J. S., CANTOR, H. & BOYSE, E. A. 1985. Cloning of Ly-5 cDNA. *Proc Natl Acad Sci U S A*, 82, 7360-3.
- SILVA, A., ANDREWS, D. M., BROOKS, A. G., SMYTH, M. J. & HAYAKAWA, Y. 2008. Application of CD27 as a marker for distinguishing human NK cell subsets. *Int Immunol*, 20, 625-30.
- SIMON, C. O., HOLTAPPELS, R., TERVO, H. M., BOHM, V., DAUBNER, T., OEHRLEIN-KARPI, S. A., KUHNAPFEL, B., RENZAHO, A., STRAND, D., PODLECH, J., REDDEHASE, M. J. & GRZIMEK, N. K. 2006. CD8 T cells control cytomegalovirus latency by epitope-specific sensing of transcriptional reactivation. *J Virol*, 80, 10436-56.
- SMITH, H. R., HEUSEL, J. W., MEHTA, I. K., KIM, S., DORNER, B. G., NAIDENKO, O. V., IIZUKA, K., FURUKAWA, H., BECKMAN, D. L., PINGEL, J. T., SCALZO, A. A., FREMONT, D. H. & YOKOYAMA, W. M. 2002. Recognition of a virus-encoded ligand by a natural killer cell activation receptor. *Proc Natl Acad Sci U S A*, 99, 8826-31.
- SNYDER, C. M., ALLAN, J. E., BONNETT, E. L., DOOM, C. M. & HILL, A. B. 2010. Cross-presentation of a spread-defective MCMV is sufficient to prime the majority of virus-specific CD8+ T cells. *PLoS One*, 5, e9681.
- SOJKA, D. K., PLOUGASTEL-DOUGLAS, B., YANG, L., PAK-WITTEL, M. A., ARTYOMOV, M. N., IVANOVA, Y., ZHONG, C., CHASE, J. M., ROTHMAN, P. B., YU, J., RILEY, J. K., ZHU, J., TIAN, Z. & YOKOYAMA, W. M. 2014. Tissue-resident

Bibliography

- natural killer (NK) cells are cell lineages distinct from thymic and conventional splenic NK cells. *Elife*, 3, e01659.
- SONNENBERG, G. F., MONTICELLI, L. A., ALENGHAT, T., FUNG, T. C., HUTNICK, N. A., KUNISAWA, J., SHIBATA, N., GRUNBERG, S., SINHA, R., ZAHM, A. M., TARDIF, M. R., SATHALIYAWALA, T., KUBOTA, M., FARBER, D. L., COLLMAN, R. G., SHAKED, A., FOUUSER, L. A., WEINER, D. B., TESSIER, P. A., FRIEDMAN, J. R., KIYONO, H., BUSHMAN, F. D., CHANG, K. M. & ARTIS, D. 2012. Innate lymphoid cells promote anatomical containment of lymphoid-resident commensal bacteria. *Science*, 336, 1321-5.
- SPITS, H., ARTIS, D., COLONNA, M., DIEFENBACH, A., DI SANTO, J. P., EBERL, G., KOYASU, S., LOCKSLEY, R. M., MCKENZIE, A. N., MEBIUS, R. E., POWRIE, F. & VIVIER, E. 2013. Innate lymphoid cells--a proposal for uniform nomenclature. *Nat Rev Immunol*, 13, 145-9.
- STEGMANN, K. A., ROBERTSON, F., HANSI, N., GILL, U., PALLANT, C., CHRISTOPHIDES, T., PALLETT, L. J., PEPPA, D., DUNN, C., FUSAI, G., MALE, V., DAVIDSON, B. R., KENNEDY, P. & MAINI, M. K. 2016. CXCR6 marks a novel subset of T-bet(lo)Eomes(hi) natural killer cells residing in human liver. *Sci Rep*, 6, 26157.
- STEMBERGER, C., HUSTER, K. M., KOFFLER, M., ANDERL, F., SCHIEMANN, M., WAGNER, H. & BUSCH, D. H. 2007. A single naive CD8+ T cell precursor can develop into diverse effector and memory subsets. *Immunity*, 27, 985-97.
- STERN, P., GIDLUND, M., ORN, A. & WIGZELL, H. 1980. Natural killer cells mediate lysis of embryonal carcinoma cells lacking MHC. *Nature*, 285, 341-2.
- SUN, J. C., BEILKE, J. N. & LANIER, L. L. 2009. Adaptive immune features of natural killer cells. *Nature*, 457, 557-61.
- TAKATORI, H., KANNO, Y., WATFORD, W. T., TATO, C. M., WEISS, G., IVANOV, II, LITTMAN, D. R. & O'SHEA, J. J. 2009. Lymphoid tissue inducer-like cells are an innate source of IL-17 and IL-22. *J Exp Med*, 206, 35-41.
- TESSMER, M. S., REILLY, E. C. & BROSSAY, L. 2011. Salivary gland NK cells are phenotypically and functionally unique. *PLoS Pathog*, 7, e1001254.
- TOMASEC, P., BRAUD, V. M., RICKARDS, C., POWELL, M. B., MCSHARRY, B. P., GADOLA, S., CERUNDOLO, V., BORYSIEWICZ, L. K., MCMICHAEL, A. J. & WILKINSON, G. W. 2000. Surface expression of HLA-E, an inhibitor of natural killer cells, enhanced by human cytomegalovirus gpUL40. *Science*, 287, 1031.
- TORTI, N., WALTON, S. M., MURPHY, K. M. & OXENIUS, A. 2011. Batf3 transcription factor-dependent DC subsets in murine CMV infection: differential impact on T-cell priming and memory inflation. *Eur J Immunol*, 41, 2612-8.
- TU, M. M., MAHMOUD, A. B. & MAKRIGIANNIS, A. P. 2016. Licensed and Unlicensed NK Cells: Differential Roles in Cancer and Viral Control. *Front Immunol*, 7, 166.

Bibliography

- TU, T. C., BROWN, N. K., KIM, T. J., WROBLEWSKA, J., YANG, X., GUO, X., LEE, S. H., KUMAR, V., LEE, K. M. & FU, Y. X. 2015. CD160 is essential for NK-mediated IFN-gamma production. *J Exp Med*, 212, 415-29.
- ULBRECHT, M., MARTINOZZI, S., GRZESCHIK, M., HENGEL, H., ELLWART, J. W., PLA, M. & WEISS, E. H. 2000. Cutting edge: the human cytomegalovirus UL40 gene product contains a ligand for HLA-E and prevents NK cell-mediated lysis. *J Immunol*, 164, 5019-22.
- UPPENDAHL, L. D., FELICES, M., BENDZICK, L., RYAN, C., KODAL, B., HINDERLIE, P., BOYLAN, K. L. M., SKUBITZ, A. P. N., MILLER, J. S. & GELLER, M. A. 2019. Cytokine-induced memory-like natural killer cells have enhanced function, proliferation, and in vivo expansion against ovarian cancer cells. *Gynecol Oncol*, 153, 149-157.
- VAN DEN BOORN, J. G., JAKOBS, C., HAGEN, C., RENN, M., LUITEN, R. M., MELIEF, C. J., TUTING, T., GARBI, N., HARTMANN, G. & HORNUNG, V. 2016. Inflammasome-Dependent Induction of Adaptive NK Cell Memory. *Immunity*, 44, 1406-21.
- VARGAS, C. L., POURSIENE-LAURENT, J., YANG, L. & YOKOYAMA, W. M. 2011. Development of thymic NK cells from double negative 1 thymocyte precursors. *Blood*, 118, 3570-8.
- VIVIER, E., ARTIS, D., COLONNA, M., DIEFENBACH, A., DI SANTO, J. P., EBERL, G., KOYASU, S., LOCKSLEY, R. M., MCKENZIE, A. N. J., MEBIUS, R. E., POWRIE, F. & SPITS, H. 2018. Innate Lymphoid Cells: 10 Years On. *Cell*, 174, 1054-1066.
- VIVIER, E., NUNES, J. A. & VELY, F. 2004. Natural killer cell signaling pathways. *Science*, 306, 1517-9.
- VOSSEN, M. T., MATMATI, M., HERTOOGHS, K. M., BAARS, P. A., GENT, M. R., LECLERCQ, G., HAMANN, J., KUIJPERS, T. W. & VAN LIER, R. A. 2008. CD27 defines phenotypically and functionally different human NK cell subsets. *J Immunol*, 180, 3739-45.
- VOSSHENRICH, C. A., GARCIA-OJEDA, M. E., SAMSON-VILLEGGER, S. I., PASQUALETTO, V., ENAULT, L., RICHARD-LE GOFF, O., CORCUFF, E., GUY-GRAND, D., ROCHA, B., CUMANO, A., ROGGE, L., EZINE, S. & DI SANTO, J. P. 2006. A thymic pathway of mouse natural killer cell development characterized by expression of GATA-3 and CD127. *Nat Immunol*, 7, 1217-24.
- VOSSHENRICH, C. A., RANSON, T., SAMSON, S. I., CORCUFF, E., COLUCCI, F., ROSMARAKI, E. E. & DI SANTO, J. P. 2005. Roles for common cytokine receptor gamma-chain-dependent cytokines in the generation, differentiation, and maturation of NK cell precursors and peripheral NK cells in vivo. *J Immunol*, 174, 1213-21.
- WALLACH, D., FELLOUS, M. & REVEL, M. 1982. Preferential effect of gamma interferon on the synthesis of HLA antigens and their mRNAs in human cells. *Nature*, 299, 833-6.
- WALZER, T., BLERY, M., CHAIX, J., FUSERI, N., CHASSON, L., ROBBINS, S. H., JAEGER, S., ANDRE, P., GAUTHIER, L., DANIEL, L., CHEMIN, K., MOREL, Y., DALOD, M., IMBERT, J., PIERRES, M., MORETTA, A., ROMAGNE, F. & VIVIER,

Bibliography

- E. 2007. Identification, activation, and selective in vivo ablation of mouse NK cells via NKp46. *Proc Natl Acad Sci U S A*, 104, 3384-9.
- WEIZMAN, O. E., ADAMS, N. M., SCHUSTER, I. S., KRISHNA, C., PRITYKIN, Y., LAU, C., DEGLI-ESPOSTI, M. A., LESLIE, C. S., SUN, J. C. & O'SULLIVAN, T. E. 2017. ILC1 Confer Early Host Protection at Initial Sites of Viral Infection. *Cell*, 171, 795-808 e12.
- WEIZMAN, O. E., SONG, E., ADAMS, N. M., HILDRETH, A. D., RIGGAN, L., KRISHNA, C., AGUILAR, O. A., LESLIE, C. S., CARLYLE, J. R., SUN, J. C. & O'SULLIVAN, T. E. 2019. Mouse cytomegalovirus-experienced ILC1s acquire a memory response dependent on the viral glycoprotein m12. *Nat Immunol*, 20, 1004-1011.
- WIGHT, A., MAHMOUD, A. B., SCUR, M., TU, M. M., RAHIM, M. M. A., SAD, S. & MAKRIGIANNIS, A. P. 2018. Critical role for the Ly49 family of class I MHC receptors in adaptive natural killer cell responses. *Proc Natl Acad Sci U S A*, 115, 11579-11584.
- WILLIAMS, K. J., WILSON, E., DAVIDSON, C. L., AGUILAR, O. A., FU, L., CARLYLE, J. R. & BURSHTYN, D. N. 2012. Poxvirus infection-associated downregulation of C-type lectin-related-b prevents NK cell inhibition by NK receptor protein-1B. *J Immunol*, 188, 4980-91.
- WOLF, F. A., ANGERER, P. & THEIS, F. J. 2018. SCANPY: large-scale single-cell gene expression data analysis. *Genome Biol*, 19, 15.
- WONG, S. H., WALKER, J. A., JOLIN, H. E., DRYNAN, L. F., HAMS, E., CAMELO, A., BARLOW, J. L., NEILL, D. R., PANOVA, V., KOCH, U., RADTKE, F., HARDMAN, C. S., HWANG, Y. Y., FALLON, P. G. & MCKENZIE, A. N. 2012. Transcription factor RORalpha is critical for nuocyte development. *Nat Immunol*, 13, 229-36.
- WU, C., ESPINOZA, D. A., KOELLE, S. J., YANG, D., TRUITT, L., SCHLUMS, H., LAFONT, B. A., DAVIDSON-MONCADA, J. K., LU, R., KAUR, A., HAMMER, Q., LI, B., PANCH, S., ALLAN, D. A., DONAHUE, R. E., CHILDS, R. W., ROMAGNANI, C., BRYCESON, Y. T. & DUNBAR, C. E. 2018. Clonal expansion and compartmentalized maintenance of rhesus macaque NK cell subsets. *Sci Immunol*, 3.
- WU, C., LI, B., LU, R., KOELLE, S. J., YANG, Y., JARES, A., KROUSE, A. E., METZGER, M., LIANG, F., LORE, K., WU, C. O., DONAHUE, R. E., CHEN, I. S. Y., WEISSMAN, I. & DUNBAR, C. E. 2014. Clonal tracking of rhesus macaque hematopoiesis highlights a distinct lineage origin for natural killer cells. *Cell Stem Cell*, 14, 486-499.
- YADI, H., BURKE, S., MADEJA, Z., HEMBERGER, M., MOFFETT, A. & COLUCCI, F. 2008. Unique receptor repertoire in mouse uterine NK cells. *J Immunol*, 181, 6140-7.
- ZHENG, Y., VALDEZ, P. A., DANILENKO, D. M., HU, Y., SA, S. M., GONG, Q., ABBAS, A. R., MODRUSAN, Z., GHILARDI, N., DE SAUVAGE, F. J. & OUYANG, W. 2008. Interleukin-22 mediates early host defense against attaching and effacing bacterial pathogens. *Nat Med*, 14, 282-9.
- ZHUANG, L., FULTON, R. J., RETTMAN, P., SAYAN, A. E., COAD, J., AL-SHAMKHANI, A. & KHAKOO, S. I. 2019. Activity of IL-12/15/18 primed natural killer cells against hepatocellular carcinoma. *Hepatol Int*, 13, 75-83.

ZIEGLER, H., THALE, R., LUCIN, P., MURANYI, W., FLOHR, T., HENGEL, H., FARRELL, H., RAWLINSON, W. & KOSZINOWSKI, U. H. 1997. A mouse cytomegalovirus glycoprotein retains MHC class I complexes in the ERGIC/cis-Golgi compartments. *Immunity*, 6, 57-66.

8 Acknowledgements

The completion of this thesis would not have been possible without the enormous support from many important people throughout this work to whom I am deeply grateful.

First, I would like to thank my supervisors Veit Buchholz and Simon Graßmann for their support, inspiring scientific discussions and helpful suggestions that were a major contribution to the success of this work and for creating such a great research environment. Furthermore, I want to thank Benjamin Schusser and Dirk Busch for their interest, scientific discussions and their agreement to supervise and mentor my thesis.

Several fruitful collaborations critically contributed to the advance of this project. Here, I would like express my gratitude to Jan Böttcher and Philippa Meiser for the enormous effort they put into conduction and analysis of the immunofluorescence imaging. I would like to thank Gabriel Victora and Jonatan Ersching for performing the parabiosis experiments as well as Luka Cicin-Sain and M. Zeeshan Chaudhry for providing MCMV stocks and measuring MCMV titers. I am deeply grateful to Michael Floßdorf, Simon Graßmann, Sebastian Jarosch and Thomas Höfer for their contribution to RNA sequencing as well as subsequent data analysis. Finally, I want to thank Eric Vivier, Yakup Tanriver and Joseph Sun for provding mice for this study.

This project was part of the SFB 1054 “Control and Plasticity of Cell-Fate Decisions in the Immune System” that provided an outstanding environment to develop the project and discuss data with renowned experts in the field.

I am enormously thankful for the friendships I made during my time at the institute. I would especially like to thank Justin Leube, Inge Hensel, Simon Graßmann, Ludwig Pachmayr, Thomas Müller, Immanuel Andrä, Julia Ritter, Anton Mühlbauer and Julian Hönninger who made these years at the institute unforgettable.

And last but not least, I am extremely grateful for my family. I would like to thank my parents, Kathrin and Thomas, as well as my brothers, Johannes and Constantin, for their unconditional support. Finally, I want to thank my boyfriend, Sebastian, for his emotional support and for always believing in me!